UNIVERSITÄT OSNABRÜCK

Remote sensing large-scale surface structures in the Wadden Sea.

Application of satellite SAR data (TerraSAR-X) to record spatial distribution and dynamics of habitats and geomorphic structures for monitoring and long-term ecological research

Thesis

for obtaining the academic degree Doctor of Science
– Dr. rer. nat. –

submitted to the
Department of Mathematics/Computer Science
at the University of Osnabrück

by

Inga Winny Adolph

June 2020

Supervisors:

Prof. Dr.-Ing. Manfred Ehlers (em.)
University of Osnabrück

Hon.-Prof. Dr.-Ing. Peter Reinartz
German Aerospace Center (DLR)

Prof. Dr. Jochen Schiewe
Hafencity University Hamburg

Abstract

The Wadden Sea off the coast of the southern North Sea is the largest coherent area of tidal flats worldwide. As a highly productive ecosystem it is of global importance, e.g. as nursery for fish and as a feeding and resting area for 10 – 12 million migratory birds following the East Atlantic Flyway. The outstanding ecological significance of this region corresponds to a high level of protection by EU directives and national law and by inscription as UNESCO World Heritage Site, all of which requires regular monitoring and assessment. Apart from the ecological aspects, the Wadden Sea is also of great importance for coastal protection. To survey the extensive, often inaccessible tidal area, remote sensing is essential and while mainly airborne techniques have been carried out for decades, now high-resolution satellite-borne sensors open up new possibilities relevant for monitoring and long-term ecological research. Especially satellite synthetic aperture radar (SAR) sensors offer a high availability of acquisitions as they operate largely independently of daylight and weather. The aim of the studies presented here was to explore the use of data from the TerraSAR-X satellite to record geomorphological structures and habitats for Wadden Sea Monitoring. More than 100 TerraSAR-X acquisitions from 2009 to 2016 were analyzed to distinguish various and variable surface types continuously influenced by tidal dynamics in the main study area, the tidal flats near the island of Norderney.

Visual image interpretation supported by extensive in-situ verification proved to be a suitable and unsophisticated approach which is unspecific enough to identify mussel beds, fields of shell-detritus, gully structures, mud fields, and intertidal bedforms in the upper flats of the East Frisian Islands. The method proved to be robust against changes in geometry of acquisition and environmental influences, which permitted a large database. Several time series of TerraSAR-X data enabled to follow inter-annual and seasonal dynamics as well as event effects (Adolph et al. 2018). The high-frequency TerraSAR-X data revealed novel evidence of an intertidal bedform shift in an easterly direction during the study period. To this aim, an unsupervised ISODATA classification of textural parameters was developed to vectorize and compare the bedforms positions in a GIS (Adolph et al. 2017a). The same intertidal bedform area was chosen as test-site for comparison of different remote sensing methods, namely airborne lidar, satellite-based radar (TerraSAR-X) and electro-optical sensors (RapidEye) (Adolph et al. 2017b).

High-resolution SAR data offer a relevant component for Wadden Sea Monitoring and Research, as they provide reliable, regular data with a high repetition rate. In particular, habitats with noticeable surface roughness, specific structures and textures are well reflected. Geomorphic Structures and their dynamics can be observed indirectly via detection of residual water trapped within. A comprehensive concept for Wadden Sea Monitoring however, requires automatized classifications and an integrative, multi-sensor approach (SAR, LIDAR, multi-spectral data, drones) in which different and complementary information, coverage and resolutions (spatial and temporal) contribute to an overall picture.

The studies were carried out as part of the joint research project “Scientific monitoring concepts for the German Bight” (WIMO), jointly funded by the Ministry of Environment, Energy and Climate Protection (NMU) and the Ministry of Science and Culture (NMWK) of the Federal State of Lower Saxony. The findings have been published in *Geo-Marine Letters 37/2* (2017) and in *Remote Sensing 10/7* (2018).

Zusammenfassung

Das trilaterale Wattenmeer entlang der südlichen Nordseeküste ist das weltweit größte zusammenhängende Wattengebiet. Als hochproduktives Ökosystem ist es von globaler Bedeutung, z.B. als Kinderstube für Fische und als Nahrungs- und Rastplatz für 10 – 12 Millionen Zugvögel auf dem Ostatlantischen Zugweg. Dem wird durch einen sehr hohen Schutzstatus Rechnung getragen: Nationalparke, EU-Richtlinien und die Anerkennung als UNESCO Weltnaturerbe verpflichten u.a. zu regelmäßigem Monitoring und Bewertung des ökologischen Zustandes. Um das ausgedehnte, oft schwer zugängliche Gezeitengebiet zu überwachen, sind Methoden der Fernerkundung unerlässlich. Bislang werden dafür flugzeug-getragene Sensoren verwendet, nun eröffnen hochauflösende satellitengestützte Sensoren neue Möglichkeiten für Wattenmeer-Monitoring und -Forschung. Insbesondere Radar mit synthetischer Apertur (SAR), das weitgehend unbeeinflusst von Tageslicht und Wetter operiert, bietet eine hohe Verfügbarkeit von Aufnahmen während der Niedrigwasserzeit. Übergeordnetes Ziel der hier vorgestellten Studien war, die Verwendung von Daten des Satelliten TerraSAR-X zur Erfassung geomorphologischer Strukturen und Lebensräume im Hauptuntersuchungsgebiet zwischen der Insel Norderney und dem Festland für das Wattenmeer-Monitoring zu untersuchen. Mehr als 100 TerraSAR-X Szenen von 2009 bis 2016 wurden analysiert, um verschiedene und äußerst variable Oberflächentypen zu unterscheiden, die kontinuierlich unter dem Einfluss der Gezeitendynamik stehen.

Visuelle Bildinterpretation kombiniert mit extensiver in-situ Verifikation der Interpretations-ergebnisse erwies sich als geeigneter und unspezifischer Ansatz zur zeitnahen Detektion von Muschelbänken, Schlick- und Schillfeldern, Prielstrukturen und geomorphen Strukturen der Sedimentoberfläche, sogenannten „bedforms“. Die Methode erwies sich als robust gegenüber Umwelteinflüssen und Änderungen der Aufnahmegeometrie, was die Nutzung einer großen Datenbasis ermöglicht. In mehreren Zeitreihen von TerraSAR-X Aufnahmen wurden inter-annuelle und saisonale Veränderungen sowie Ereigniseffekte beobachtet (Adolph et al. 2018). Aufgrund der hohen Aufnahmefrequenz der TerraSAR-X Daten konnte erstmals eine ostwärts gerichtete Verlagerung der bedforms während des Untersuchungszeitraumes aufgezeigt werden. Zu diesem Zweck wurde eine unbeaufsichtigte ISODATA-Klassifizierung von Texturparametern entwickelt, um die Positionen der „bedforms“ zu vektorisieren und in einem GIS zu vergleichen (Adolph et al. 2017a). Dasselbe Areal wurde als Testgebiet gewählt, in dem die Aufnahmeeigenschaften von flugzeug-getragenem Lidar und satelliten-gestütztem SAR (TerraSAR-X) sowie elektro-optischen Sensoren (RapidEye) verglichen wurden (Adolph et al. 2017b).

Hochauflösende SAR-Daten stellen eine relevante Komponente für das Monitoring und die Forschung im Wattenmeer dar, da sie zuverlässig und regelmäßig Daten mit einer hohen Wiederholungsrate liefern. Geomorphe Strukturen und ihre Dynamik können indirekt durch die Erkennung von darin eingeschlossenem Restwasser erfasst werden. Ein umfassendes Konzept für das Wattenmeer Monitoring wird jedoch automatisierte Klassifizierungen erfordern sowie einen multi-sensor Ansatz (SAR, LIDAR, multispektrale Daten, Drohnen), bei dem unterschiedliche und komplementäre Informationen, Abdeckungen und Auflösungen (räumlich und zeitlich) zu einem Gesamtbild beitragen.

Die Untersuchungen waren Teil des gemeinsamen Forschungsprojekts „Wissenschaftliche Überwachungskonzepte für die Deutsche Bucht“ (WIMO), das vom Nds. Ministerium für Umwelt, Energie und Klimaschutz (NMU) und dem Nds. Ministerium für Wissenschaft und Kultur (NMWK) finanziert wurde. Die Ergebnisse wurden in *Geo-Marine Letters 37/2* (2017) und in *Remote Sensing 10/7* (2018) veröffentlicht.

Contents

1 General Introduction – Background and Motivation

1.1 Protection, Monitoring and Assessment of the Wadden Sea

The outstanding ecological significance attributed to the Dutch, German and Danish Wadden Sea is met by a particularly high level of protection. As a national park the Wadden Sea has the highest protection status according to national nature protection legislation in Germany and in Denmark. Beyond the national laws and borders, the Trilateral Wadden Sea Cooperation (TWSC), an intergovernmental cooperation of The Netherlands, Germany and Denmark is to protect and conserve the Wadden Sea as an ecological entity through common policies and management. At EU level, the Wadden Sea is protected as part of the European Natura 2000 network of protected areas according to the provisions of the Fauna-Flora-Habitat Directive (Directive 92/43/EEC, FFH) and the Birds Directive (Directive 79/147/EC, BD) as well as under the EU Water Framework Directive (Directive 2000/60/EC, WFD) and the Marine Strategy Framework Directive (Directive 2008/56/EC, MSFD). Furthermore, the Wadden Sea is subject to a large number of international conventions, agreements and treaties such as, e.g., the Ramsar Convention (Convention on Wetlands of International Importance Especially as Waterfowl Habitat), the Convention on Biological Diversity (CBD) and many more, which are listed by Marencic (2009) and CWSS (2017). The recognition as a UNESCO World Heritage area (2009) underlines the peculiarity of the Wadden Sea in a worldwide context.

This legal status at national and EU level, but also the international conventions and the UNESCO require assessments of the ecological status of the Wadden Sea in regular intervals. For the understanding of the ecosystem and its future development, extensive monitoring and research are needed and there has been a long tradition of ecological research in the area (Wolff 2013). Nevertheless, with the number of environmental directives relating to the Wadden Sea, the demands of monitoring and reporting obligations have increased during the last decades. For example, every 6 years status reports that are based on data related assessments have to be carried out for the FFH Directive, the Water Framework Directive and the Marine Strategy Framework Directive, aiming at a favorable conservation status or good status (WFD) respectively good environmental status (MSFD) of species, habitats or waterbodies. Monitoring programs providing actual comprehensive data of different components of the Wadden Sea ecosystem are fundamental for these assessments.

However, not only for reasons of environmental protection, but also for coastal protection, the recording of morphological changes or salt marsh status in this highly dynamic marine environment is of great value for the management of the area. It becomes even more essential against the background of global climate change and rising sea levels which will increasingly place this area under the pressure of coastal squeezing (Delafontaine & Flemming 2000, Reise 2005).

1.2 Relevance of Remote Sensing for Wadden Sea Monitoring and Research

The Wadden Sea area covers approximately 14,700 km^2 when defined as the area seaward the main dike where present, respectively the spring-high-tide-water line or the brackish-water limit in the rivers. Towards the North Sea, it reaches up to 3 nautical miles from the baseline or the offshore boundaries of the Conservation Area (CWSS 2017). Of this area, intertidal sand and mud flats and saltmarshes take 4,700km^2 and 400 km^2 respectively. Due to the changing tides, this large and rough terrain is accessible only in tight time frames around low water time. Muddy sediment and tidal channels further complicate the direct access. Due to this constellation of regularly required data on the state of the Wadden Sea, the sheer size of the area and the restricted accessibility, methods of remote sensing are essential, as they allow periodic surveys and assessments of large areas with comparatively less effort.

Fig. 1-1 The Trilateral Wadden Sea in the German Bight. Satellite image mosaic, 2015. Based on 20 individual images from the American earth observation satellite Landsat 8, © albedo39 Satellitenbildwerkstatt.

2 Objective – Overarching Goals and Issues

Aerial mapping and interpretation of aerial color and infrared imagery as well as airborne lidar have proven to provide the high resolution needed to identify tidal surface structures, salt marsh vegetation types or even numbers of waterbirds or marine mammals. These airborne observation methods have been used operationally for a long time and they are currently being used. At the same time, however, satellite-borne sensors have been improved and the use of satellite data for monitoring, protection and management of coastal areas such as the Wadden Sea has become increasingly realistic. An overview of previous research on satellite-based remote sensing for the tidal flats of the Wadden Sea is given e.g. by Müller et al. (2016). To reach the overall goal of an area-wide and regular survey of the Wadden Sea, providing the relevant information at minimum expense, the available sensor classes – including a progressive multitude of space-borne sensors – are to be used efficiently according to their respective advantages. To this aim, monitoring requirements have to be checked against the sensor`s features especially regarding areal coverage, spatial resolution, temporal availability, sensitivity and geometric accuracy. The studies leading to the published manuscripts presented below were carried out as part of the joint research project “Scientific monitoring concepts for the German Bight” (WIMO). It was conducted from 2010 to 2015 to develop innovative scientific monitoring concepts for the German Bight as a model region (for overviews see Winter et al. 2016, Winter 2017, wimo-nordsee.de). One of the focal points in WIMO was the applicability of established and new methods of remote sensing for monitoring intertidal areas and subtidal seafloor. Four sub-projects contributed to the WIMO internal project-group “Habitat Mapping” by investigating and comparing high-resolution electro-optical and SAR data, airborne laser scanning (Schmidt et al. 2013, Jung et al. 2016, Adolph et al. 2017a, b., Adolph et al, 2018) and sublittoral habitat mapping by side-scan sonar (Holler et al. 2017). The studies presented here mainly result from investigations on the applicability of SAR data for intertidal monitoring (WIMO subproject TP 1.4 “Application of high resolution SAR-data (TerraSAR-X) for monitoring eulittoral surface structures and habitats”). Since it is highly probable that an integrative monitoring concept is required to fulfil the monitoring needs, one of the publications also reflects the close cooperation between the subprojects dealing with different sensor classes (Publication III, chap. 5.3).

3 Thematic Introduction

3.1 The Wadden Sea

3.1.1 Physical Setting – Geology, Hydrology, Morphology

Tidal flat areas off shallow coasts can be found worldwide occurring as transitional areas between the open sea and the shore. They are formed by the tides in marine and brackish areas where the sea floor rises gradually towards the coast. The world's largest coherent intertidal flat area is the Wadden Sea bordering the North Sea coast of The Netherlands, Germany, and Denmark. Over a length of 450 km, the Wadden Sea stretches from Den Helder in the southwest up to the Skallingen peninsula in the northeast. The average width is 10 km, but can be up to 40 km in some places (Scheiffarth 2004). Thus, the Wadden Sea holds about 60% of the whole intertidal area at the north-eastern Atlantic shores (Reise et al. 2010). In geomorphological and evolutionary terms the Wadden Sea is a very young ecosystem that has developed after the last ice age (CWSS 2017). The evolution of the Wadden Sea barrier island system commenced at 7,500−8,000 years BP when the rising post-glacial sea reached the southern margin of the North Sea basin and entered local river valleys, turning them into estuaries (Flemming & Davies 1994). The geomorphology of the landscape continuously changed due to Holocene sea-level rise, the geometry of the Pleistocene surface, the development of sedimentary environments, sediment transport mechanisms (tides and wind) and, relatively recently, the human interference in the landscape (Oost et al. 2017). Man-made interventions influence the current landscape of the Wadden Sea through coastal protection measures, maritime maintenance and uses such as fishing and tourism (Ehlers 1994). Today`s shoreline is the result of the post-glacial sea-level rise, of storm surges that led to land losses, and of subsequent embankments, coastal defense structures and sand nourishments. Approximately 10,000 km^2 of Wadden Sea habitats have been impoldered since the medieval times (Wolff 1991). Nevertheless, the natural geological and biological processes are still highly effective at work in the coastal and marine environment of the Wadden Sea, generating the enormous dynamics that characterize especially the tidal flat system. The interaction of tidal and wave energy, the transport, erosion and sedimentation of sand and mud, result in an ever-changing morphology of the channels, tidal flats and islands (e.g. Wang et al. 2012, Hellwig & Stock 2014). The 4,700 km^2 of bare sand and mud flats emerge at low tide, partially sheltered against winds and the waves of a rough sea by a seaward barrier of dynamic sandy shoals and dune islands (Reise et al. 2010). Tidal range today spans from 1.5 to 4 m increasing from the edges towards the inner German Bay (Reise et al. 2010). In the south and the north, mesotidal regions with tidal ranges between 1.5 to 3 m form a system of tidal flats sheltered by the seaward chain of barrier islands, whose size decreases towards the center. These areas extend from Texel to the Jade mouth in the south and from the Süderoogsand to the island of Fanø in the north. In the central Wadden Sea, mean tidal range exceeds 2.90 m, this is the macrotidal region with no barrier islands. These open tidal flats can be limited to the seafront by small, highly variable sandbars at the most (Ehlers 1994, Reise et al. 2010). Barrier islands and elevated sands generate an internal structure of the Wadden Sea comprising a series of 33 tidal basins interrupted only by the four major estuaries of the Ems, Weser, Elbe and Eider. The tidal basins are distinctive, hydrological features of the Wadden Sea, which, disregarding the tides, can be compared to riverine catchment areas. (CWSS 2008). The lateral connection of the tidal basins is provided by some overflow at the tidal divides (watersheds) in the back-barrier area, where the flood waters of adjacent tidal basins meet, and by the long-shore current seaward of the islands (CWSS 2008).

Twice a day an average volume of 15 km^3 of sea water is moved through the inlets and tidal channels into and out of the tidal basins while roughly the same volume stays there at low tide. In this process, compression of the tidal flow between adjacent islands leads to strong current velocities with a mean

flow of about 1 m s^{-1} (Reise et al. 2010), scouring tidal inlets of up to 50 m depths (CWSS 2008). Strong onshore winds may increase high tides up to 4 m above mean high tide and strong offshore winds may push low tides down to 1.5 m below mean low tide level (Reise et al. 2010). The high daily flow velocities, and especially storm events with high swell, can cause strong displacements of tidal channels, gullies and flats. Having passed the barrier islands, most inlets divide into major tidal channels, which successively branch into smaller tidal creeks, gullies and runnels. In the areas of high energy, under the influence of inlets and major channels, sand flats are formed, whereas with decreasing energy-level mixed flats and subsequently mud flats develop corresponding to flow-velocity, wave exposition and times of coverage by sea water. Thus, mud flats are found mainly in sheltered areas close to the shoreline or to the watershed.

To sum it up, the Wadden Sea is a highly dynamic and amphibious coastal landscape characterized by constant change and a multitude of transitions and extremes. It represents the ongoing adaption of coastal environments to a rising sea level. Moreover, the geological and geomorphological features are closely entwined with ecological and biological processes, thus creating a complex coastal ecosystem with strong bio-geomorphological interactions at all scales.

3.1.2 Ecology and Habitats

Major habitats of the Wadden Sea ecosystem can be distinguished according to their location in an offshore-inshore gradient. It reaches from the subtidal (sublittoral) areas, the offshore belt (seaward of the islands up to 15m depth) and the system of inlets, channels and gullies extending into the actual intertidal area, the eulittoral sand and mud flats and sandbanks falling dry at low tide. Closer to the shore, the supra-littoral zone follows, which is only sporadically flooded at high water levels such as higher springtides or storm surges. This area includes the salt marshes and high beaches of the mainland coast and of the dune islands.

The productivity of the Wadden Sea in terms of biomass is one of the highest in the world (CWSS 2008). Primary production is dominated by microscopic algae, mainly diatoms, which in places cover the sediment surface of the flats or drift in the shallow waters as planktonic algae. Additionally, there is an essential import of phytoplankton from the offshore belt through the tidal inlets. These unicellular algae are consumed by invertebrate herbivores and constitute an abundant and highly effective food supply for rich zoobenthos numbers and biomass in and on the sediment: molluscan suspension feeders such as mussel and oyster beds, deposit feeding worms and small snails (Beukema 1978, Beukema et al. 2002, Asmus 1987, Reise et al. 1994). This biological production in turn, provides plenty of food for small crabs, shrimp and fish (Smidt 1951, Kuipers 1977, Strasser 2002) as well as for wading birds, gulls and ducks (Piersma 1987, Scheiffarth & Nehls 1997). The biomass of marine invertebrates on the tidal flats is on average 20 times higher than for offshore benthic systems in the North Sea (CWSS 2008). For this reason, the Wadden Sea is an important nursery area for fish, foraging and resting ground for seals, waders and other waterfowl from in- and outside the Wadden Sea region. About 10 million birds migrating on the East Atlantic Flyway use the area as an indispensable stepping stone every year to generate the fat reserves needed for their long distance flights to the Arctic or to Africa.

The different types of sediment forming the tidal flats and the subtidal areas, provide differing environmental conditions for the benthic organisms living in or on the bottom of the Wadden Sea. Depending on flow velocity, wave energy and inundation time, they have to cope with very unstable, nutrient-poor but well oxygenated conditions in exposed sands on the one hand, and with stable and nutrient-rich, but low oxygen conditions in mud flats on the other hand. These extremes cause high specialization of the organisms for distinct environments forming habitats with typical species communities. It has been shown that the spatial distribution of benthic communities is directly

dependent on sediment grain size, water depth and exposure to hydrodynamic energy (e.g. Markert et al. 2015). Open flats may consist of wave rippled sands, mixed flats, mud flats and bumpy mud fields. Additionally, surfaces may be featured e.g. by coiled strings of sand which are the fecal mounds of millions of lugworms (*Arenicola marina*) reworking the sediment, by dense fields of Sand Masons (*Lanice conchilega*) whose tubes protrude above the sediment, by accumulated shell detritus, by residual water coverage or by the more or less brownish-colored coverings of diatoms. More conspicuous structures are formed by ecosystem engineers such as beds of Blue Mussels (*Mytilus edulis*) and Pacific Oysters (*Magallana gigas*, syn. *Crassostrea gigas*) or seagrass beds established by two species of vascular plants inhabiting the tidal flats, Dwarf Eelgrass (*Zostera noltii*) and Common Eelgrass (*Z. marina*). Both, mussel beds and seagrass beds, are home and/or feeding ground for a species-rich fauna, epiphytes and microflora. The transition from tidal flats to island or mainland coasts is primarily formed by saltmarshes, a special habitat characterized by salt-tolerant plant communities and a species-rich fauna adapted to it including many endemic taxa.

Altogether, a mosaic of different habitats and microhabitats results from the dynamics characterizing the Wadden Sea – from environmental gradients, transition zones and small-scale changes of important environmental conditions such as sediment structure, flow conditions, depth, temperature and salinity. To these habitats, a large number of animal and plant species have adapted as a mixture of residents, migrants and casual visitors. Reise et al. (2010) emphasize this complex matrix of habitats occurring in dynamic sequences in a repetitive pattern due to the long chain of islands and shoals, tidal basins and estuaries. They estimate a total number of about 10,000 species populating the Wadden Sea ecosystem and in particular the saltmarshes harbor a large number of species. Yet, the actual intertidal area, the tidal flats, are characterized rather by high abundances of individuals instead of high biodiversity (CWSS 2008).

From the ecological perspective, the Wadden Sea is one of the last large-scale and near-natural ecosystems in Central Europe with ecosystem services such as filtration and decomposition of organic matter and a very high biological productivity that fulfill important ecological functions far beyond its spatial limits in the adjacent North Sea, and also worldwide, e.g. in bird migration. Nevertheless, the Wadden Sea also plays a vital role in coastal protection and has a very high economic importance. Human activities such as tourism (more than eight million overnight stays a year only regarding the Lower Saxon coast), fishing, agriculture, dredging and maritime transport are on the one hand crucial economic factors for the coastal region, but on the other hand also pose a significant potential for disturbance and pollution in the Wadden Sea area. In order to sustainably reconcile these different interests and demands on the area, monitoring, management and protective measures are required (CWSS 1997).

3.2 Remote Sensing in the Wadden Sea

3.2.1 Airborne Remote Sensing

Airborne remote sensing techniques such as aerial mapping and imagery have for long been applied in research projects and some have been included in current operational monitoring programs. The oldest series of aerial photographs (panchromatic, 1:25 000, pers. comm. NLPV) covering the Lower Saxony tidal area date back to the years 1936-1939 (Reichsluftbilder, Federal Archives, Koblenz).

The aerial survey of selected species seems to have the longest history of environmental monitoring in the Wadden Sea. In Lower Saxony, first counts of waterbirds from the aircraft have been carried out in the 1950s, with surveys of moulting Shelduck (*Tadorna tadorna*) on Knechtsand (Goethe 1961). Since 1986, wintering stocks and moulting stocks of Common Eider (*Somateria mollissima*) have been

recorded regularly by aerial surveys in coordination with Schleswig-Holstein (Nehls et al. 1988, Swennen et al. 1989, Scheiffarth & Frank 2005). And since 1992, regular aerial counts for Common Eider in winter and for Common Shelduck during wing moult (July/August) are carried out trilaterally coordinated as part of the Joint Monitoring of Migratory Birds in the Wadden Sea (JMMB) in the framework of the TMAP (Blew et al. 2005, Blew et al. 2017). Aerial counts to determine the population of Harbour Seal (*Phoca vitulina*) are carried out regularly since 1975 (Abt 2002, Lienau 2010). With the return of the Grey Seal (*Halichoerus grypus*) to the Wadden Sea, the monitoring has been extended to cover this species as well (Jensen et al. 2017). Currently, trilaterally coordinated flights take place annually, according to the 'Seal Management Plan' and the data are part of the Trilateral Monitoring and Assessment Program (TMAP).

Results of a first systematic inventory of intertidal habitats based on a comprehensive data base, including aerial photographs (panchromatic, 1:15 000 to 1:60 000) were compiled by Dijkema et al.(1989) into 24 habitat maps (1:100 000) of the Dutch, German and Danish Wadden Sea. Due to the base material used, these habitat maps represent the situation of the Wadden Sea at the end of the 1970s (Dijkema 1991).

Since the 1990s, aerial imagery has been applied conceptually and regularly in operational monitoring programs to survey intertidal habitats of the Lower Saxony Wadden Sea. Since 1994, the monitoring of mussel bed area is based on the analysis of aerial photographs and since 1999, aerophotos are taken annually for this purpose (Millat 1996, Herlyn & Millat 2004, Herlyn 2005), starting with panchromatic images (scale 1:15 000) and changing to true color (scale 1:20 000) in 2006 (Folmer et al. 2014). Aerial imagery also contributes to biotope type mapping of the salt marshes since 1991 (Ringot 1992/1993, Millat 1996, Esselink et al. 2009, Petersen et al. 2010) and is used by the responsible authorities for coastal protection to monitor tidal inlets and deltas (NLWKN, unpublished data). The use of aerial photographs in support of seagrass mappings has been examined by Kolbe (2011), who showed that total seagrass cover must exceed 15% to be detectable with sufficient reliability. In majority, seagrass beds along the coast of Lower Saxony are not that densely covered currently. However, the density of intertidal seagrass beds varies within Wadden Sea regions and aerial mappings and imagery contribute to annual surveys of seagrass beds with a cover of more than approximately 20% in Schleswig-Holstein and Denmark. In The Netherlands, long-term seagrass monitoring was changed in 2009 from the analysis of color-infrared (CIR) aerial photography to ground survey due to the sparse seagrass coverage (Dolch et al 2017).

As a state-of-the-art three-dimensional terrain survey technique, also airborne lidar (light detecting and ranging) is applied to derive highly accurate digital terrain models (DTMs) of the intertidal area (Brzank et al. 2009). Lidar serves as a standard method for DTM generation in coastal zones, it delivers dense and accurate data for large areas. However, only the intertidal zone can be covered by standard laser because the near-infrared laser pulses are not able to penetrate residual water which remains in some tidal areas and especially in channels even during low tide (Brzank et al. 2009, Schmidt et al. 2013).

3.2.2 Satellite-borne Remote Sensing

Early investigations on the use of satellite data for remote sensing the Wadden Sea are based on data from the Thematic Mapper (TM) and the Multispectral Scanner (MSS) on board Landsat (e.g. Pröber 1981, Dennert-Möller 1982, Bartholdy & Folving 1986), or synthetic aperture radar (SAR) data from ERS-1/2 (e.g. Wang & Koopmanns 1995, Geoscan 1996, Lehner et al. 2001). Spatial resolution was in the scale of about 30 m for ERS-1/2 SAR imaging and spectral Landsat (4–5) TM data (ESA Earth Online 2000−2019, NASA 2019a). The Landsat (1–5) MSS collected at a spatial resolution of 68 m x 83 m,

commonly resampled to 57 m or 60 m (NASA 2019b). Increasing spatial and/or spectral resolution of electro-optical systems (e.g., Landsat-8, RapidEye, SPOT-4, World-View, or currently, Sentinel-2) and significant advances in synthetic aperture radar (SAR) technology also resulted in expanded research on data analysis and furthered the development of image classification methods (see e.g. Moreira et al. 2013, Müller et al. 2016).

The availability of increasingly relevant data was taken into account in a series of publicly funded research projects. The EU-project HIMOM (2002–2005) was designed to provide a "system of Hierarchical Monitoring Methods (HMM) for assessing changes in the biological and physical state of intertidal areas" (HIMOM 2005, unpublished.). As part of the HIMOM project, data from Landsat 5 TM and Landsat 7 ETM were used to generate an atlas of sediment types and vegetation coverage of 5 European estuaries, including selected parts of the German Wadden Sea. From 2005–2007, HIMOM was followed by the German project OFEW (operationalization of remote sensing methods for monitoring the Wadden Sea) to further develop satellite-borne remote sensing methods and techniques for the Wadden Sea monitoring. The objective of OFEW was to develop standardized methods for automated classification of sediment type, vegetation, mussel beds and chlorophyll-a concentration (Brockmann Consult 2007, Stelzer et al. 2007). A central result of the project is a classification methodology using linear spectral unmixing and knowledge-based decision trees for electro-optical remote sensing data of medium spatial resolution, which is tens of meters (Stelzer et al. 2007). This classification method was subsequently improved in the following projects DeMarine-1-Environment TP4 (2008–2011) and DeMarine-2 SAMOWatt (2012–2015), both part of the European GMES program (Global Monitoring for Environment and Security, 2012 renamed Copernicus). To provide area-wide information on the Wadden Sea surface, within these consecutive DeMarine subprojects, high-resolution SAR data was integrated into the hitherto purely electro-optical data base to develop a synergistic classification which led to significant improvements especially regarding the identification of mussel beds (Stelzer et al. 2010). Additionally, the classification methods developed for electro-optical data have been refined, applied and adapted to satellite data of different spatial and spectral resolution (Stelzer et al. 2010, Müller et al. 2016). The application of satellite-borne remote sensing and of Lidar to monitor the Wadden Sea was also a focal point of the WIMO project and the frame for this dissertation (see chap. 2).

As a significant advantage of the projects listed above, the active cooperation between scientific institutions and users such as representatives from public authorities has to be emphasized, being a forward-looking approach.

3.2.3 SAR data for Remote Sensing in the Wadden Sea – State of the Art

A new class of high-resolution SAR sensors has enabled a new level of spatial resolution. Since the launch of TerraSAR-X in 2007, followed by TanDEM-X (both X-band), the COSMO-SkyMed satellite constellation (X-band), and Radarsat-2 (C-band), these satellites provide SAR data with resolutions in the scale of meters (Moreira et al. 2013). The radar satellite Sentinel-1 with a slightly lower resolution (5 m in stripmap mode) has been available since 2014 with open data policy. Due to their active functionality, SAR sensors can record independently from daylight and cloud cover, which considerably raises the availability of satellite acquisitions during low water time. For these reasons, SAR data has a high potential for remote sensing in intertidal areas. Unlike electro-optical sensors and depending on the wavelength used, synthetic aperture radar can be regarded as a measure of surface roughness (e.g. Van der Wal et al. 2005, Aubert et al. 2011, Moreira et al. 2013), adding another valuable perspective to remote sensing. Stelzer et al. (2010), Dehouck et al. (2012) and later Gade et al. (2014, 2015), Jung et al. (2015) and Müller et al. (2016) demonstrated the potential of SAR data as a synergistic input to multi-sensor approaches for the remote sensing of intertidal areas.

Waterline detection and residual water:

An essential feature of SAR imagery is the ability to distinguish water cover from sediment surfaces. Different approaches of waterline detection from SAR data have been developed and applied to tidal flat areas in several regions worldwide with the aim to generate topographic maps and digital elevation models (DEMs) of the intertidal zone and to monitor the longer-term evolution of tidal flats and tidal inlets. For instance, Mason and Davenport (1996) developed a semiautomatic method for coastline detection using a multi-scale approach, and Dellepiane et al. (2004) proposed to exploit coherence measures of interferometric SAR couples. To detect waterlines in SAR images of the German Bight in the south-eastern North Sea, Niedermeier et al. (2005) and Heygster et al. (2010) proposed wavelet-based algorithms which they applied to map tidal flats of the large estuaries of the Elbe and Eider rivers, and of an area of 50×100 km along the North Sea coast of Schleswig-Holstein and Lower Saxony. The same method was used by Li et al. (2014) to generate annual topographic maps analyzing SAR images collected over 8 years (1996−1999 and 2006−2009) for the northern German Wadden Sea. These maps enable a view on tidal flats and sandbanks and the changes they undergo during these years. More recently, Wiehle & Lehner (2015) presented an algorithm combining edge detection, brightness thresholding and a previously determined coarse landmask which they applied to TerraSAR-X acquisitions covering flats of the Schleswig-Holstein Wadden Sea. The objective of all these studies was to use SAR data to detect the edges delimiting the contours of the exposed flats from the surrounding tidal waters. In contrast, the residual water remaining on the flats during low tide has not been investigated so far (cf. review of SAR applications by Lehner & Tings 2015). But it should not be neglected, that residual water demarcates even shallow features of the sediment surface such as depressions, puddles and bedforms in the SAR data. Thereby, it helps to identify geomorphic surface structures which can provide insight into water drainage systems or further the understanding of morphodynamic processes. For instance, satellite SAR was used by Kim et al. (2011) to detect puddles related to groundwater discharge on tidal flats of the Korean Peninsula. Areas with higher abundances of puddles could be distinguished from areas with lower abundances due to darker backscattering in SAR images over the tidal flats.

Sediment composition:

Exposed and bare tidal flats have been studied with regard to sediment grain-size and surface characteristics in connection with the contribution of surface roughness and moisture to the radar backscattering. In tidal flats, soil moisture as the main factor affecting the dielectric properties usually is very high, and the contribution of variations in such high values to variations in backscatter are considered to be negligible compared to roughness (Van der Wal & Herman 2007, Gade et al. 2008). Van der Wal et al. (2005) found correlations between mud content as well as sediment grain size and backscatter coefficient extracted from ERS SAR data (C band) of intertidal flats in the Westerschelde. Likewise, the studies of Deroin (2012) on radar backscattering of tidal sediments in the Baie des Veys, Normandy, France, showed that backscattering is mainly influenced by the surface roughness. Gade et al. (2008) used multifrequency data from SIR-C/X-SAR (L, C, and X band) for a crude sediment classification based on surface roughness parameters in a tidal flat area off Dithmarschen (Schleswig-Holstein, Germany) and Park et al. (2009) retrieved roughness parameters of intertidal mudflats which can be related to surface sediment textures of biogenic, depositional or also land-use characteristics by using polarimetric airborne SAR data (L band) in Suncheon Bay on the southern coast of the Korean peninsula. A classification chain for mudflats and sand flats in intertidal zones using fully polarimetric SAR data is proposed by Wang et al. (2017a) as a result of their studies on ALOS PALSAR-2 data (L band) of the Chinese east coast. Concerning sediment classification on exposed intertidal flats, the use of multi-frequency or multi-satellite data sets and also the complementary combination with electro-optical remote sensing data which has been found to be sensitive to the correlation of grain-size and

moisture conditions is emphasized by various authors dealing with the subject (e.g. Van der Wal & Herman 2006, 2007, Gade et al. 2014, Wang et al. 2016, 2017).

Mussel beds:

Mussel beds formed as biogenic structures on tidal flats by bivalves such as Blue Mussel and Pacific Oyster create a specific surface roughness which should be reflected in the SAR data. Choe et al. (2012), Kim et al. (2013) and Cheng et al. (2013) detected specific microwave signatures backscattered from oyster reefs, respectively from oyster farms using fully polarimetric C-band data (RADARSAT-2). Nieuwhof et al. (2015) demonstrated that dual-polarized X- and C-band SAR data (TerraSAR-X and RADARSAT-2) can be used to distinguish bare sediment (with up to 5% dispersed shellfish cover) and shellfish substrates (>5% cover). The use of dual-co-polarization TerraSAR-X data was suggested by Gade et al. (2015) and by Gade & Melchionna (2016).

Vegetation cover:

Dehouck et al. (2011) identified Cordgrass (*Spartina spec.*) and the complex of intermediate and upper salt-marsh vegetation in TerraSAR-X imagery and Lee et al. (2012) also showed that high resolution SAR, such as TerraSAR-X and Cosmo-SkyMed can also be used for mapping halophytes in tidal flats.

4 Specific Objectives and Research Questions

This chapter presents the specific objectives and issues of the three publications that form the cumulative part of this study:

The studies were started in 2011 as a part of the WIMO project (subproject TP 1.4 “Application of high resolution SAR-data (TerraSAR-X) for monitoring eulittoral surface structures and habitats”, see chap. 2). The overall goal was to evaluate the suitability of high-resolution imagery acquired by TerraSAR-X to detect and map characteristic tidal habitats and geomorphological structures of the intertidal Wadden Sea area.

At the beginning of the investigations, a reliable interpretation of the TerraSAR-X recordings had to be developed and tested. Because of the widely varying appearances of most surfaces that are permanently influenced by tidal dynamics, wind effects on water-covered surfaces as well as by biological and morphological processes, it was necessary to find a non-specific, generic approach which would also be quick and easily applicable. A quick evaluation was required to be able to carry out timely inspections on the site and to be able to detect and verify the interpretation of the surface type and potential changes. Therefore, regarding interpretation of the satellite data, the following questions were in focus:

- Which TerraSAR-X products relating to footprint and resolution (StripMap, SpotLight, high resolution SpotLight) are most suitable to detect and map characteristic intertidal habitats and large scale surface structures of the Wadden Sea?
- Does statistical analysis of backscatter provide sufficient information to identify habitats and geomorphic surface structures or is additional information needed – e.g. about patterns of internal structures or textures?
- Is interpretability of the images affected by geometry of acquisition? Are there any limitations or advantages of different angles of incidence?
- How far can visual interpretation, as a non-specific, generic approach, be used to achieve a reliable and fast interpretation of the TerraSAR-X data to capture the tidal areas?

- Which intertidal habitats and large-scale surface structures are reproduced by TerraSAR-X and how are they displayed?
- Can habitats and large-scale surface structures be reliably distinguished from each other in the TerraSAR-X data? How reliable are the interpretation results compared to extensive field observations?

With regard to Wadden Sea monitoring not only the identification, location and distribution of the characteristic habitats and of large-scale geomorphological structures is of interest, but also areal information is required to determine spatial extents and their development. Therefore, the question arises:

- Is it possible to define reliable outlines of habitats and large-scale surface structures from TerraSAR-X data?

Having in mind transitional zones between different habitats or structures, a clear demarcation may not always be possible:

- Which properties delimit the discrimination of tidal surfaces imaged by TerraSAR-X and the determination of defined contours?

These questions have been dealt with in Publication I ("Remote Sensing Intertidal Flats with TerraSAR-X. A SAR Perspective of the Structural Elements of a Tidal Basin for Monitoring the Wadden Sea", chap. 5.1) which gives a broad overview of how habitats and structures are imaged by TerraSAR-X data, whether and how they can be identified and contoured.

One of the detected structures, a type of intertidal bedforms, is examined in more detail in Publication II ("Monitoring spatiotemporal trends in intertidal bedforms of the German Wadden Sea in 2009–2015 with TerraSAR-X, including links with sediments and benthic macrofauna", chap. 5.2). Based on this example, more specific questions related to detection of geomorphological surface structures and their dynamics are investigated:

- Is the detection of residual water in the bedform troughs suitable to survey the bedforms as a whole?

And, as the patterns created by the residual water proved indicative of the described intertidal bedforms:

- How can the areas of residual water cover be extracted and vectorized for comparison in a time series of TerraSAR-X acquisitions?
- Is the available spatial and temporal resolution of TerraSAR-X data sufficient to track the dynamics of geomorphological surface structures such as the observed bedforms?

The same intertidal bedform area was used in the investigations for Publication III ("Integration of TerraSAR-X, RapidEye and airborne lidar for remote sensing of intertidal bedforms on the upper flats of Norderney (German Wadden Sea)", chap. 5.3) in which the TerraSAR-X data are compared to electro-optical and lidar data from two parallel WIMO subprojects. The general questions, which basically motivate the studies presented here, in this publication are dealt with by way of example:

- Which could be the contribution of TerraSAR-X data for an integrative monitoring concept for future Wadden Sea Monitoring?
- What are the specific qualities of TerraSAR-X data in a multi-sensor approach for remote sensing of tidal flats?

5 Cumulative Section

This chapter comprises one publication in *Remote sensing 10/7* (2018) and two publications in *Geo-Marine letters 37/2* (2017). In the following, the accepted manuscript versions are cited, therefore the layout differs from that of the final publications.

5.1 Remote Sensing Intertidal Flats with TerraSAR-X. A SAR Perspective of the Structural Elements of a Tidal Basin for Monitoring the Wadden Sea

Adolph, W.; Farke, H.; Lehner, S.; Ehlers, M. (2018). *Remote Sens.* 10 (7), 1085–1108. DOI: 10.3390/rs10071085.

Abstract

Spatial distribution and dynamics of intertidal habitats are integral elements of the Wadden Sea ecosystem, essential for the preservation of ecosystem functions and interlocked with geomorphological processes. Protection and monitoring of the Wadden Sea is mandatory and remote sensing is required to survey the extensive, often inaccessible tidal area. Mainly airborne techniques are carried out for decades. High-resolution satellite-borne sensors now enable new possibilities with satellite synthetic aperture radar (SAR) offering high availability of acquisitions during low water time due to independence from daylight and cloud cover. More than 100 TerraSAR-X images from 2009 to 2016 were used to examine the reproduction of intertidal habitats and macrostructures from the flats south of the island of Norderney and comparative areas in the Lower Saxony Wadden Sea. As a non-specific, generic approach to distinguish various and variable surface types continuously influenced by tidal dynamics, visual analysis was chosen which was supported by extensive in situ data. This technically unsophisticated access enabled us to identify mussel beds, fields of shell-detritus, gully structures, mud fields, and bedforms, the latter detected in the upper flats of every East Frisian island. Based on the high frequency of TerraSAR-X recordings for the Norderney area, a bedform shift was observed in a time-series from 2009 to 2015. For the same period, the development of a mud field with an adjoining depression was traced. Beside seasonal variations of the mud field, the formation of a mussel bed settling in the depression was imaged over the years. This study exemplifies the relevance of TerraSAR-X imagery for Wadden Sea remote sensing. Further development of classification methods for current SAR data together with open access availability should contribute to large-scale surveys of intertidal surface structures of geomorphic or biogenic origin and improve monitoring and long-term ecological research in the Wadden Sea and related tidal areas.

5.1.1 Introduction

Tidal flat areas off shallow coasts can be found worldwide. The world's largest coherent intertidal area, the Wadden Sea, is stretching for over 500 km along the North Sea coast of The Netherlands, Germany, and Denmark with a width of up to 20 km. The system of barrier islands, intertidal flats and sandbanks, channels, gullies, and salt marshes forms the transition between the mainland and the open North Sea. The Wadden Sea is one of the last large-scale and near-natural ecosystems in Central Europe, whose ecological functions are supraregional and of far-reaching importance, e.g., as an indispensable stepping stone for birds migrating on the East Atlantic Flyway. In addition, it also plays an important role in coastal protection. The Wadden Sea is protected by a high national as well as international conservation status and it is listed as UNESCO world heritage site. Regular monitoring of the area is

mandatory but complex and expensive because of the large area of rough terrain which is accessible only in tight timeframes due to the changing tides. Therefore, remote sensing techniques are required and aerial mapping and photography (e.g., mussel beds, seagrass meadows, salt marsh vegetation) as well as airborne lidar (light detection and ranging) provide the high resolution needed to determine surface structures of the tidal flats or salt marsh vegetation types. Today they are applied in operational monitoring programs of the Wadden Sea. Aerial photographs have been used in the Lower Saxony Wadden Sea since the 1990s for the monitoring of mussel beds [1–3] and for biotope mapping of the salt marshes [4–6]. Aerial photography and lidar are also used by the responsible authorities for coastal protection (NLWKN, unpublished data). A possible support of the seagrass mappings by aerial photographs was examined by Ref. [7].

Advances in synthetic aperture radar (SAR) technology have enabled a high level of spatial resolution also for satellite-borne sensors implemented by a new class of high-resolution SAR satellites. Since the launch of TerraSAR-X in 2007, followed by TanDEM-X (both X-band), the COSMO-SkyMed satellite constellation (X-band), and Radarsat-2 (C-band), these satellites provide SAR data with resolutions in the scale of meters [8]. The radar satellite Sentinel-1 with a slightly lower resolution (5 m in stripmap mode) has been available since 2014 with open data policy.

With the technical improvements not only offered by the SAR sensors, but also with increasing spatial and/or spectral resolution of electro-optical systems (e.g., Landsat-8, RapidEye, SPOT-4, World-View, or currently, Sentinel-2), the use of satellite data for the protection and management of coastal areas such as the Wadden Sea is becoming increasingly realistic. Against this background, a number of German research projects such as OFEW (2005–2007), DeMarine-1-Environment TP4 (2008–2011), DeMarine-2 SAMOWatt (2012–2015), and WIMO (2011–2015) was conducted to apply high-resolution satellite data for the requirements of monitoring and long-term ecological research in the Wadden Sea; for overviews, see [9–13]. Various authors have demonstrated the value of state-of-the-art satellite data for the exploration of tidal areas [10,11,14–20]. The further development of image classification methods designed for the tidal area has gained pace, for example, regarding the exploitation of polarimetric information from SAR data, whose potential has already been documented by, e.g., Refs. [21–23].

The aim of the present study is to determine the potential of the high-resolution intensity images acquired by TerraSAR-X to identify the distribution and development of the main geomorphological structures and habitats in a whole tidal basin and their dynamics which are of utmost importance for monitoring and long term ecological research but also for the management of the area. In order to recognize as many different surface structures as possible, this study focuses on visual image interpretation, which takes into account backscatter intensity and contrast as well as shapes, patterns, and textures of surface features reflected by the SAR data, but also their configuration or surrounding context. This is of particular importance because the Wadden Sea, characterized by a flat topography, a very dynamic variability, the variety of gradients, transitional zones, and surface structures under the influence of constantly changing water levels and weather conditions, poses great challenges to classification of intertidal surfaces. In this context, visual analysis should provide technically unsophisticated access to as much of the information contained in the SAR data as possible.

Previous knowledge and experience play an important role in the visual interpretation process, with recognition and interpretation running through an iterative process, where both steps heavily rely on one another [24]. That is, context information, such as environmental conditions (acquisition time related to tidal cycle, water level, weather conditions) and processes, field experience, and in situ data, which is difficult to quantify automatically, are essential components flowing into the analysis. Therefore, in this study, extended field observations partly synchronous to the satellite acquisition are

carried out throughout the period of the investigations to validate the image interpretation results. An initial basis of the terrain knowledge was laid during the comprehensive mapping of the main study area as part of the DeMarine-1 project.

TerraSAR-X spotlights and high resolution spotlights proved most suitable to investigate typical intertidal surface structures and habitats such as mussel beds, shell-detritus, gully systems, mud fields, and bedforms which are clearly reproduced and can be drawn from the intensity images by visual analysis. Regarding intertidal bedforms, visual image analysis raised the assumption of bedform movement, therefore the positions of bedform structures in the upper flats of Norderney were further analyzed using the extensive time series of satellite images available for this study. For this purpose, the water-covered bedform troughs were extracted from the TerraSAR-X images using an automated method developed by Ref. [19].

The studies presented here were part of the German research project WIMO (Scientific monitoring concepts for the German Bight) with subproject TP 1.4 (Application of high resolution SAR-data (TerraSar-X) for monitoring of eulittoral surface structures and habitats). In addition, data from the DeMarine-1 and DeMarine-2 projects with the subprojects TP4 (Integration of Optical and SAR Earth Observation Data and in situ Data into Wadden Sea Monitoring) and SAMOWatt (Satellite data for Monitoring in the Wadden Sea) have been included in the investigations.

5.1.2 Materials and Methods

5.1.2.1 Study Site in the Tidal Flats of Norderney (German Wadden Sea)

The study was carried out in the East Frisian Wadden Sea, which forms the western part of the German North Sea coast between the river Ems and the Weser estuary. Towards the open North Sea, the Wadden Sea is bordered by a chain of barrier islands (Figure 5.1-1a). The tidal flats between the island of Norderney and the mainland coast were selected as the main study area. For comparative purposes, surface structures from other parts of the East Frisian Wadden Sea are also included (Figure 5.1-1b).

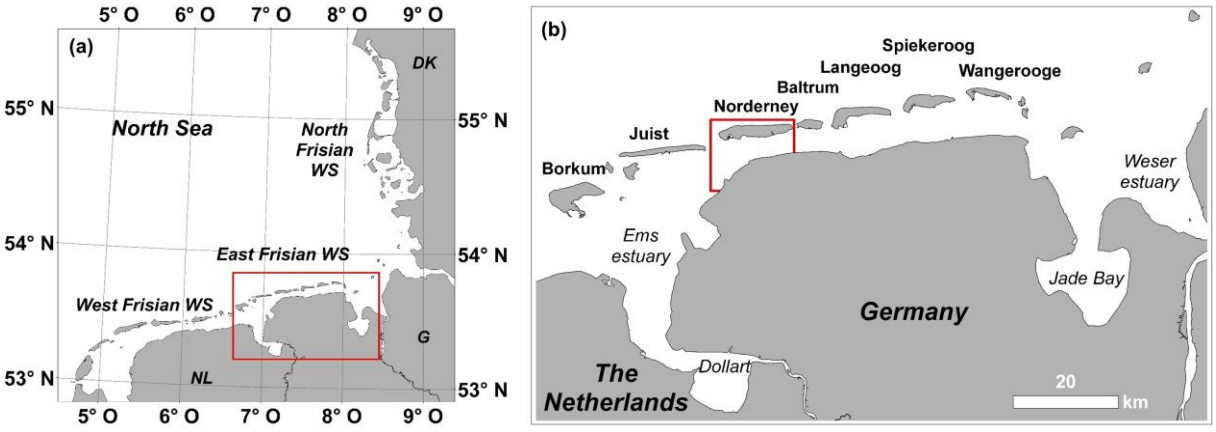

Fig. 5.1-1 The study area in the German Wadden Sea: (**a**) the Trilateral Wadden Sea in the German Bight; (**b**) the main investigation area located at Norderney in the East Frisian Wadden Sea.

The back-barrier tidal basin of Norderney covers the geomorphic structures and habitats which are frequent and characteristic for Wadden Sea flats: mussel beds, fields of shell detritus, seagrass beds, low lying areas collecting residual waters, a drainage system of channels and gullies and the tidal flats varying in sediment composition from the more sheltered muddy regions near the mainland coast and the watershed to the more exposed sandflats close to the Norderney inlet which connects the tidal basin with the open sea. The different sediment types on the tidal flats and in the subtidal significantly

influence the environmental conditions for the organisms living in or on the bottom of the Wadden Sea thus forming habitats with typical species communities. With a mean tidal range of 2.4 m ± 0.7 m [25], the back-barrier tidal basin of Norderney is classified as upper mesotidal according to Ref. [26].

5.1.2.2 TerraSAR-X Data Base

SAR data were acquired by the high-frequency (9.6 GHz) X-band sensor of TerraSAR-X with a wavelength of 3.1 cm, operating at 514 km altitude. The data were collected in Spotlight (SL) and High Resolution Spotlight (HRS) mode, which provide ground range resolutions of 1.5–3.5 m [27], few images were taken in stripmap mode with a resolution of 3 m. Since the SAR data should be combined with extensive in situ data and to perform spatio-temporal analyses, Geocoded Ellipsoid Corrected images (GEC) were chosen which can be easily imported into geographic information systems (GIS). To allow acquisition times close to the time of low tide on the one hand, and to obtain a sufficient amount of data on the other hand, SAR data had to be collected at varying orbits and incidence angles. This enabled us to acquire extensive and detailed time series, as well as recordings before and after events such as storm and storm tide or ice drift. From the resulting set of more than 100 TerraSAR-X images available for the years 2009 to 2016, the SAR data documented in this study are listed in Table 5.1-1. These images were acquired within the time period 1.5 h before and after low tide and apart from the stripmap image recorded in HH-polarization, the data were taken vertically co-polarized (VV).

5.1.2.3 Image Analysis

The TerraSAR-X data were calibrated to “sigma naught” (σ0), the radar reflectivity per unit area in ground range using ERDAS Imagine (version 2013–2016), to correct for geometry of acquisition cf. [28]. For image interpretation and analysis the intensity images were directly imported into the geographic information system (GIS) of ESRI ArcGIS 10.1 where the data was repetitively verified with geospatial in situ data or compared to monitoring results.

According to initial tests, statistical analysis of backscatter differences such as height, mean value, amplitude, or variance seemed not sufficient for the clear demarcation of most intertidal surfaces. Therefore, in this study the images are analyzed via visual interpretation integrating i.a. the patterns of internal structures or textures characterizing the surface structures reflected by TerraSAR-X data as well as contextual data including extensive in situ data or weather and gauge level data (cf. Introduction).

5.1.2.3.1 Visual Image Analysis

The radar backscatter recorded by the SAR sensor can be considered as a measure of the surface roughness, with smoother surfaces rendered dark in the resulting image and rougher surfaces appearing brighter. Characteristic surface properties of the various structures and habitats in the tidal area therefore lead to corresponding patterns and textures in the radar image. A major difference is seen between water-covered areas and exposed areas such as sediment surfaces and biogenic structures. Although the water surface appears highly variable due to currents, wind, and waves—sometimes in interaction with surface active agents such as biofilms—it can be clearly distinguished from the emerged tidal flats, especially if the edges are markedly distinct. Even from gradual transitions, which are also common in tidal areas, visual references to the surface morphology can be obtained. On the flats, residual water trapped in hollow surface structures helps to detect or identify geomorphic surface characteristics from TerraSAR-X images, such as depressed areas, bedforms, or draining systems. Residual water also contributes to the identification of typical large-scale structures and habitats with specific roughness properties such as mussel beds, fields of shell detritus or mud fields. Associated puddles caught in the humpy sediment surface of a mud field or pools within mussel beds are characteristic features reflected by specific patterns of backscatter in the SAR image.

Tab. 5.1-1 TerraSAR-X acquisitions used in this study. Image mode: HRS = High Resolution Spotlight, SL = Spotlight, SM = Stripmap, Inc. = Incidence angle, Orbit direction: A = ascending, D = descending, Δ tLT = Acquisition time related to low tide (*positive values*: acquisition at rising tide), Gauge level related to normal height null (NHN), WS, WD = wind speed, wind direction.

Site	Date	Image Mode	Rel. Orbit	Inc. [°]	Orbit Dir.	Δ tLT [min]	Gauge [cm < NHN]	WS [m/s]	WD [°]
Norderney	21/07/2009	HRS	131	20.8	A	63	111 [2]	3.9 [7]	60
Juist/Borkum	05/04/2011	SM	63	37.4	D	9	136 [1]	10.9 [6]	210
Spiekeroog	17/05/2011	SL	40	37.0	A	14	142 [3]	7.6 [8]	270
Norderney	02/06/2011	HRS	116	45.1	A	11	145 [2]	5.4 [7]	360
Norderney	04/06/2011	SL	139	23.3	D	0	160 [2]	5.5 [7]	60
Norderney	16/07/2011	HRS	116	45.1	A	−18	152 [2]	3.2 [7]	160
Norderney	19/07/2011	SL	154	46.6	D	−82	106 [2]	5.5 [7]	190
Norderney	14/10/2011	SL	139	23.6	D	15	174 [2]	3.2 [7]	130
Norderney	10/01/2012	HRS	139	23.5	D	43	116 [2]	3.6 [7]	270
Wangerooge	19/05/2012	SL	116	47.9	A	50	144 [5]	4.8 [8]	30
Baltrum	07/06/2012	SL	63	35.3	D	−52	144 [2]	3.1 [7]	150
Wangerooge	15/10/2012	HRS	40	38.1	A	−2	142 [4]	6.2 [8]	160
Norderney	30/11/2012	SL	63	36.4	D	21	129 [2]	5.4 [7]	10
Norderney	09/06/2013	HRS	131	21.1	A	−23	144 [2]	6.9 [7]	360
Norderney	28/02/2014	HRS	131	21.1	A	63	67 [2]	3.4 [7]	60
Norderney	14/06/2014	HRS	63	36.1	D	46	132 [2]	9.9 [7]	350
Norderney	11/08/2014	HRS	116	45.1	A	6	111 [2]	8.5 [7]	220
Norderney	07/12/2014	HRS	63	36.1	D	56	102 [2]	7.6 [7]	190
Norderney	19/04/2015	HRS	78	54.3	D	40	166 [2]	2.9 [7]	260
Langeoog	21/06/2016	HRS	78	54.2	D	26	105 [2]	2.5 [7]	310

Water level data (source: Federal Waterways and Shipping Administration WSV, provided by Federal Institute for Hydrology BfG) are from the gauges: [1] Borkum Fischerbalje, [2] Norderney Riffgat, [3] Spiekeroog, [4] Wangerooge West, and [5] Wangerooge East. Wind speed and wind direction (source: German Weather Service DWD) are from the weather stations: [6] Borkum, [7] Norderney, and [8] Spiekeroog.

5.1.2.3.2 Digital Image Analysis

Visual image analysis raised the assumption of bedform movement in the upper flats of the island of Norderney, therefore a spatio-temporal analysis of bedform positions was performed using the extensive time series of satellite images collected during this study. To extract relevant markers from the SAR data, bedform positions were determined by detection of the water-covered troughs according to the method proposed by Ref. [19] which is based on textural analysis combined with an unsupervised classification: For comparison with the complete set of TerraSAR-X data, the images were re-sampled at their highest common resolution, a pixel size of 1.25 m. Speckle reduction was performed by edge-preserving Frost and Median filtering and followed by a textural analysis calculating Gray Level Co-occurrence Matrix (GLCM) statistical parameters (variance, homogeneity, and mean) according to Ref. [29]. From the resulting feature images, the water-covered troughs were derived by means of unsupervised ISODATA classification. Image processing was carried out using ERDAS imagine (2013–2015) and ENVI 4.7 software. The classification output was vectorized and imported into ESRI ArcGIS 10.1 for further analysis. The correct assignment of classes was verified by regularly collected in situ data combined with visual interpretation of the SAR images.

5.1.2.4 Ground Truth, Monitoring and Environmental Data

Visual image interpretation was performed in conjunction with extensive ground truth data. The background of the terrain knowledge comes from a survey carried out as part of the DeMarine-1 project in 2008/2009 [10,30]. In this context, the tidal areas of Norderney were surveyed according to

a comprehensive protocol and photographically documented in a 300 × 300 m grid of stations. In 2014, sections of the grid were revisited for comparison with the 2008/2009 situation. During the current research on the WIMO project, all of the structures described below have been extensively validated by GPS measurements and photo documentation, in part simultaneously with SAR acquisition (cf. Figure 5.1-2). Garmin's GPSmap 62s was used for the GPS measurements, the photos were taken with cameras with GPS functionality. Additionally, the bedforms in the upper flats of Norderney were validated by high-precision height measurements recorded by Real Time Kinematic Differential GPS (RTK-DGPS) with a Leica Differential-GPS SR530 and AT 502 antenna type, see [19,20]. Furthermore, data from the annual mussel monitoring program of the National Park authority in Lower Saxony (NLPV) were used which are obtained by interpretation of aerial photographs. These data are available as shapefiles and indicate the location and areal extent of the intertidal mussel beds of Lower Saxony [31]. Environmental background information included water level data from the gauges at Borkum Fischerbalje, Norderney Riffgat, Spiekeroog, Wangerooge West and Wangerooge East (source: Federal Waterways and Shipping Administration WSV, provided by Federal Institute for Hydrology BfG), as well as wind speed and direction data from the weather stations on Borkum, Norderney and Spiekeroog (source: German Weather Service DWD).

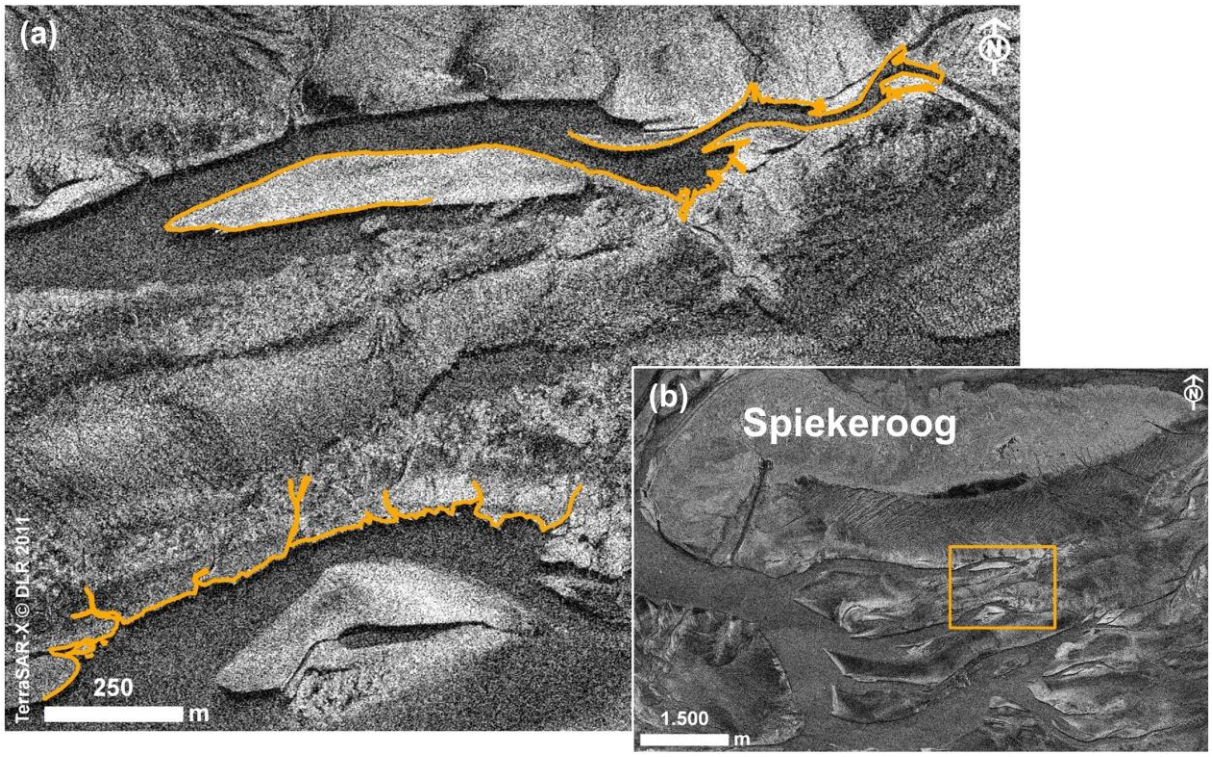

Fig.5.1-2 In situ verification of land-water-lines: (**a**) GPS measurement of channel edges synchronous to satellite overflight at 14 min. after low tide (*yellow line*); (**b**) location of study area (*rectangle*) in the tidal flats of Spiekeroog (SL of 17/05/2011, ascending orbit).

5.1.3 Results

Many characteristic habitats and large-scale surface structures of the tidal flats are clearly reproduced by the TerraSAR-X data. They can be visually identified and analyzed from high-resolution (HRS), spotlight (SL), and, depending on the size of the structure, even in stripmap (SM) images. Figure 5.1-3 gives an overview of the main study area, the tidal flats south of the island of Norderney, reproduced by TerraSAR-X. The added in situ photographs illustrate some of the macrostructures imaged by the SAR sensor. Some of them, such as mussel beds or fields of shell detritus, are usually displayed very clearly due to their outstanding surface roughness and specific textures. Edges also, in particular the

steeper slopes of channels and gullies or the steeply sloping edges of high sandflats, are clearly shown depending on their orientation relative to the sensor.

Other intertidal structures, however, are specifically reproduced due to the contrasting water and sediment surfaces. Most obvious, water level lines delineate the sub-littoral from the tidal area at low tide or flooded areas from exposed flats in the course of the tides. But also residual water caught in troughs and depressions helps to recognize the relief of tidal flat surfaces indicating structures such as intertidal bedforms, depressed areas, or mud fields

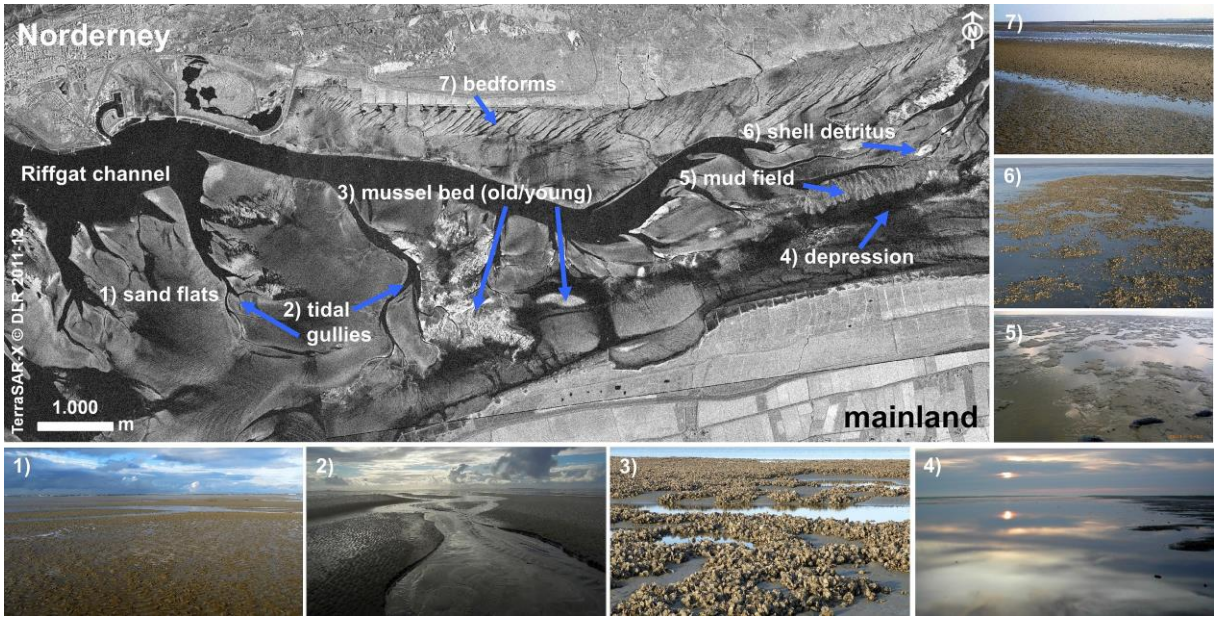

Fig. 5.1-3 Overview of characteristic habitats and large-scale surface structures of the tidal flats south of Norderney, imaged by TerraSAR-X (02/06/2011 and 30/11/2012, *large picture*) and the corresponding in situ photographs (*small pictures*).

5.1.3.1 Tidal Channels and Gullies

Twice a day, in the course of the tides, the tidal flats are flooded and drained through the system of tideways, such as channels and gullies. Depending on their position in this system these tideways are exposed to high flow velocities, which especially in sandy environments, causes regular shifts of the edges and leads to highly dynamic channel courses. These tideways can be identified from TerraSAR-X imagery (Figure 5.1-4) and over time, also the shifting of their courses or their positional stability. Furthermore, characteristic shapes formed by the branches may provide information about the surrounding sediment.

Channels and gullies are mapped in the TerraSAR-X data depending on their width, the shape of the edges and the surface of the water they contain. In case of water-filled channels, the waterline will mark the edge, whereas for smaller and dry-fallen gullies especially the steep edges eaten into the sediment will be reproduced. The intertidal area shown in Figure 5.1-4a exposed to the direct influence of the inlet between the islands of Norderney and Juist open to the North Sea exemplifies morphological development in dynamic tidal areas. TerraSAR-X data from 2009–2012 enables one to observe the shifting of the channel section during that period. Over the entire time, the channel has been relocated by a maximum of over 100 m locally (Figure 5.1-4c). The branching arms, by contrast, have remained largely stable. Part of the channel, north of the first branch in the upper part of the image section, is stabilized by an adjoining mussel bed (indicated by internal structures and high backscatter).

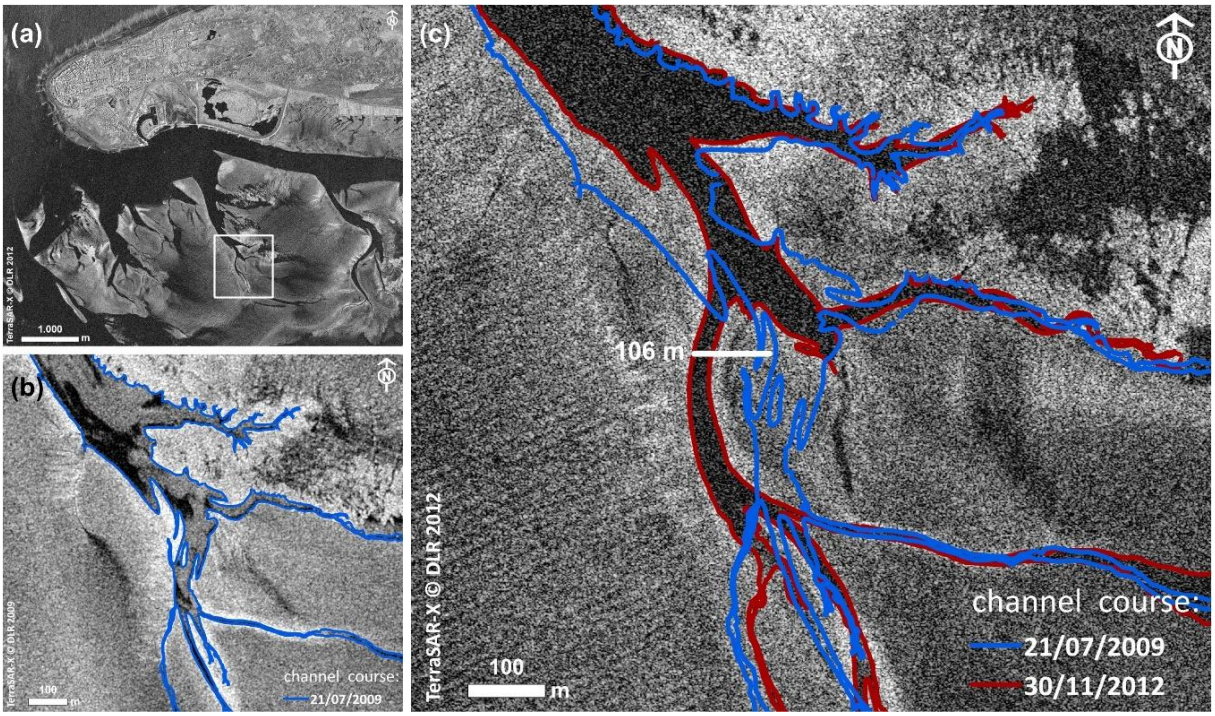

Fig. 5.1-4 Relocation of tidal channels imaged by TerraSAR-X: (**a**) location of study area (*rectangle*) in the tidal flats of Norderney (SL of 30/11/2012); (**b**) channel course in 2009 (HRS of 21/07/2009, 111 cm < NHN, ascending orbit); (**c**) shifted channel course in 2012 (*red lines*) compared to course of 2009 (*blue lines*) (SL of 30/11/2012, 129 cm < NHN, descending orbit).

By means of visual analysis, the channels are clearly visible in the TerraSAR-X data (Figure 5.1-4b,c). However, Figure 5.1-4b also illustrates how automatic channel detection may be difficult due to the varying representation of the water surface and to internal patterns e.g., depending on the presence of surface-active agents, weather, or flow conditions at the time of acquisition.

5.1.3.2 Intertidal Bedforms

5.1.3.2.1 Intertidal Bedforms in the Upper Island Flats of the East Frisian Islands

In large areas of the upper back-barrier tidal flats of the East Frisian islands, the sediment surface forms a pattern of periodic crests and troughs thus creating bedform fields of considerable size. The troughs are covered with water throughout the whole time of emergence, therefore the bedforms are clearly reproduced by TerraSAR-X imagery and they can be detected in the whole set of images (acquired from 2009 to 2016) and in the upper island flat of each of the East Frisian islands. In Figure 5.1-5, an overview of the bedform fields of the East Frisian islands is given, it shows the bedforms directly adjoining the southern island's shores are generally oriented in a north-easterly direction, but especially in the lower flats also cross-profiles can appear. The dimensions and the exact orientations may vary from island to island.

In the study area at Norderney the bedform positions and their dynamics were examined in detail. The photograph (Figure 5.1-6a) gives an impression of their appearance in the field. The bedforms imaged by TerraSAR-X and the vectorized classification result for the water-covered troughs are given in Figure 5.1-6b,c.

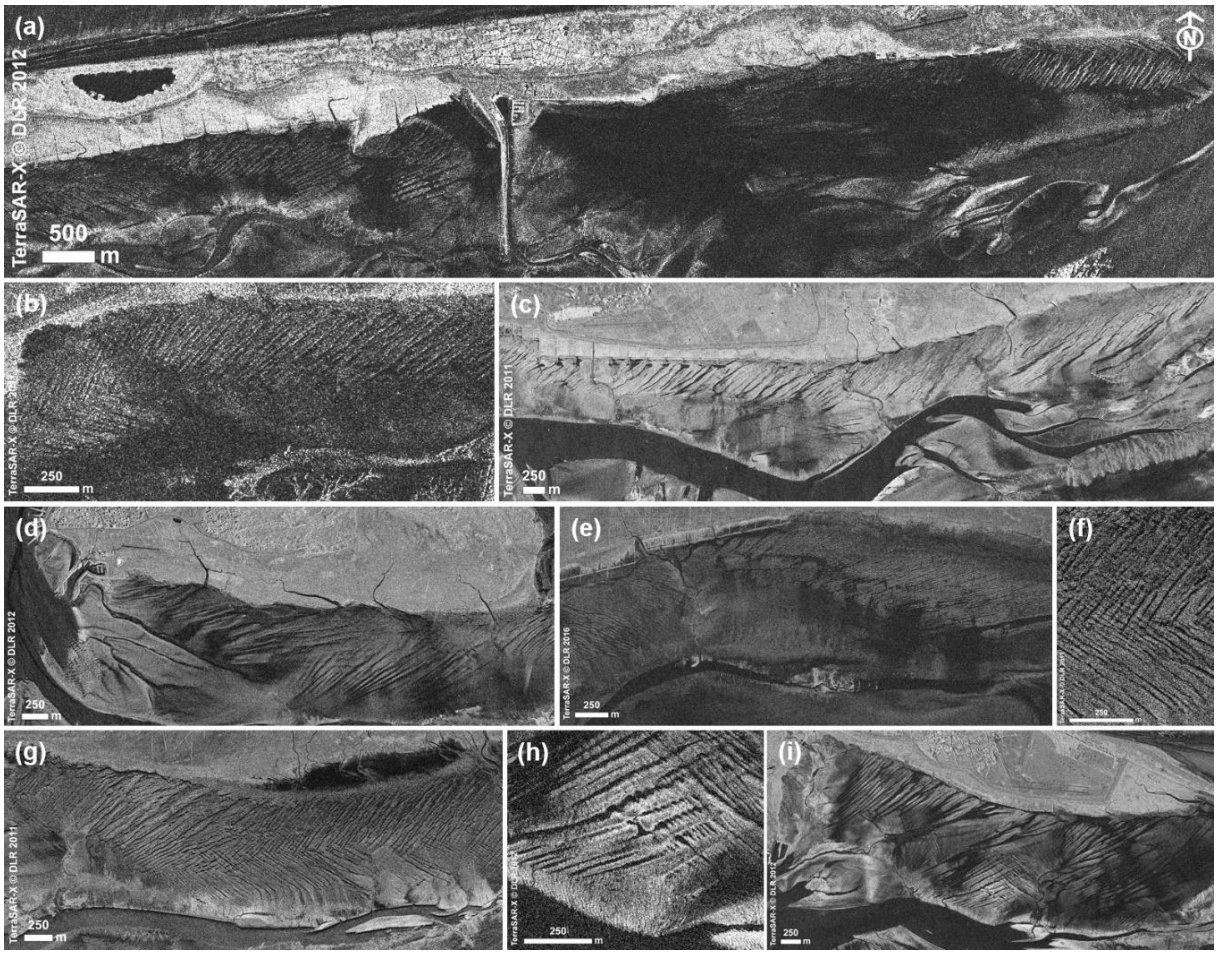

Fig. 5.1-5 Bedforms in the upper flats of the East Frisian islands imaged by TerraSAR-X: (**a**) Juist (SM of 05/04/2011, desc.); (**b**) Borkum (SM of 05/04/2011, desc.); (**c**) Norderney (HRS of 02/06/2011, asc.); (**d**) Baltrum (SL of 07/06/2012, desc.); (**e**) Langeoog (HRS of 21/06/2016, desc.); (**f**) cross-patterns, detail of (**g**); (**g**) Spiekeroog (SL of 17/05/2011, asc.); (**h**) cross-patterns, detail of (**i**);(**i**) Wangerooge (SL of 15/10/2012, asc.). HRS = High resolution Spotlight, SL = Spotlight, SM = Stripmap acquisition mode of TerraSAR-X, asc. = ascending orbit, desc. = descending orbit.

The results of the survey are described in detail by Ref. [19], who demonstrate that visual trough detection as well as results from unsupervised ISODATA classification of textural parameters from TerraSAR-X data are in good accordance with the in situ measurements of the bedforms. Spatio-temporal GIS-analysis of trough positions extracted from a time-series of TerraSAR-X images then revealed a shifting of the bedforms in an easterly direction during the study period from 2009–2015. This general bedform shift is demonstrated for the years 2012–2015 in Figure 5.1-7. The western trough edges are highlighted because in situ measurements as well as TerraSAR-X data reproducing variable states of water-cover indicate an asymmetry of the bedforms leading to steeper western trough edges and smoother eastern edges. Therefore the waterlines of the western edges proved to be a better indicator for the trough positions even with a slightly varying amount of residual water on the exposed flats due to environmental conditions or tidal state.

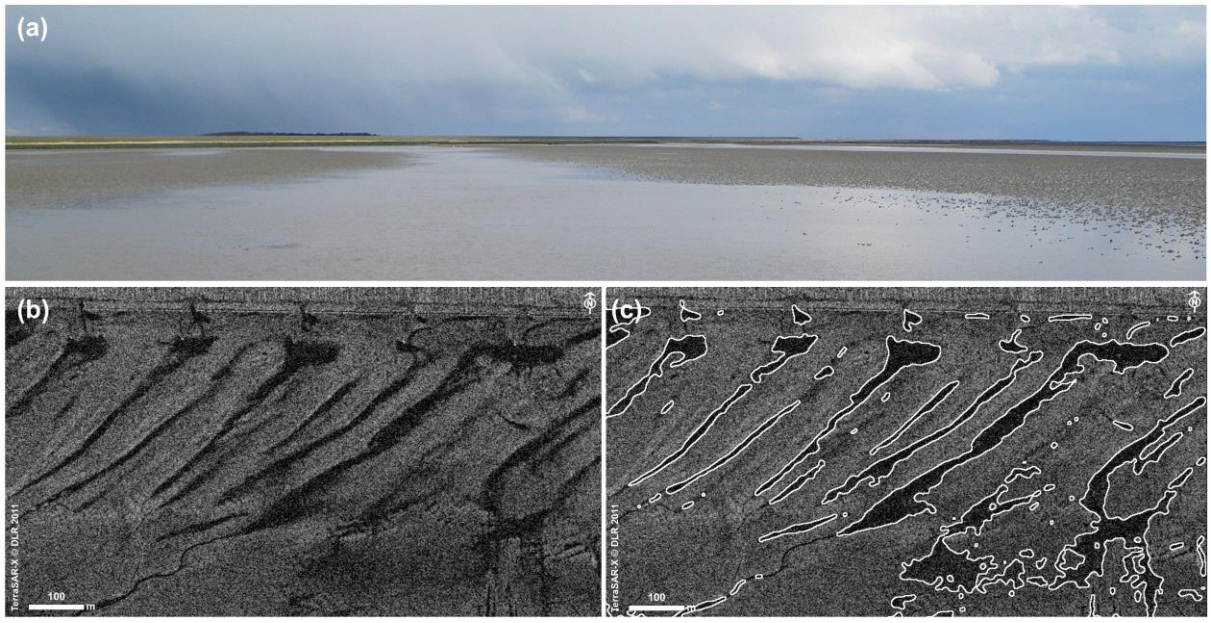

Fig. 5.1-6 Intertidal bedforms at Norderney: (**a**) photography of intertidal bedforms in the test area (26/03/2014); (**b**) image section: test area in the flats of Norderney (HRS of 02/06/2011, asc.); (**c**) Trough extraction result (*white lines*) from the same TerraSAR-X data.

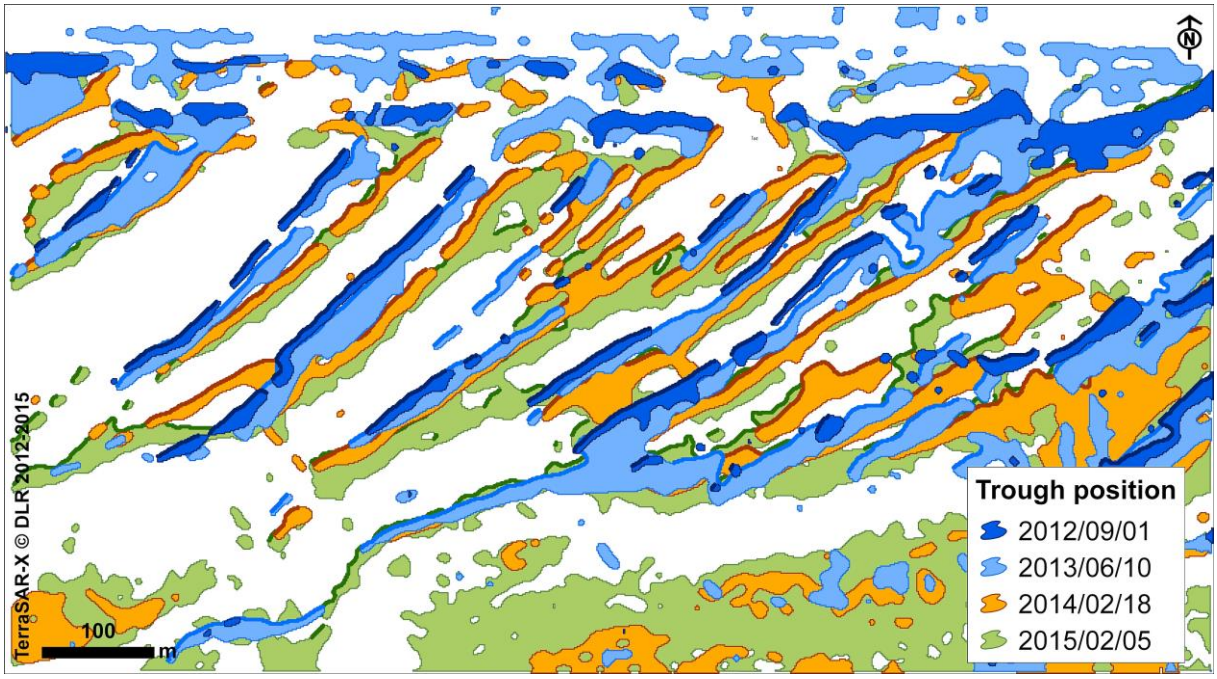

Fig. 5.1-7 Trough positions extracted from TerraSAR-X images of 2012–2015. Western trough edges are highlighted (reprinted by permission from Springer Nature Terms and Conditions for RightsLink Permissions Springer Customer Service Centre GmbH: Springer Nature, Geo-Marine Letters: Monitoring spatiotemporal trends in intertidal bedforms of the German Wadden Sea in 2009–2015 with TerraSAR-X, including links with sediments and benthic macrofauna, Adolph et al. 2016).

The high frequency of TerraSAR-X data acquisition also enabled us to study the bedform positions in the course of the year and in connection with the effects of storm events. Adolph et al. [19] showed that the trough positions extracted from TerraSAR-X data generally remained stable from late winter to late summer and a shift to the east regularly occurred during winter. The change from the summer to the winter situation in 2013 provides a good insight into the shifting forces. In that year, the troughs kept their positions in every TerraSAR-X acquisition from February to August. However, the TerraSAR-X data from mid-December show a clear bedform shift which is most likely the effect of two very heavy gales in late October and early December with maximum wind speeds exceeding 130 and 120 km/h, respectively [19].

5.1.3.2.2 Temporary Surface Structures

Observing the tidal areas by means of TerraSAR-X data, different types of linear structures of the sediment surface were identified. So far, no further investigation of any of these structures has been carried out but similar characteristics were found in TerraSAR-X images of tidal areas throughout the East Frisian Wadden Sea, and also in transition from the tidal to the subtidal areas. In this way, TerraSAR-X imagery opens up new insights into large-scale tidal flat morphology and provides an opportunity to examine its genesis, development, and the significance for the tidal areas.

Southeast of the island of Wangerooge, as an example, in the near-shore area close to the mainland, linear surface structures were detected on a TerraSAR-X image from 2012 and verified in situ. A field of common cockle (*Cerastoderma edule*) apparently stabilized the linear structures and made them both more durable and more conspicuous in the TerraSAR-X data. Additionally, the elevated ridges of the sediment and cockle surface were covered by green algae, which contributed to the clear picture (Figure 5.1-8). In situ observations in 2016 have shown that in the meantime, the cockle field had been occupied by blue mussels (*Mytilus edulis*) and turned into a patchy mussel bed.

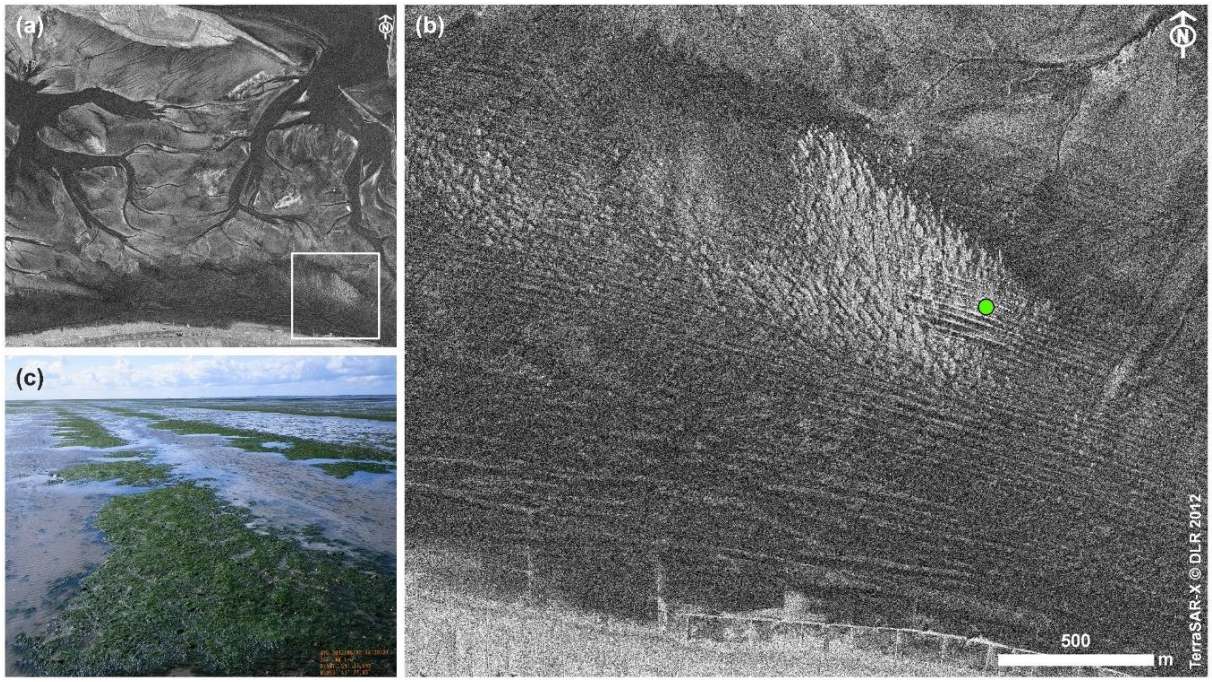

Fig. 5.1-8 Temporary linear surface structures in the tidal area south of Wangerooge: (**a**) Tidal flats between the island of Wangerooge and the mainland coast, rectangle marks image Section b (SL of 19/05/2012, asc.); (**b**) linear surface structures within and in the surroundings of a cockle field (C. *edule*), point marks position of photographer; (**c**) photography of surface structures (02/06/2012).

5.1.3.3 Mud Field

The large mud field close to the watershed of the tidal flats beneath the island of Norderney extends over ca. 1.8 km along the Riffgat channel (see Figure 5.1-9) with a width of 300–400 m. On the wavy to humpy sediment surface, water puddles formed between the muddy humps resulting in a characteristic pattern (see Figure 5.1-9e), leading to a relatively high backscatter in the TerraSAR-X data. In addition, the mud field is traversed by a dense network of highly branched gully structures which drain the water from the adjacent depression in the south of the mud field to the channel in the north. These properties lead to a specific reproduction of the mud field in the TerraSAR-X images characterized by a high backscatter and the recognizable texture of the many gully structures (see Figure 5.1-9b). The contrast with the Riffgat channel and the water covering the area of the depression also facilitate to determine the contours of this mud field. In situ the southern edge of the mud field is clearly marked by the finely branched gullies originating from the water-covered depression. Here, the surface of the muddy deposits stands out from the more solid, smoother sediment surface of the depressed area (see Figure 5.1-9c,d). Therefore, GPS measurements of the mud field's edge carried out in summer 2011 (27/07/2011) show very good agreement with the contours reproduced by the TerraSAR-X acquisition recorded within a short time frame (16/07/2011). In Figure 5.1-9b, the yellow line represents the GPS measurement.

Fig. 5.1-9 Large mud field in the tidal area of Norderney: (**a**) location of the mud field close to the watershed, marked by oval line (HRS of 02/06/2011, asc.); (**b**) GPS measurement of mud field's edge taken on 27/07/2011 (*yellow line*) compared to TerraSAR-X HRS of 16/07/2011, asc.; (**c**) photography along the mud field's edge (27/07/2011); (**d**) gully delta at the mud field's edge (27/07/2011); (**e**) humpy mud field surface with water puddles (27/07/2011).

Seasonal Aspects

In situ studies show variations in the surface form of the mud field. Extent and height of the muddy humps vary as well as their shape, which can be smooth and wavy or in contrast have steep erosive

edges. These variations may occur locally, e.g., the silt surface always tends to be smoother on the edge of the mud field towards the depression. Overall, however, the field surveys showed that the mud field surface was more pronounced during the calmer season of the year (usually the summer) than after the stormy time of winter. When GPS-measuring the mud field's edge in summer 2011 (27/07/2011), the mud deposits clearly stood out from the depressed area covered with water. Thus, the boundary of the mud field was obvious and also well defined by the waterline (see Figure 5.1-9b,c). In the following January (17/01/2012), after two storms had passed through in the first days of the month (03–06/01/2012), a much more gradual transition was observed from the depression to the mud field. While the gully deltas where still in place, the smooth, slightly wavy surface of the silt accumulation began to emerge only gradually from the lower area, just beyond the ends of the gully deltas.

In fact, regarding the mud field over several years (2011–2015) in the TerraSAR-X data, seasonal changes are observed. During summer, the mud field surface is displayed in full width with high backscatter, in winter, however, the area of high backscattering retreats towards the Riffgat channel. The internal gully structures, on the other hand, remain visible throughout the year, across the entire width from channel to depression. This can be seen in Figure 5.1-10a–d showing the reproduction of the mud field in TerraSAR-X acquisitions from summer 2013, the following winter (02/2014) and the next summer (06/14) and winter (12/2014). The formation of similar mud fields between tidal channels or expanded gully deltas and low-lying, often water-covered flat areas (depressions) with a network of gullies connecting both across the mud field, can also be seen in SAR images covering the tidal areas of other East Frisian islands.

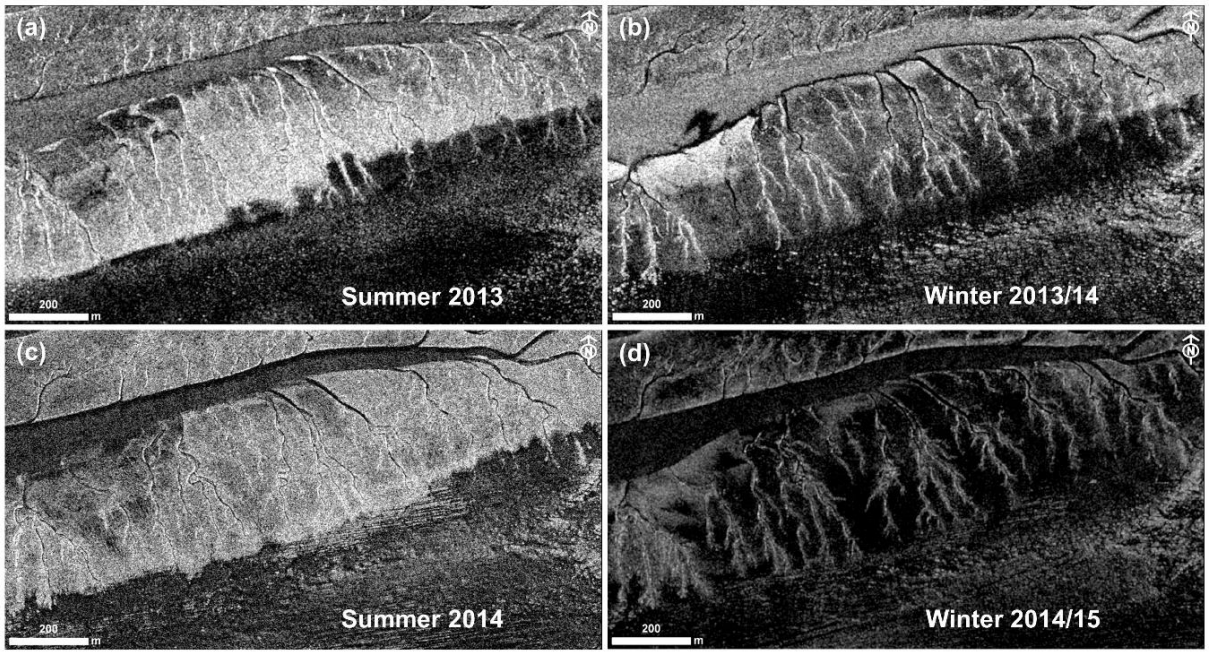

Fig. 5.1-10 Seasonal aspects of the large mud field close to the watershed of the tidal area of Norderney reproduced by TerraSAR-X HRS acquisitions, VV polarised, ©DLR: (**a**) 09/06/2013, orbit 131, asc., 144 cm < NHN; (**b**) 28/02/2014, orbit 131, 67 cm < NHN; (**c**) 14/06/2014, orbit 63, desc., 132 cm < NHN; (**d**) 07/12/2014, orbit 63, 102 cm < NHN.

5.1.3.4 Mussel Beds

Intertidal settlements of blue mussels (*M. edulis*) associated with Pacific oysters (*Crassostrea gigas*) form solid structures sticking out above the sediment surface. These biogenic structures are characterized by a high surface roughness caused by the mussels and by the larger Pacific oysters often

growing upright. They are reflected with high backscatter in the SAR images and the varying forms of appearance in which mussel beds occur in situ are also reproduced by the TerraSAR-X data: Young beds that have settled during an actual spat fall are relatively homogeneously occupied by mussels or by homogeneously distributed smaller patches. Over the years, a typical structure of mature beds develops, in which more or less elevated areas covered by mussels form an irregular pattern with open interspaces. This is reflected in the TerraSAR-X data accordingly, with young beds showing homogenous backscatter, while old mussel beds have characteristic internal structures (Figure 5.1-11a). In most cases the mussel beds reflected by TerraSAR-X are in good agreement with field observations or with the monitoring results currently obtained from aerial photographs. This is exemplified in Figure 5.1-11b, where the yellow line represents the monitoring result from the year of the TerraSAR-X acquisition.

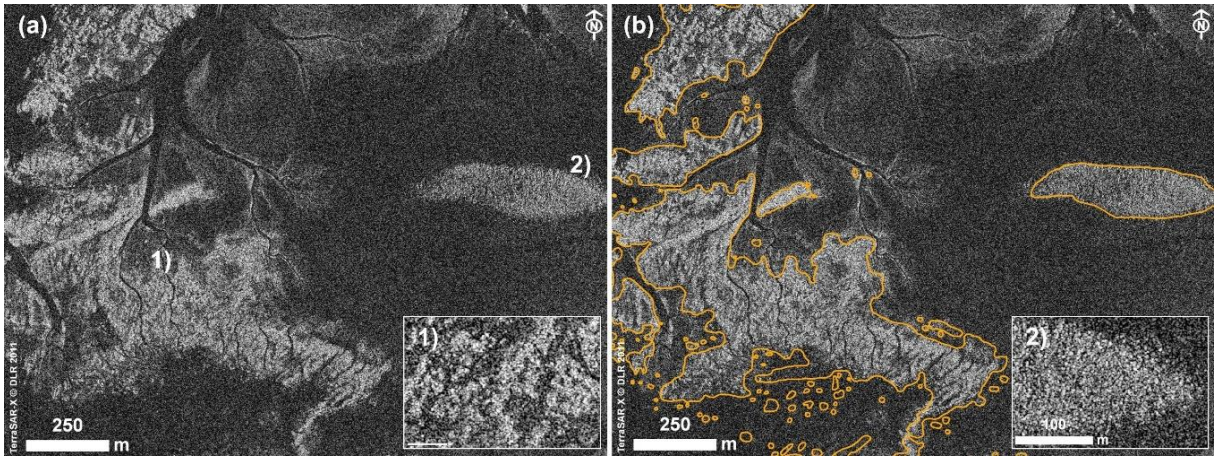

Fig. 5.1-11 Mussel beds in the central area of the tidal flats south of Norderney imaged by TerraSAR-X (SL of 19/07/2011, desc.): (**a**) established old mussel bed (1) and young mussel bed (2); (**b**) *yellow line* represents monitoring result from aerial photography interpretation (2011).

5.1.3.5 Tidal Flat Dynamics Imaged by TerraSAR-X

The tidal area close to the watershed of the Norderney basin between the eastern Riffgat channel and the mainland coast may serve as an example to demonstrate both the stability and the variability of tidal areas and their reproduction in the TerraSAR-X data. A time series of TerraSAR-X images shows the developments taking place in this area from 2009–2015 (Figure 5.1-12). The branches of the Riffgat channel, at the top of the picture, do not change their courses during this period. Likewise, the large mud field (Figure 5.1-12, Region 1) remains as such, only the shape of the southern edge, constituting the boundary to the adjacent depression, changes slightly. The gully structures within the mud field remain essentially the same, even if displacements occur in the course of the smaller branches. Since the TerraSAR-X data were recorded in April to July, the mud field is shown in the aspect of the calmer season in each of the four SAR acquisitions. Compared to 2009, the area increased slightly in 2011, 2014, and 2015.

Most obvious in the SAR data, however, is the development of mussel beds in the low lying area south of the mud field (Figure 5.1-12, Region 2–4): in the field surveys of 2008/2009, this area proved to be a depression with open sediment surface, often water-covered, and in wide areas densely populated by common cockles (*C. edule*) and the polychaete worm sand mason (*Lanice conchilega*). Sand masons build tubes protruding up to a few centimeters above the sediment surface which leads to an increased roughness, particularly when they break through the surface of shallow water covering the flats (Figure 5.1-12a, Region 4, see also photography in Figure 5.1-12a). Just like the shell detritus of cockles (cf.

chap. 3.2), sand masons can serve as a substrate for the settlement of blue mussels. In 2011, the first mussel settlement in this location was reproduced in the TerraSAR-X image (Figure 5.1-12b, Region 4), and in the data from 2014, the mussel bed with its internal structures is already well recognizable as such (Figure 5.1-12c, Region 4, photography in Figure 5.1-12c). The typical pattern of an established mussel bed can be seen here in 2015 (Figure 5.1-12b–d). Southwest of the mud field however, a mussel bed with open structures developed from 2009 to 2011, which in the following years recedes and confines to a few central bed structures in 2014/2015 (Figure 5.1-12, Region 3).

In effect, the area of the extensive depression clearly discernible in 2008–2011, has narrowed until 2015. It has been taken up, in particular, by scattered mussel settlements but also by accumulations of muddy sediment, partly forming temporary linear structures (Figure 5.1-12c,d, Region 2) which are visible at the mud field's edge in 2014 and throughout the area of the formerly water covered depression. These may be due to the unusually turbulent summer season of that year [32,33].

South of the mussel bed in Region 3, higher backscatter is visible especially in the 2014 acquisitions (Figure 5.1-12c). From the field surveys it is known that, in this area, fields of seagrass patches occur. Seagrass itself was not detected in the TerraSAR-X data according to this study, as it lies flat on the sediment at low tide and is characterized mainly by its spectral features. In some cases, though, the seagrass vegetation leads to the formation of elevated surface structures, which are reflected in the SAR data.

In summary, certain habitats and structures such as the mud field, mussel bed, or the water-covered depression are clearly recognizable in the TerraSAR-X data due to typical characteristics and patterns. Intermediate states of developments or vague surface structures, on the other hand, can only be identified through field observations or context knowledge. This applies, for example, to the extensive fields of sand mason, which can be recognized at the appropriate level of residual water due to the disturbance of the smooth water surface, to scattered young mussel settlements and oyster scree scattered by winter storms, or to the surface structures sometimes generated by seagrasses.

For monitoring, often it is sufficient to carry out a correct identification of a structure in situ once, to determine its characteristics and boundaries. Further development can then be monitored via TerraSAR-X data.

5.1.4 Discussion

The results of the present study show the great potential of satellite SAR data to contribute to the monitoring of the tidal Wadden Sea area. Visual image interpretation of TerraSAR-X data combined with extensive in situ data enable the detection and observation of various large-scale surface structures and characteristic habitats. This is to be emphasized as the smooth and dynamic relief of the Wadden Sea, influenced by variable water levels and weather conditions, places great demands on classification methods in general.

5.1.4.1 Geometry of Acquisition

In general, using different geometries of acquisition, different angles of incidence, and ascending and descending orbit directions, we found that the reproduction of surface structures indicated or amplified by the contrast of sediment and water surfaces is relatively insensitive to geometry of acquisition when making use of visual image interpretation. The same holds for habitats with an extensive three-dimensional surface roughness, such as mussel beds, mud fields, and fields of shell detritus which can be visually identified by their specific patterns and textures under the differing geometries we used.

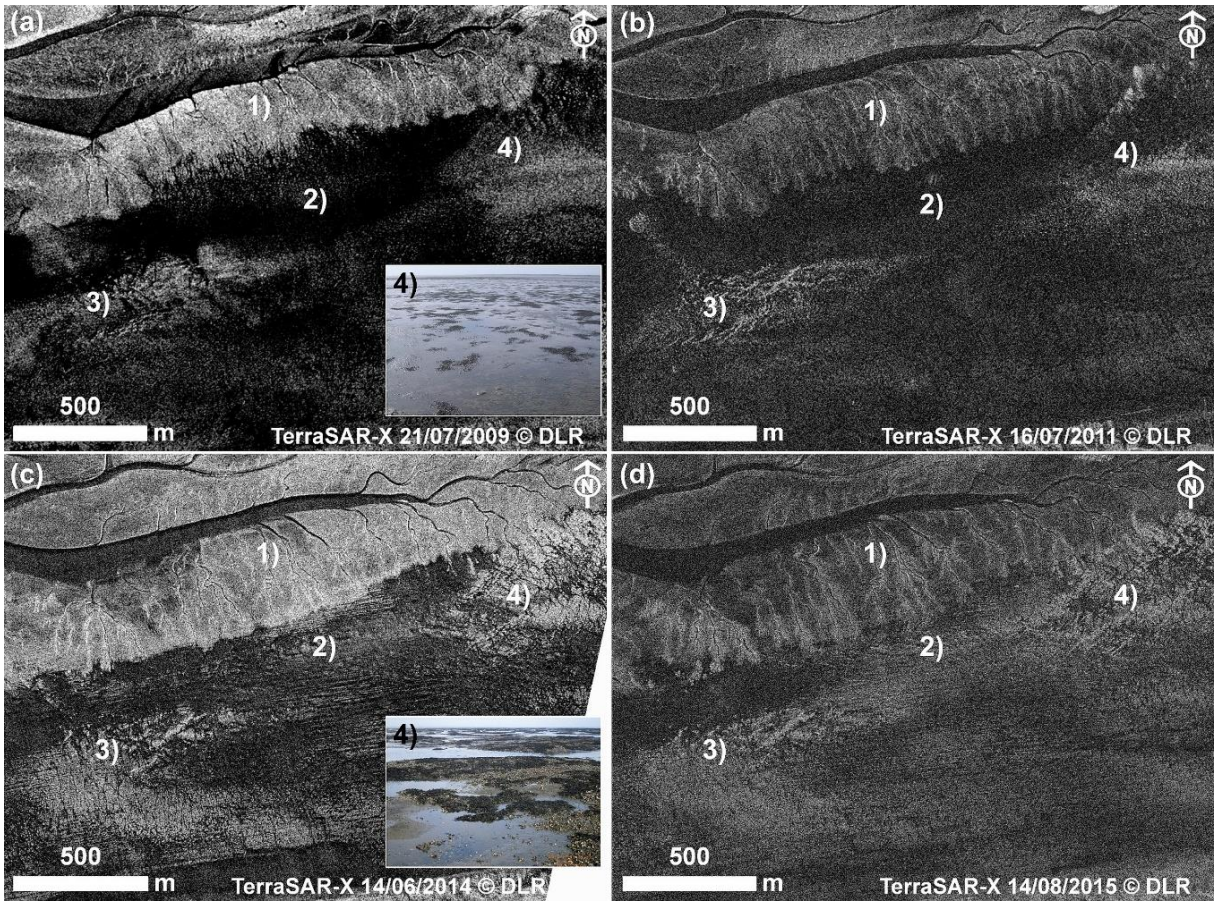

Fig. 5.1-12 Time series 2009–2015 of tidal area imaged by TerraSAR-X, HRS: (**a**) 21/07/2009, asc., 111 cm < NHN and photograph of 14/07/2008; (**b**) 16/07/2011, asc., 152 cm < NHN; (**c**) 14/06/2014, desc., 132 cm < NHN and photograph of 17/10/2014; (**d**) 19/04/2015, desc., 166 cm < NHN. (1) mud flat; (2) depression; (3) area of patchy mussel bed; (4) area of solid mussel bed.

However, we found some variations in the characteristics of the TerraSAR-X images are due to varying incidence angles of the geometry of acquisition. In near range, that is at small incidence angles <24° (relative orbits 131, 139), the images show sharp contrasts and widespread high backscatter. Therefore, strongly scattering structures that are not well demarcated from each other. Mussel beds, humpy mud fields with a dense network of gullies, sediment surfaces roughened by sandworm (*Arenicola marina*) heaps, and steep sandy slopes (depending on exposition in relation to sensor, orbit direction) are displayed similarly brightly which makes the differentiation of these surfaces more difficult. Furthermore, in mussel beds, internal structures are less recognizable. However, when surrounded by smooth surfaces, e.g., smooth water cover, these scatterers stand out sharply. Any roughness of the water surface, on the other hand, is also highlighted and eddies and currents can clearly be seen when biofilms or other surface-active agents are present. As backscatter values of the flooded areas can be quite high, they often exceed those of smooth intertidal surfaces.

With incidence angles of 30–40° (rel. orbits 40, 63), the water surface becomes more uniform and scatters less, the images are less sharp in contrast and more differentiated in the backscatter values. Mussel beds and other structures with high backscatter are better distinguished from each other and from rougher surroundings.

Increasing incidence angles of 40–47° (rel. orbits 116, 154), amplify further differentiation of backscatter intensities. Mussel beds, for example, stand out more clearly from their surroundings,

from other rougher surfaces, or from steep edges with high backscatter, which is also due to the fact that the internal structures are better recognizable. Fine linear structures of the sediment surfaces are clearly visible.

All of this is reinforced with incidence angles above 50° (rel. orbits 25, 78). Mussel beds are clearly recognizable. However, gradual transitions are now displayed very fluently and demarcations are therefore less obvious. Under good environmental conditions, i.e., with well drained flats, fine surface structures are clearly visible (e.g., linear structures).

In summary, for most intertidal surface types acquisitions at incidence angles between 30–47° therefore are most suitable. For specific questions smaller or higher incidences can be useful.

5.1.4.2 Environmental Influences—Water Cover

An essential aspect in the interpretation of SAR images from tidal areas is the varying presence of water. Apart from the tidal cycle, the water regime is influenced by external conditions affecting tidal water level and, to a lesser extent, also residual water remaining on the flats. Therefore, knowledge of weather and environmental conditions at the time of recording or in the time before may be essential for image analysis. Time of exposure, wind speed and direction, as well as spring/neap tides affect the water coverage in the area but they may also influence the roughness of water and sediment surfaces or sediment moisture. Hence, the same area may appear partly different in SAR acquisitions taken at different times. In general, the flats are better drained after low tide compared to the time of falling tide, even at the same gauge level. Such effects should be taken into account as well as knowledge about general processes and phenomena occurring in tidal areas.

As an example, the appearance of tidal channels, creeks, and gullies reproduced in SAR images is heavily dependent on water level as soon as the water reaches the tideway's edges or goes beyond. Therefore, changes in water level due to weather conditions or even wind-drift may have an effect especially on the gently rising slip-off slopes in contrast to the steep edges of the eroding banks, whose positions will not be markedly affected even for larger variations of the water levels. Thus, to observe and compare the courses of channels and gullies, they should on the one hand be imaged close to maximum drained stage, and on the other hand the steep eroding banks should be used as markers. The same applies when determining migration rates for bedforms in the upper island flats, whose slopes have been found to be slightly asymmetrical [19]. Conversely, in the case of multi-temporal acquisitions, the magnitude of changes in the water level lines would indicate the slope inclination.

On the whole, the SAR data used in this study not only image the channel network and drainage system in tidal areas but they also provide a valuable source of insight into surface morphology of tidal flats mapped due to accumulation of residual water on the exposed flats. Such are the distribution of depressed areas indicated by frequent water coverage or troughs marking bedforms of the sediment surface.

5.1.4.3 Visual Analysis and Classification

Overall, the visual approach proved generic enough to provide an overview of most elements structuring the main research area at Norderney by taking into account not only statistical parameters such as backscatter intensity and contrast, but also shapes, sizes, patterns, and textures of surface features reflected by the SAR data, as well as their spatial distribution and surroundings. Especially patterns, texture, and context information proved to have a great significance for the image interpretation. The importance of contextual information—site and time specific—in SAR image interpretation is also emphasized by Ref. [34] who studied the effects of environmental factors and natural processes on radar backscattering in the Korean tidal areas.

Although successful application of TerraSAR-X images is shown, the results also indicate problem zones and variations with the risk of misinterpretation. Areas with no clearly distinctive features or with broad transition zones between habitats may demonstrate the limits of exact demarcation. Mussel beds can exemplify both clearly identifiable areas and problem zones, which will be discussed in the following.

Mussel beds are particularly well recognized by their specific internal structures of beds and interspaces, which also allow a certain understanding of their maturity and compactness. Still, due to variability in the appearance of habitats and structures, misinterpretation can occur, e.g., with shell detritus. Mostly, fields of shell detritus are easy to distinguish from mussel beds, because they lack the characteristic internal structures. However, for young mussel beds or very densely covered areas of mussel beds, internal structures may be similar. In these cases, supplementary in situ data is necessary for correct interpretation of the SAR data. Likewise, steeply sloping edges of high sand flats exposed to the sensor could be mistaken for dense beds of mussels or shell detritus, although these are often recognizable from their location, or from comparison with acquisitions of a different recording geometry. In case of doubt, the structure should be clarified on site. Surfaces that have been identified and verified can then be tracked over time in the SAR data with little effort. Or they can also be identified in other places with this acquired knowledge.

The sole visual analysis of the TerraSAR-X images may also reach its limits when it comes to determining the exact demarcation of surfaces which directly merge into each other with flowing transitions e.g., where mussel beds are directly surrounded by humpy mud flats or fields of shell detritus that extend far beyond the mussel bed and represent their own habitats. In such cases, again, field observations are needed. Preferably, additional distinguishing characteristics are to be found to design a specific classification method, for example, by exploiting the polarized information of the SAR data. Various authors have shown the additional potential of multi-polarization SAR imagery for the detection of bivalve beds, using fully polarimetric e.g., [35,36] or dual-copolarized SAR data [37,38]. Wang et al. [22] discriminated bivalve beds from the surrounding bare sediments through polarimetric decomposition based on dual-copolarized SAR data. Further research is needed to investigate to what extent polarimetric information can be used for the detection of other surface types in the tidal area. Geng et al. [21] identified different surface cover types (i.e., seawater, mud flats, and aquaculture algae farms) through polarimetric decomposition, and Ref [39], and recently Ref [23] pointed to the potential of fully polarimetric interpretation of SAR imagery for classification purposes in tidal areas.

Gade et al. [23] found evidence of mapping characteristics of seagrass beds in SAR data from the Schleswig-Holstein Wadden Sea, whereas in the present study, no general detection of seagrass is proven. In some cases, areas of which seagrass vegetation is known from the field surveys, were characterized by diffusely elevated backscatter values, which may be due to elevated structures of the sediment surface induced by the seagrass cover. Comparative areas vegetated by seagrass, however, could be completely inconspicuous in the SAR data. However, the seagrass stocks in the Lower Saxony Wadden Sea are smaller and of significantly lower density than those in the Schleswig-Holstein Wadden Sea. For these reasons, recognition of seagrass was not pursued in this study. Still, seagrass is a parameter required for Wadden Sea monitoring. For test areas in the Schleswig-Holstein Wadden Sea, Ref. [11] showed that seagrass meadows can be classified based on optical satellite data with a high degree of detail. At present, electro-optical sensors seem to be essential for the detection of seagrass—respectively of vegetated areas—but merging with SAR data could also include surface roughness information. If it is proven that seagrass meadows produce characteristic surface structures reflected by the radar return, this could facilitate their differentiation from green algae or diatoms.

Sediment distribution on tidal flats is another information that would be important for monitoring, but could not be directly obtained from the SAR data by visual interpretation. In some cases indirect detection methods are conceivable, e.g., for mud fields, which are characterized by a humpy surface with puddles and dense gully structures. Also channel network features i.e., the meandering patterns, density and complexity of creeks and gullies and their branches provide, among others, information about the surrounding sediment. The authors of Refs. [40,41], who extracted the geometric information of tidal channels from aerial photography as well as Ref. [42], using electro-optical satellite data (KOMPSAT-2), found lower tidal channel density in areas of higher sand percentage, while complex and dendritic channel patterns were found in mud flat areas. Regarding movement of sediment, Ref. [43] applied the waterline technique to satellite SAR to form a Digital Elevation Model (DEM) of the intertidal zone of Morecambe Bay, U.K. for measurement of long-term morphological change in tidal flat areas. Automated waterline extraction from SAR imagery is used by Ref. [44] for determination of changes in coastal outlines.

The present study shows that visual interpretation of SAR imagery has its own value in support of monitoring and questions of ecological or morphological research in tidal areas. It provides technically unsophisticated access to remote sensing information about characteristic surface structures which can be used by nature protection managers or researches of various disciplines. As a first analysis approach, visual interpretation can also indicate the potential of the satellite SAR data for further investigation and thus may provide pointers for the development of automatable classification methods with regard to monitoring requirements. Currently, Sentinel-1 is providing an increasing base of SAR data available with open and free access which can be screened for monitoring and research for the Wadden Sea.

5.1.4.4 Contribution of Satellite SAR for Future Monitoring of Tidal Flats

The regular recording of position, area, and status of characteristic spatial structures in defined time intervals is an indispensable condition for monitoring tidal flat areas such as the Wadden Sea. Monitoring this area has to integrate differing requirements which cannot be provided by a single sensor system. Therefore, a spatially and temporally differentiated monitoring concept combining the benefits of different sensor classes has to be developed. This study has shown that particularly habitats and geomorphic structures characterized by their surface roughness combined with specific textures and patterns are clearly recognizable in TerraSAR-X acquisitions. Other surface structures are virtually marked by residual water, which is an outstanding advantage of this sensor technology. Because of the high temporal availability, SAR data are also predestined to cover periods between sumptuous in situ campaigns, expensive recordings such as lidar scans, or electro-optical acquisitions dependent on daylight and weather. Thus, continuity in the tracking of dynamic structures can be ensured or new events can be discovered in a timely manner by the SAR sensors.

Another approach to meet the monitoring requirements is to directly fuse data from different sensor systems to leverage their respective benefits concerning areal coverage, spatial and temporal resolution, sensitivity, and geometric accuracy while also taking into account financial aspects. In this regard, the advances in satellite technology and the open data policy for imagery from an increasing number of sensors, such as recently the sentinel satellites from the ESA Copernicus program, has already promoted the development of image classification methods. Against the background of the different sensor properties, the combination of different SAR sensors as well as SAR and optical sensors has been examined to refine the differentiation between scatterers or to obtain high-resolution multispectral images e.g., [45–48]. For tidal areas, e.g., Ref. [49] used information from both space-borne microwave (SAR) and optical/shortwave infrared remote sensing to determine sediment grain-size of tidal flats in the Westerschelde, and Ref. [50] investigated the use of multi-frequency SAR data

for sediment classification and for the detection of bivalve beds. Results from the DeMarine projects [10,11,14] and the WIMO project [15,17,20] have also shown that a combination of high spatial resolution SAR data and specific spectral resolution (specific wavelengths) benefits the classification of intertidal habitats. New algorithms and procedures in the area of neural network deep learning [51,52] may also bring advances in information extraction from satellite data.

So, to develop operational methods that harness satellite-based remote sensing data for Wadden Sea monitoring and meet the requirements of monitoring obligations from national and international legislation, the advantages of various sensor classes and methods of information extraction will have to be combined. Regarding the exponential growth of technology and methods of information extraction, interdisciplinary research as well as collaboration of nature protection managers with experts in electro-optical and SAR remote sensing will be absolutely beneficial.

5.1.5 Conclusions

- High-resolution SAR data as recorded by TerraSAR-X enables identification of essential geomorphic surface structures and habitats of the Wadden Sea ecosystem and their dynamics.
- Independence of SAR sensors from daylight and weather and a high repetition rate (11 days for TerraSAR-X) offer high temporal availability of data and allow to record long-term developments, short-term (e.g., seasonal) developments, and also event effects (e.g., storms, human intervention).
- Even in the spotlight modes providing highest spatial resolution, the footprint of one acquisition covers about the area of a tidal basin. This allows one to determine the status, size, and distribution of the intertidal macrostructures and habitats of a whole sub-unit of the Wadden Sea ecosystem.
- Visual interpretation of TerraSAR-X data combined with context information such as ground truth, monitoring results, or data on environmental conditions, both integrated in a GIS, proved to be a technically unsophisticated access to the information contained in the SAR data. As a first analysis approach, it can also provide basics for the further development of automatable classification methods.
- High-resolution SAR sensors can contribute relevant data for remote sensing the Wadden Sea. For future Wadden Sea monitoring or long-term ecological research, the combination or fusion of appropriate sensor data (e.g., SAR, multi-spectral data) is promising to significantly expand the interpretation options of advanced satellite-borne remote sensing techniques and to develop automated classification methods.
- In this study, the integration of diverse spatial data (such as large-scale remote sensing data and local sampling data) in a GIS has emerged as an essential component assisting the visual analysis. Beyond that, in a broader context, GIS allow to merge classification results and thus to compose a multifarious overall picture (respectively data base) of the Wadden Sea ecosystem which can support the inter-disciplinary analysis of complex relationships and processes.
- The overview of the geomorphic and biogenic structural elements and habitats of the Wadden Sea ecosystem, their spatial arrangement and dynamics, seen from the perspective of satellite remote sensing using both optical and SAR sensors should be used to contribute to a holistic approach to monitor and further explore the eco-morphological evolution of the tidal system of the Wadden Sea and related tidal systems worldwide.

Author Contributions: H.F. and S.L. conceived and designed the basic project, managed the funding acquisition (WIMO) and provided resources. W.A. refined the project, conducted the research and investigation, performed the data collection and analysis and synthesized the data in the GIS. W.A. wrote the paper, which was commented on by H.F. and reviewed by S.L. and M.E. Validation of the data in the field were carried out by W.A. and H.F. M.E. was involved as external mentor and contributed to the financing.

Funding: This research was carried out as part of the project "Scientific Monitoring Concepts for the German Bight" (WIMO) funded by the Lower Saxony Ministry for the Environment, Energy and Climate Change and the Lower Saxony Ministry for Research and Culture (grant numbers VWZN2564., VWZN2869, VWZN2881). The APC was funded by DLR-MF.

Acknowledgments: The Ministries are highly acknowledged for the funding. We thank DLR for providing the TerraSAR-X data via project COA1075. We are grateful to Ursula Marschalk und Achim Roth (DLR) for their support in acquiring data, which had to be in sync with field campaigns, and also to the colleagues from the DLR Forschungsstelle Maritime Sicherheit, Bremen for the workplace, help and fruitful discussions. We also thank the Institute for Advanced Study (HWK) in Delmenhorst, especially Doris Meyerdierks and Verena Backer for the WIMO overall project management and the function of HWK as platform for discussions and workshops. In the WIMO subproject "Remote sensing", the cooperation with the colleagues from the University of Osnabrück (IGF), especially Richard Jung, the University of Hannover (IPI) with Alena Schmidt and the Senckenberg Institute in Wilhelmhaven with Ruggero Capperucci and Alexander Bartholomä gave insights into the possibilities of the different sensory systems and their pro and cons. We thank our colleagues for the good teamwork especially in the joint field campaigns and the many fruitful discussions. Equally we thank our colleagues from the projects DeMarine-1 and DeMarine-2, Martin Gade, Kerstin Stelzer, Gabriele Müller, Kai Eskildsen, and Jörn Kohlus and also the colleagues from the DLR, Andrey Pleskachevsky, Stephan Brusch and Wolfgang Rosenthal for close cooperation over many years. Personal thanks to Gerald Millat und Gregor Scheiffarth from the National Park Administration Lower Saxon Wadden Sea, whose support of our work was of particular importance and who were always willing to discuss or help.

Conflicts of Interest: The authors declare no conflict of interest. The founding sponsors had no role in the design of the study; in the collection, analyses, or interpretation of data; in the writing of the manuscript, and in the decision to publish the results.

5.1.6 References

1. Millat, G. *Entwicklung Eines Methodisch-Inhaltlichen Konzeptes zum Einsatz von Fernerkundungsdaten für ein Umweltmonitoring im Niedersächsischen Wattenmeer.* Schriftenreihe der Nationalparkverwaltung Niedersächsisches Wattenmeer: Wilhelmshaven, Germany, 1996, Volume 1, pp. 1–125.
2. Herlyn, M.; Millat, G. *Wissenschaftliche Begleituntersuchungen zur Aufbauphase des Miesmuschelmanagements im Nationalpark "Niedersächsisches Wattenmeer"*; Abschlussbericht der Niedersächsischen Wattenmeerstiftung; Wilhelmshaven, Germany, 2004 (unpublished data).
3. Herlyn, M. Quantitative assessment of intertidal blue mussel (*Mytilus edulis* L.) stocks: Combined methods of remote sensing, field investigation and sampling. *J. Sea Res.* **2005**, *53*, 243–253, doi:10.1016/j.seares.2004.07.002.
4. Ringot, J.L. Erstellen eines Interpretationsschlüssels und Kartierung der Biotoptypen terrestrischer Bereiche des Nationalparks Niedersächsisches Wattenmeer auf der Basis des CIR-Bildfluges vom 21.08.1991. 1992/1993 (unpublished data).
5. Esselink, P.; Petersen, J.; Arens, S.; Bakker, J.P.; Bunje, J.; Dijkema, K.S.; Hecker, N.; Hellwig, U.; Jensen, A.-V.; Kers, A.S.; et al. Salt Marshes. Thematic Report No. 8. In *Quality Status Report 2009—Wadden Sea Ecosystem 25*; Marencic, H., Vlas, J., Eds.; Common Wadden Sea Secretariat, Trilateral Monitoring and Assessment Group: Wilhelmshaven, Germany, 2009.
6. Petersen, J.; Dassau, O.; Dauck, H.-P.; Janinhoff, N. Applied vegetation mapping of large-scale areas based on high resolution aerial photographs—A combined method of remote sensing, GIS and near comprehensive field verification. *Wadden Sea Ecosyst.* **2010**, *26*, 75–79.

7. Kolbe, K. Erfassung der Seegrasbestände im niedersächsischen Wattenmeer über visuelle Luftbildinterpretation—2008. *Küstengewässer und Ästuare* **2011**, *4*, 1–35.
8. Moreira, A.; Prats-Iraola, P.; Younis, M.; Krieger, G.; Hajnsek, I.; Papathanassiou, K.P. A tutorial on synthetic aperture radar. *IEEE Geosci. Remote Sens. Mag.* **2013**, *1*, 6–43, doi:10.1109/MGRS.2013.2248301.
9. Stelzer, K.; Brockmann, C. Operationalisierung von Fernerkundungsmethoden fürs Wattenmeermonitoring (OFEW). Abschlussbericht, 2007. Available online: http://docplayer.org/7506004-Operationalisierung-von-fernerkundungsmethoden-fuer-das-wattenmeermonitoring-zusammenfassung.html (accessed on 27 April 2018).
10. Stelzer, K.; Geißler, J.; Gade, M.; Eskildsen, K.; Kohlus, J.; Farke, H.; Reimers, H.-C. *DeMarine Umwelt: Operationalisierung Mariner GMES-Dienste in Deutschland. Integration optischer und SAR Erdbeobachtungsdaten für das Wattenmeermonitoring; Jahresbericht 2009–2010,* Bundesamt für Seeschifffahrt und Hydrographie: Hamburg, Germany, 2010, pp. 37–55.
11. Müller, G.; Stelzer, K.; Smollich, S.; Gade, M.; Adolph, W.; Melchionna, S.; Kemme, L.; Geißler, J.; Millat, G.; Reimers, H.-C.; et al. Remotely sensing the German Wadden Sea—A new approach to address national and international environmental legislation. *Environ. Monit. Assess.* ***2016***, *188*, 595, doi:10.1007/s10661-016-5591-x.
12. Winter, C.; Backer, V.; Adolph, W.; Bartholomä, A.; Becker, M.; Behr, D.; Callies, C.;Capperucci, R.; Ehlers, M.; Farke, H.; et al. *WIMO—Wissenschaftliche Monitoringkonzepte für die Deutsche Bucht*; Abschlussbericht; 2016; pp. 1–159, doi:10.2314/GBV:860303926. Available online: http://dx.doi.org/10.2314/gbv:860303926 (accessed on 05 July 2018).
13. Winter, C. Monitoring concepts for an evaluation of marine environmental states in the German Bight. *Geo-Mar. Lett.* **2017**, *37*, 75–78, doi:10.1007/s00367-017-0496-4.
14. Gade, M.; Alpers, W.; Melsheimer, C.; Tanck, G. Classification of sediments on exposed tidal flats in the German Bight using multi-frequency radar data. *Remote Sens. Environ.* **2008**, *112*, 1603–1613, doi:10.1016/j.rse.2007.08.015.
15. Jung, R.; Adolph, W.; Ehlers, M.; Farke, H. A multi-sensor approach for detecting the different land covers of tidal flats in the German Wadden Sea—A case study at Norderney. *Remote Sens. Environ.* **2015**, *170*, 188–202, doi:10.1016/j.rse.2015.09.018.
16. Gade, M. A polarimetric radar view at exposed intertidal flats. In Proceedings of the 2016 IEEE International Geoscience and Remote Sensing Symposium (IGARSS), Beijing, China, 10–15 July 2016.
17. Jung, R. A Multi-Sensor Approach for Land Cover Classification and Monitoring of Tidal Flats in the German Wadden Sea. Ph.D. Dissertation, University of Osnabrueck, Osnabrueck, Germany, December 2015.
18. Wang, W.; Yang, X.; Liu, G.; Zhou, H.; Ma, W.; Yu, Y.; Li, Z. Random Forest Classification of Sediments on Exposed Intertidal Flats Using ALOS-2 Quad-Polarimetric SAR Data. *Int. Arch. Photogramm. Remote Sens. Spat. Inf. Sci.* **2016**, *8*, 1191–1194, doi:10.5194/isprsarchives-XLI-B8-1191-2016.
19. Adolph, W.; Schückel, U.; Son, C.S.; Jung, R.; Bartholomä, A.; Ehlers, M.; Kröncke, I.; Lehner, S.; Farke, H. Monitoring spatiotemporal trends in intertidal bedforms of the German Wadden Sea in 2009–2015 with TerraSAR-X, including links with sediments and benthic macrofauna. *Geo-Mar. Lett.* **2017**, *37*, 79–91, doi:10.1007/s00367-016-0478-y.
20. Adolph, W.; Jung, R.; Schmidt, A.; Ehlers, M.; Heipke, C.; Bartholomä, A.; Farke, H. Integration of TerraSAR-X, RapidEye and airborne lidar for remote sensing of intertidal bedforms on the upper flats of Norderney (German Wadden Sea). *Geo-Mar. Lett.* **2017**, *37*, 193–205, doi:10.1007/s00367-016-0485-z.
21. Geng, X.-M.; Li, X.-M.; Velotto, D.; Chen, K.-S. Study of the polarimetric characteristics of mud flats in an intertidal zone using C- and X-band spaceborne SAR data. *Remote Sens. Environ.* **2016**, *176*, 56–68, doi:10.1016/j.rse.2016.01.009.
22. Wang, W.; Gade, M. A new SAR classification scheme for sediments on intertidal flats based on multi-frequency polarimetric SAR imagery. *Int. Arch. Photogramm. Remote Sens. Spat. Inf. Sci.* **2017**, *XLII-3/W2*, 223–228, doi:10.5194/isprs-archives-XLII-3-W2-223-2017.
23. Gade, M.; Wang, W.; Kemme, L. On the imaging of exposed intertidal flats by single- and dual-co-polarization Synthetic Aperture Radar. *Remote Sens. Environ.* **2018**, *205*, 315–328, doi:10.1016/j.rse.2017.12.004.
24. Albertz, J. *Einführung in die Fernerkundung. Grundlagen der Interpretation von Luft- und Satellitenbildern*, 4th ed.; Wissenschaftliche Buchgesellschaft: Darmstadt, Germany, 2009; ISBN 978-3-534-23150-8.

25. Eitner, V.; Kaiser, R.; Niemeyer, H.D. Nearshore sediment transport processes due to moderate hydrodynamic conditions. In *Geology of Siliciclastic Shelf Seas*; de Batist, M., Jacobs, P., Eds.; Geological Society: London, UK, 1996; pp. 267–288.
26. Hayes, M.O. Barrier islands morphology as a function of tidal and wave regime. In *Barrier Islands*; Leatherman, S.P., Ed.; Academic Press: New York, NY, USA, 1979; pp. 1–28.
27. Fritz, T.; Eineder, M. TerraSAR-X Ground Segment Basic Product Specification Document. Available online: http://sss.terrasar-x.dlr.de/docs/TX-GS-DD-3302.pdf (accessed on 27 April 2018).
28. Airbus Defence & Space. Radiometric Calibration of TerraSAR-X Data. Beta Naught and Sigma Naught Coefficient Calculation. TSXX-ITD-TN-0049-radiometric_calculations_I3.00.doc. Available online: https://dep1doc.gfz-potsdam.de/attachments/download/365/r465_9_tsx-x-itd-tn-0049-radiometric_calculations_i3.00.pdf (accessed on 27 April 2018).
29. Haralick, R.M.; Shanmugam, K.; Dinstein, I. Textural Features for Image Classification. *IEEE Trans. Syst. Man. Cybern.* **1973**, *3*, 610–621.
30. Farke, H. *DeMarine-Umwelt: TP 4—Integration Optischer und SAR Beobachtungsdaten für das Wattenmeermonitoring*; Schlussbericht; 2011, doi:10.2314/GBV:722405367. Available online: http://dx.doi.org/10.2314/gbv: 722405367 (accessed on 05 July 2018).
31. NLPV. Monitoring Data: Aerial Mapping for Annual Mussel Monitoring. Available online: http://www.nationalpark-wattenmeer.de/nds/service/publikationen/1130_muschelwildbänke-von-borkum-bis-cuxhaven-gis-daten (accessed on 26 April 2018).
32. Deutscher Wetterdienst (DWD). Available online: www.dwd.de/DE/presse/pressemitteilungen/DE/2014/20140730_Deutschlandwetter_Juli_2014.html (accessed on 28 April 2018).
33. UnwetterZentrale. Available online: http://www.unwetterzentrale.de/uwz/955.html (accessed on 28 April 2018).
34. Lee, H.; Chae, H.; Cho, S.-J. Radar Backscattering of Intertidal Mudflats Observed by Radarsat-1 SAR Images and Ground-Based Scatterometer Experiments. *IEEE Trans. Geosci. Remote Sens.* **2011**, *49*, 1701–1711, doi:10.1109/TGRS.2010.2084094.
35. Choe, B.-H.; Kim, D.-J.; Hwang, J.-H.; Oh, Y.; Moon, W.M. Detection of oyster habitat in tidal flats using multi-frequency polarimetric SAR data. *Estuar. Coast. Shelf Sci.* **2012**, *97*, 28–37, doi:10.1016/j.ecss.2011.11.007.
36. Cheng, T.-Y.; Yamaguchi, Y.; Chen, K.-S.; Lee, J.-S.; Cui, Y. Sandbank and Oyster Farm Monitoring with Multi-Temporal Polarimetric SAR Data Using Four-Component Scattering Power Decomposition. *IEICE Trans. Commun.* **2013**, *96*, 2573–2579, doi:10.1587/transcom.E96.B.2573.
37. Gade, M.; Melchionna, S.; Kemme, L. Analyses of multi-year synthetic aperture radar imagery of dry-fallen intertidal flats. *Int. Arch. Photogramm. Remote Sens. Spat. Inf. Sci*. **2015**, *XL-7/W3*, 941–947, doi:10.5194/isprsarchives-XL-7-W3-941-2015.
38. Gade, M.; Melchionna, S. Joint use of multiple Synthetic Aperture Radar imagery for the detection of bivalve beds and morphological changes on intertidal flats. *Estuar. Coast. Shelf Sci.* **2016**, *171*, 1–10, doi:10.1016/j.ecss.2016.01.025.
39. Park, S.-E.; Moon, W.M.; Kim, D.-J. Estimation of Surface Roughness Parameter in Intertidal Mudflat Using Airborne Polarimetric SAR Data. *IEEE Trans. Geosci. Remote Sens.* **2009**, *47*, 1022–1031, doi:10.1109/TGRS.2008.2008908.
40. Ryu, J.-H.; Eom, J.A.; Choi, J.-K. Application of airborne remote sensing to the surface sediment classification in a tidal flat. In Proceedings of the IGARSS 2010: 2010 IEEE International Geoscience and Remote Sensing Symposium, Honolulu, HI, USA, 25–30 July 2010; pp. 942–945, doi:10.1109/IGARSS.2010.5653413.
41. Eom, J.A.; Choi, J.-K.; Ryu, J.-H.; Woo, H.J.; Won, J.-S.; Jang, S. Tidal channel distribution in relation to surface sedimentary facies based on remotely sensed data. *Geosci. J.* **2012**, *16*, 127–137, doi:10.1007/s12303-012-0015-6.
42. Choi, J.-K.; Eom, J.A.; Ryu, J.-H. Spatial relationships between surface sedimentary facies distribution and topography using remotely sensed data: Example from the Ganghwa tidal flat, Korea. *Mar. Geol.* **2011**, *280*, 205–211, doi:10.1016/j.margeo.2010.10.022.
43. Mason, D.C.; Scott, T.R.; Dance, S.L. Remote sensing of intertidal morphological change in Morecambe Bay, U.K., between 1991 and 2007. *Estuar. Coast. Shelf Sci.* **2010**, *87*, 487–496, doi:10.1016/j.ecss.2010.01.015.

44. Wiehle, S.; Lehner, S.; Pleskachevsky, A. Waterline detection and monitoring in the German Wadden Sea using high resolution satellite-based Radar measurements. *Int. Arch. Photogramm. Remote Sens. Spat. Inf. Sci*. **2015**, *XL-7/W3*, 1029–1033, doi:10.5194/isprsarchives-XL-7-W3-1029-2015.
45. Klonus, S.; Rosso, P.; Ehlers, M. Image Fusion of High Resolution TerraSAR-X and Multispectral Electro-Optical Data for Improved Spatial Resolution. In *Remote Sensing—New Challenges of High Resolution*; Jürgens, C., Ed.; EARsel Joint Workshop: Bochum, Germany, 2008; pp. 249–264, ISBN 978-3-925143-79-3.
46. Klonus, S.; Ehlers, M. Additional Benefit of Image Fusion Method from Combined High Resolution TerraSAR-X and Multispectral SPOT Data for Classification. In Proceedings of the 29th Annual EARSeL Symposium, Chania, Kreta, 15–18 June 2009.
47. Rosso, P.H.; Michel, U.; Civco, D.L.; Ehlers, M.; Klonus, S. Interpretability of TerraSAR-X fused data. In Proceedings of the SPIE Europe Remote Sensing, Berlin, Germany, 31 August 2009, doi:10.1117/12.830528.
48. Metz, A.; Schmitt, A.; Esch, T.; Reinartz, P.; Klonus, S.; Ehlers, M. Synergetic use of TerraSAR-X and Radarsat-2 time series data for identification and characterization of grassland types—A case study in Southern Bavaria, Germany. In Proceedings of the 2012 IEEE International Geoscience and Remote Sensing Symposium, IGARSS, Munich, Germany, 22–27 July 2012; pp. 3560–3563, doi:10.1109/IGARSS.2012.6350649.
49. Van der Wal, D.; Herman, P.M.J. Regression-based synergy of optical, shortwave infrared and microwave remote sensing for monitoring the grain-size of intertidal sediments. *Remote Sens. Environ.* **2007**, *111*, 89–106, doi:10.1016/j.rse.2007.03.019.
50. Gade, M.; Melchionna, S.; Stelzer, K.; Kohlus, J. Multi-frequency SAR data help improving the monitoring of intertidal flats on the German North Sea coast. *Estuar. Coast. Shelf Sci.* **2014**, *140*, 32–42, doi:10.1016/j.ecss.2014.01.007.
51. Luus, F.P.S.; Salmon, B.P.; van den Bergh, F.; Maharaj, B.T.J. Multiview Deep Learning for Land-Use Classification. *IEEE Geosci. Remote Sens. Lett.* **2015**, *12*, 2448–2452, doi:10.1109/LGRS.2015.2483680.
52. Cheng, G.; Yang, C.; Yao, X.; Guo, L.; Han, J. When Deep Learning Meets Metric Learning: Remote Sensing Image Scene Classification via Learning Discriminative CNNs. *IEEE Trans. Geosci. Remote Sens.* **2018**, *99*, 2811–2821, doi:10.1109/TGRS.2017.2783902.

5.2 Monitoring Spatiotemporal Trends in Intertidal Bedforms of the German Wadden Sea in 2009–2015 with TerraSAR-X, Including Links with Sediments and Benthic Macrofauna

Adolph, W.; Schückel, U.; Son, C.S.; Jung, R.; Bartholomä, A.; Ehlers, M.; Kröncke, I.; Lehner, S.; Farke, H. (2017). *Geo-Mar. Lett.* 37 (2), 79–91. DOI: 10.1007/s00367-016-0478-y.

Abstract

Satellite synthetic aperture radar (SAR) holds a high potential for remote sensing in intertidal areas. Geomorphic structures of the sediment surface generating patterns of water cover contrasting with exposed sediment surfaces can clearly be detected. This study explores intertidal bedforms on the upper flats bordering the island of Norderney in the German Wadden Sea using TerraSAR-X imagery from 2009 to 2015. Such bedforms are common in the Wadden Sea, forming crests alternating with water-covered troughs oriented in a north-easterly direction. In the western Norderney area, the crest-to-crest distance ranges from 50–130 m, and bedform length can reach 500 m. Maximum height differences between crests and troughs are 20 cm. A simple method is developed to extract the water-covered troughs from TerraSAR-X images for spatiotemporal analysis of bedform positions in a GIS. It is earmarked by unsupervised ISODATA classification of textural parameters, contrasting with various algorithm-based methods pursued in earlier studies of waterline detection. The high-frequency TerraSAR-X data reveal novel evidence of a bedform shift in an easterly direction during the study period. Height profiles measured with RTK-DGPS along defined transects support the findings from TerraSAR-X data. First investigations to characterise sediments and macrofauna show that benthic macrofauna community structure differs significantly between crests and troughs, comprising mainly fine sands. Evidently, bedform formation has implications for benthic faunal diversity in back-barrier settings of the Wadden Sea. SAR remote sensing provides pivotal data on bedform dynamics.

5.2.1 Introduction

Understanding the dynamics of geomorphic structures generated by waves and currents in many intertidal areas such as the Wadden Sea (southern North Sea) still is a challenge of importance for science to comprehend basic processes of coastal development and also for authorities responsible for coastal management. For the Wadden Sea, the outstanding qualities of the continuous and largely unbroken geomorphic processes forming this characteristic landscape have been an important criterion for inclusion in the UNESCO World Heritage List (CWSS 2008). Monitoring the dynamics of intertidal geomorphic macrostructures requires large-scale surveys in relatively short time intervals. This is made possible by a new class of high-resolution synthetic aperture radar (SAR) sensors introduced since 2007 by the launch of TerraSAR-X, followed by TanDEM-X (X-band), the COSMO-SkyMed satellite constellation (X-band) and Radarsat-2 (C-band).These SAR satellites provide images with resolutions in the scale of meters independent from daylight and cloud cover (Moreira et al. 2013), which considerably raises the feasibility of data acquisition during low tide.

Different approaches of waterline detection from SAR data have been developed and applied to tidal flat areas in several regions worldwide with the aim to generate topographic maps and digital elevation models (DEMs) of the intertidal zone and to monitor the longer-term evolution of tidal flats and tidal inlets. For instance, Mason and Davenport (1996) developed a semiautomatic method for coastline detection using a multi-scale approach, and Dellepiane et al. (2004) proposed to exploit coherence measures of interferometric SAR couples. For the detection of waterlines in SAR images of the German

Bight in the south-eastern North Sea, Niedermeier et al. (2005) and Heygster et al. (2010) proposed wavelet-based algorithms which they applied to map tidal flats of the large estuaries of the Elbe and Eider rivers, and of an area of 50×100 km along the North Sea coast of Schleswig-Holstein and Lower Saxony. The same method was used by Li et al. (2014) to generate annual topographic maps analysing SAR images collected in1996-1999 and 2006-2009 for the northern German Wadden Sea. These maps enabled an assessment of changes on these tidal flats and sandbanks. More recently, Wiehle and Lehner (2015) presented an algorithm combining edge detection, brightness thresholding and a previously determined coarse landmask applied to TerraSAR-X acquisitions covering the flats between the island of Trischen and the mainland near Friedrichskoog at low tide, and the surroundings of the island of Pellworm at high tide. The objective of all these studies was to use SAR data to detect the edges delimiting the contours of the exposed flats from the surrounding tidal waters. In contrast, the residual water remaining on the flats during low tide has not been investigated so far (cf. review of SAR applications by Lehner and Tings 2015).

In fact, residual water demarcates even shallow features of the sediment surface such as depressions, puddles and bedforms in SAR data. Thereby, it can provide insight into water drainage systems or further the understanding of morphodynamic processes. For instance, satellite SAR was used by Kim et al. (2011) to detect puddles related to groundwater discharge on tidal flats of the Korean Peninsula. Areas with higher abundances of puddles could be distinguished from areas with lower abundances due to darker backscattering in SAR images over the tidal flats.

The present study aims at the detection of residual water cover on tidal flats based on the recognition of the outlines of water-filled depressions. The methods developed to date for waterline detection (cf. above) combine extensive processing steps to cover complete SAR images and larger coastal areas. These are required to accommodate varying contrasts between tidal flats and land and sea surfaces induced by a wide range of environmental factors such as wind, currents, swell and surface types. In contrast, this study investigates surface structures indicated by residual water, which is less influenced by wind and unaffected by swell and currents in a defined area. It pursues an approach of easy applicability based on unsupervised ISODATA classification of a few textural parameters of the SAR image after edge-preserving speckle filtering. In this way, a quick overview of the subject of interest is available for spatiotemporal assessment in a GIS. The focus is on intertidal bedforms associated with water cover on the back-barrier tidal flats of the East Frisian island of Norderney in the German Wadden Sea sector (Fig. 5.2-1). In large areas of the upper island flats of this as well as neighbouring islands, the sediment surface forms a pattern of periodic crests and troughs oblique to the southern shoreline of each island. The bedforms are generally oriented in a north-easterly direction, whereas the exact dimensions and orientations may vary from island to island. Because of their permanently water-covered troughs, these bedforms should be clearly reproduced by TerraSAR-X imagery.

Bedforms of various scales are common in sandy and shallow marine environments, and have been related to the effects of currents and waves (e.g. Dalrymple et al. 1978; Allen 1980; Zarillo 1982; Ashley 1990; Davies and Flemming 1991; Ernstsen et al. 2005; Whitmeyer and FitzGerald 2008; Gómez et al. 2010) interacting with grain size (McCave 1971; Dalrymple et al. 1978; Zarillo 1982; Bartholdy et al. 2002; Ernstsen et al. 2005; Buijsman and Ridderinkhof 2008), water depth (Allen 1980; Zarillo 1982) and sediment supply (Hoekstra et al. 2004). In addition, Whitmeyer and FitzGerald (2008) and Diesing et al. (2006) emphasise the effects of episodic high-energy events on bedform morphology and dynamics. Interdependencies with benthic biota have been shown for the sublittoral by Baptist et al. (2006) and Markert et al. (2015). Both studies report significant differences in benthic assemblages related to shoreface-connected ridges offshore the East Frisian island of Spiekeroog and off The

Netherlands, and to sand waves on the Dutch continental shelf. Borsje et al. (2009) modelled the influence of biota on the occurrence and dimensions of sand waves and sandbanks off the Dutch coast.

The classification and terminology of bedforms are still being discussed controversially and various terms are currently being used, such as megaripples, sand waves and subaqueous dunes. In this paper, the sedimentary surface structures of the intertidal East Frisian island flats are described as “bedforms” to avoid any process-related ascriptions. To date, there has been no systematic investigation of these bedforms, although they have been documented on aerial photographs as well as in situ for decades (cf. Fig. 5.2-1c). These records include the current yearly aerial photographic survey of the National Park Authority (NLPV), and aerial images of the Norderney flats from 1936–1938 (Reichsluftbilder, Federal Archives, Koblenz). For the North Frisian Wadden Sea sector, Dolch and Reise (2010) describe similar “large sandy bedforms” in the intertidal zone of the island of Sylt (Fig. 5.2-1), based on high-resolution aerial photographs from 1936 to 2006. Complementing studies from sublittoral areas, they found interdependencies with benthic biota as the migration of these bedforms interfered with seagrass beds and the resettlement of mussel beds.

Although the bedform fields cover considerable areas of the upper flats adjoining each of the East Frisian islands, the forces driving their generation and dynamics have not been investigated yet, nor the implications for the sedimentology and biology of the region. Within this context, the aim of this study is (1) to develop a down-to-earth method for the detection and recording of bedforms in back-barrier tidal flats from TerraSAR-X images and (2) to apply this method to monitor bedform spatiotemporal development on the Norderney island flats based on a high availability of TerraSAR-X acquisitions spanning the years 2009 to 2015. Thereby, the seasonality of bedform dynamics and effects of storm events are evaluated. In addition, preliminary assessments of interrelationships with sediments and benthic macrofaunal communities are reported based on random sampling in 2013 and 2014.

Satellite remote sensing techniques are increasingly becoming relevant for monitoring in coastal areas. The present study forms part of the German scientific project WIMO carried out by an interdisciplinary research consortium addressing various European and German regulations to assess the state of the marine environment in the German Bight (for overviews, see Winter et al. 2014; Winter et al., Introduction article for this special issue). A companion study by Adolph et al. (2016, this special issue) compares the bedform imaging qualities of TerraSAR-X, Rapid Eye and lidar data.

5.2.2 Study site

Norderney is one of the barrier islands of the East Frisian Wadden Sea bordering the northwest coast of Germany (southern North Sea; Fig. 5.2-1a). The back-barrier tidal basin has a mean tidal range of 2.4±0.7 m (Eitner et al. 1996) and is classified as high mesotidal according to Hayes (1979). Hydrodynamic conditions in the tidal inlet and offshore Norderney have been reported by Niemeyer (1987, 1994).

Figure 5.2-1b shows Norderney with the adjoining island flats imaged by TerraSAR-X on 20 April 2011. Large bedforms are clearly visible and most pronounced in the western and eastern parts of the island flats, interspersed with smaller surface structures. On the lower island flats, cross-patterns may arise temporarily (not shown). The bedform area is about 200–500 m wide. In the west, it directly borders on groynes and, in the east, on salt marshes. In the north towards the island, larger troughs are often connected to pools formed beneath the heads of spur dikes, or to salt marsh drainage gullies. Towards the southern fringe of the bedform field, the troughs either conjoin into shallow gullies leading to the Riffgat channel, or they end blind or mouth into depressions. For the present study, a test area of 1,000×600 m was chosen in the western sector of the bedform field (cf. white rectangle in Fig. 5.2-1b).

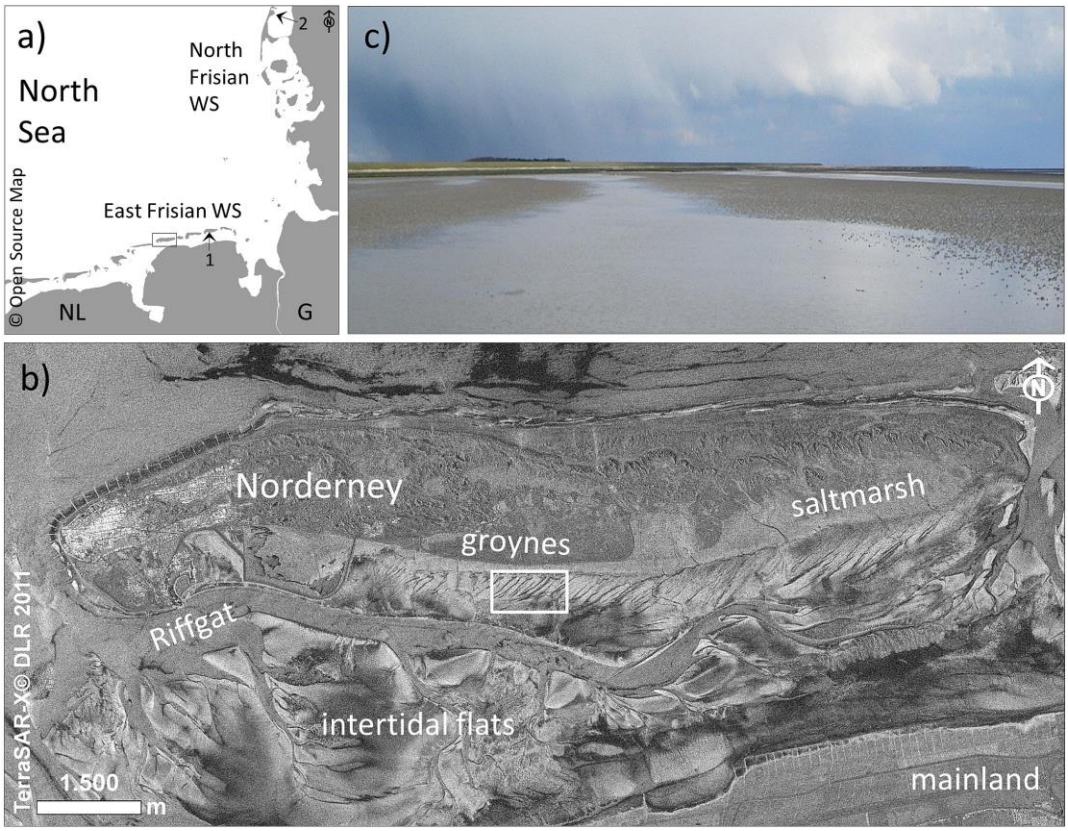

Fig. 5.2-1 Study site on the upper tidal flats of the island of Norderney (German Wadden Sea sector, southern North Sea): a regional locality map with the islands of Norderney (*rectangle*), Spiekeroog (*1*) and List/Sylt (*2*); b Norderney imaged by TerraSAR-X on 20/04/2011 (Stripmap mode) and test area (*rectangle*); c photograph of intertidal bedforms (26/03/2014)

5.2.3 Materials and methods

The positions of the bedforms were derived from TerraSAR-X data by detection of residual water cover in the troughs between the ridges of exposed sediment. Extensive field surveys showed that, although the bedforms are located on the highest island flats, the troughs remain filled with water throughout the duration of exposure. Thus, the pattern of bedforms is clearly perceptible in the satellite data due to the imaging characteristics of the SAR sensor.

A comprehensive set of TerraSAR-X data was acquired each year in the period 2009–2015, except for 2010 (see Table 5.2-A1 in the electronic supplementary material available online for this article). Results of trough detection were validated by high-precision, synchronous in situ measurements (cf. below). Environmental background information included water level data from the Riffgat gauge at Norderney (source: Federal Waterways and Shipping Administration WSV, provided by Federal Institute for Hydrology BFG), as well as wind speed and direction data from the weather station on Norderney (source: German Weather Service DWD).

5.2.3.1 Bedform detection from TerraSAR-X

TerraSAR-X data were acquired in Spotlight (SL) and High Resolution Spotlight (HS) mode providing ground range resolutions of 1.5–3.5 m (Fritz and Eineder 2010). Aiming at spatiotemporal analysis and combination with geospatial ground-truth data, Geocoded Ellipsoid Corrected intensity images (GEC) were mapped onto the Universal Transverse Mercator coordinate system (UTM) and then directly imported into the geographic information system (GIS) of ESRI ArcGIS.

Intertidal features are best imaged at maximum drained stage, which is after low tide shortly before the next inundation. Therefore, most images were acquired shortly before or up to 2 h after low tide, corresponding to satellite data collected at varying orbits and incidence angles. Additional acquisition dates were chosen in 2011 to depict different phases of the tidal cycle in order to investigate a possible correlation between tidal water level and trough width. In all, 50 TerraSAR-X images were available for the years 2009 to 2015; some were discarded because of unfavourable water levels, wind conditions or poor contrast. To correct for acquisition geometry, the selected images (cf. ESM Table 5.2-A1 in the electronic supplementary material) were pre-processed by calibration to normalised radar cross section "Sigma Naught" (σ^0) as described by Airbus Defence & Space (2014). The images were then re-sampled at a pixel size of 1.25 m, their highest common resolution.

Sigma Naught denotes the radar backscatter recorded by the SAR sensor and can be regarded as a measure of surface roughness: the smoother the surface, the less energy is returned to the radar sensor and the darker the area is represented in the resulting image. In this manner, a smooth and undisturbed water surface can be detected easily due to specular reflection, with weak or no return leading to a low intensity of related pixels (i.e. dark pixels). Wind and currents make this a seldom case in coastal areas but, irrespective of how variable the appearance of the water surface may be, the differences in surface roughness between tidal flat and water surface allow the detection of water-covered areas in most images.

The method developed here to extract the water-covered troughs from TerraSAR-X images is based on textural analysis sensitive to the contrasts in surface roughness, combined with an unsupervised classification. The latter was chosen because it clusters the pixels of a satellite image based purely based on statistics. Not utilizing any user-defined training classes or set thresholds, this method proved to be fairly insensitive to the wind-induced variability of the water surfaces and the changing states of the tidal flats due to for example e.g. lugworm activity. The correct assignment of classes was verified by regularly acquired in situ data combined with visual interpretation of the SAR images.

For speckle reduction, two edge-preserving filtering methods were employed by combining adaptive Frost filtering, window size 9×9 and one pixel distance (Frost et al. 1982; Shi and Fung 1994) with twofold median filtering of window size 5×5 and one pixel distance (Pratt 2007). Subsequently, a textural analysis was performed calculating Gray Level Co-occurrence Matrix (GLCM) statistical parameters after Haralick et al. (1973) and testing the corresponding feature images for their relevance to distinguish water cover from tidal-flat surfaces. The combination of variance, homogeneity and mean feature images proved to be the most suitable in this study. Therefore, these were added to a three-band layer stack serving as input to an unsupervised ISODATA classification (Tou and Gonzalez 1974) to derive the class "water-covered". For further analysis, the classification output was vectorised and imported into ESRI ArcGIS. Image processing was by means of ERDAS Imagine (2013–2015) and ENVI 4.7 software.

5.2.3.2 In situ bedform measurements

In situ verification of bedforms was by means of high-precision DGPS (differential global positioning system) recordings of positions, sediment surface height and waterline positions along transects crossing the bedforms perpendicularly. The measurements were taken with a real time kinematic differential GPS (RTK-DGPS) of type "Leica Differential-GPS SR530", with antennae type "AT 502 antennae". Reference data were provided by the Satellite Positioning Service of German land surveying (SAPOS®), using High Precision Real-Time Positioning Service with a horizontal accuracy of 1–2 cm and vertical accuracy of 2–3 cm (SAPOS®-HEPS) for measurements in 2013 and 2014 (17 May 2013, 6 February 2014, 13 June 2014), and Geodetic Post-processing Positioning Service with a horizontal

accuracy of at least 1 cm and vertical accuracy of 1–2 cm (SAPOS®-GPPS) for measurements on 15 February 2015.

For RTK-DGPS measurements, two fixed transects crossing the bedforms in the higher and lower parts of the island flats were marked with metal poles in February 2014 (Fig. 5.2-2), and point measurements were carried out at intervals of 2 m. Transect D6–D5 had a length of 240 m spanning the crests and troughs of a three-bedform series. Transect D13–D12 (length of 100 m) crossed one bedform trough. A longer data series spanning 3 years is available for transect D13–D12, comprising measurements of February 2014, February 2015 and also May 2013, the latter with a coarser interval of 10 m.

High-precision positioning of the trough borders was carried out on 14 June 2014 synchronously to the overflight of TerraSAR-X. The outline of the totally water-covered area was defined as the trough border; at the time of satellite data acquisition, it was marked with a pole and then measured with RTK-DGPS.

5.2.3.3 Sediment sampling

Box-cores (30 cm in depth) and surface sediment samples (upper ca. 1–2 cm) were collected in the bedform area in 2013 (March, May and June) and 2014 (February), combined with concurrent surface sampling in adjoining bedform-free areas (Fig. 5.2-2). Epoxy peels were made of the box-cores after drainage for several weeks in cold storage. Textural parameters of surface samples (mean grain size, sorting, mud content, i.e. dry wt% <63 µm fraction) were assessed by means of a high-resolution settling tube and Sedigraph 5100 particle analyser based on standard laboratory procedures (cf. Brezina 1986; Flemming and Ziegler 1995). Sedimentological terms used in this paper follow standard definitions: for grain size, phi (φ) is equivalent to –log2d where d is the grain diameter in mm; "mud" indicates sediments finer than 4 phi (62.5 µm); "sorting" is the degree of variance in grain size.

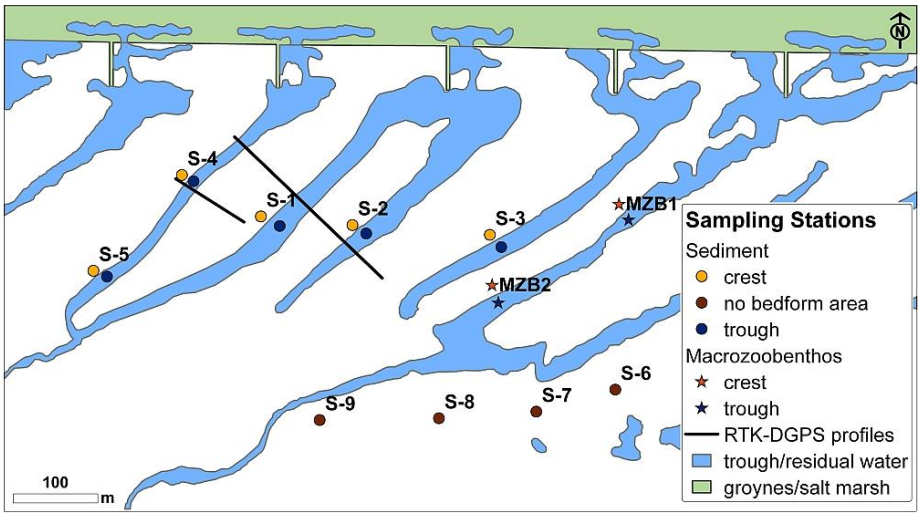

Fig. 5.2-2 Locations of RTK transects (*upper* D6–D5, *lower* D13–D12) as well as sediment and macro-zoobenthos sampling stations in relation to bedform morphology on the back-barrier tidal flats of Norderney

5.2.3.4 Macrofauna sampling and statistical analysis

For characterisation of macrofauna community structure, samples were taken in March 2013 in the upper (MZB1) and lower (MZB2) parts of the bedform area (see Fig. 5.2-2), in each case comprising a crest and a trough station with seven replicate box-cores (100 cm^2) per station. After sieving through a 1 mm mesh, the fauna were fixed with 4% buffered formaldehyde, stained with Bengal rose, identified to species level whenever possible, counted, weighed and then preserved in 70% alcohol.

Differences in species composition and community structure among and between crest and trough areas were assessed by means of multivariate analyses of species abundance per replicate at each station. Distances among replicates were calculated based on the Bray-Curtis dissimilarity index, a

measure recommended for clustering or ordination of species abundance data (Legendre and Gallagher 2001). Results were visualized by using non-metric multi-dimensional scaling (NMDS). Pair-wise analyses of variance among and between crest and trough areas were performed to examine whether differences in macrofauna community structure were significant. Groups were compared by means of the adonis-function, incorporating a permutation test (999 permutations) with F statistic. Discriminating species among and between crest and trough areas were calculated by the Similarity Percentages routine based on Bray-Curtis dissimilarities. The R package vegan (Oksanen et al. 2016) served for all calculations. For further information, the readers are referred to Anderson (2001).

Densities of the lugworm *Arenicola marina* were recorded by counting the casts within a 25×25 cm frame at 10 replicate sites per station. Numbers were compared with paired t-tests using R (R Core Team 2015).

5.2.4 Results

5.2.4.1 Bedform characteristics

Trough detection from TerraSAR-X data is in good accordance with the in situ survey of the bedforms. The height-profile data measured by RTK-DGPS confirm the surface structures responsible for the water cover leading to reproduction of the troughs as dark areas in the SAR images (Fig. 5.2-3 and 5.2-4). Trough extraction results also correspond with in situ measurements of the waterlines (Fig. 5.2-4).

In the test area on the western upper flat of Norderney (cf. white rectangle in Fig. 5.2-1b), the main bedforms occur at intervals of 50–130 m; smaller troughs can develop in between at intervals of 15–30 m. At maximum drainage stage, the water-covered troughs have a width of 7–15 m. The bedform area extends over 350 m from the island's groynes down to a lower flat area with formation of gullies draining into the main channel. Bedforms reach maximum lengths of 400–500 m; smaller troughs may end blind, or bend and join a larger one over shorter distances. The height difference from crest to trough as measured by RTK-DGPS is 13–20 cm for the main bedforms, and 5–10 cm for the smaller bedforms (cf. Fig. 5.2-3).

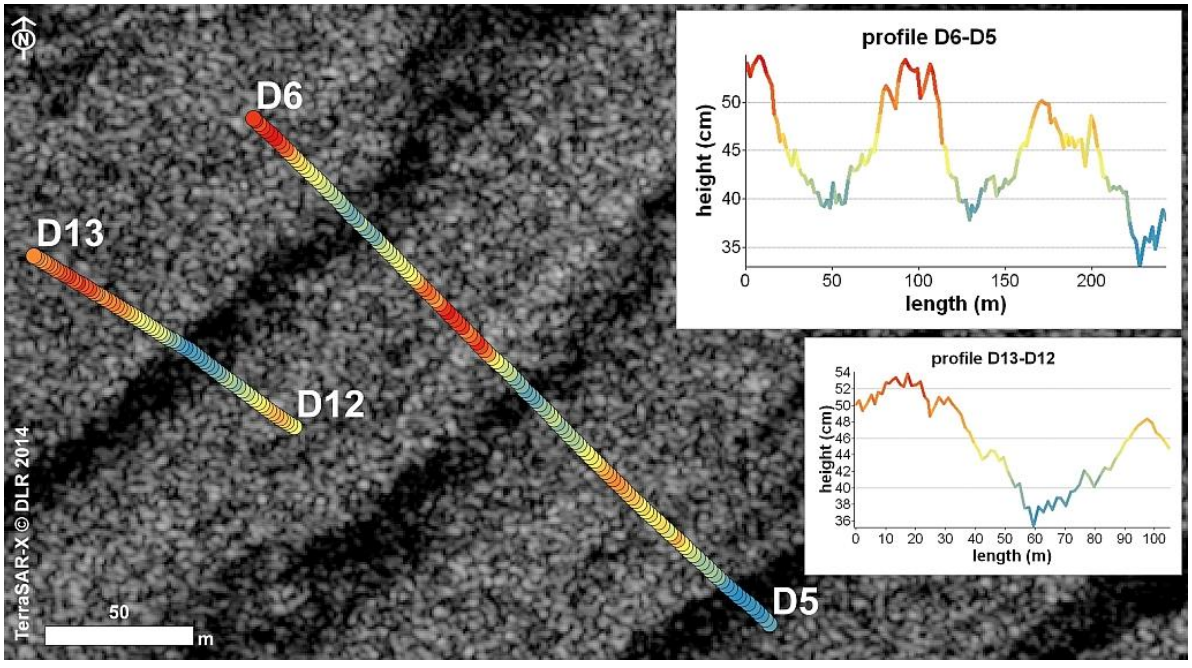

Fig. 5.2-3 Height profiles of transects D6–D5 and D13–D12 measured by RTK-DGPS (cm above normal height null, NHN) on 13/06/2014, and background TerraSAR-X image of 14/06/ 2014

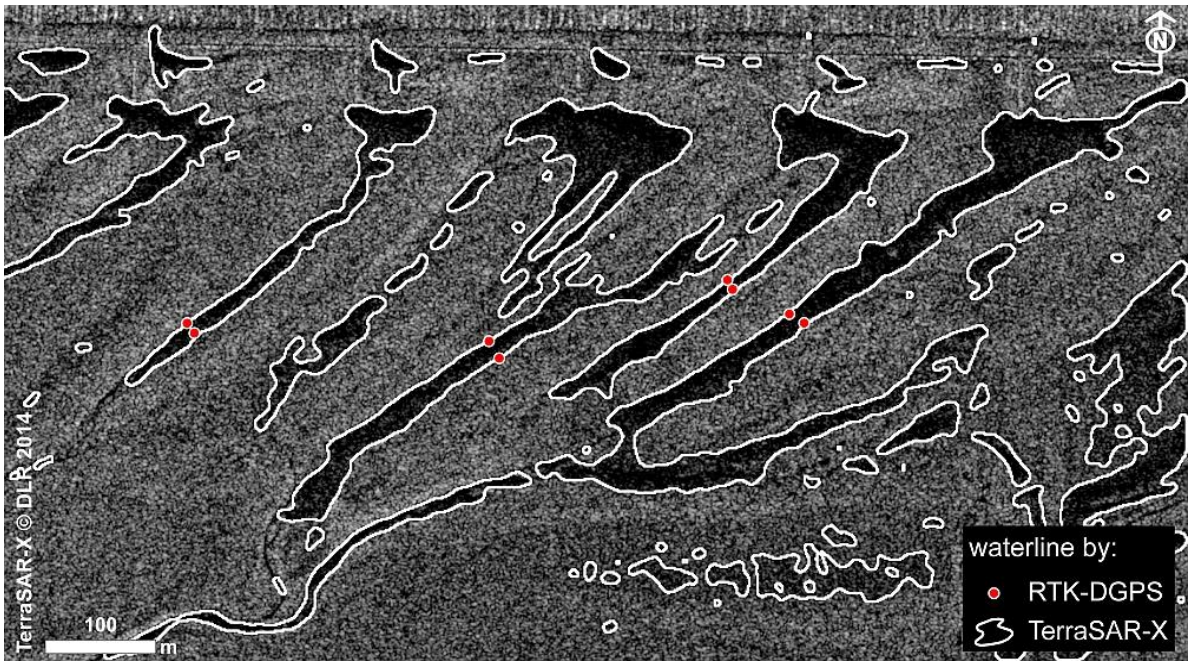

Fig. 5.2-4 Trough extraction (*white lines*) from TerraSAR-X data (*background*) and waterlines marked with RTK-DGPS (*red dots*) during synchronous overflight on 14/06/2014

Maximum variation of trough widths during time of exposure was examined in a set of 11 TerraSAR-X images taken at different tidal stages from April to November 2011 (90 minutes before to 178 minutes after low tide; see ESM Table 5.1-A1 in the online electronic supplementary material). Mean trough widths along four cross-sections of different troughs are 9.2±3.3, 6.7±2.4, 7.6±2.3 and 7.7±2.2 m. The comparison of trough widths with Riffgat gauge levels ranging from 174 cm below normal height null (NHN) to 37 cm above NHN (ESM Table 5.2-A1, source: WSV, provided by BFG) at the time of each acquisition indicates no clear relation (Fig. 5.2-5a). If at all, the time to or from low water influences the trough width: in Fig. 5.2-5a, a cluster of highest trough widths relates to image acquisitions from 1 h before to shortly after low water, although the corresponding gauge levels are the lowest in the sample. After low water the gauge level is rising, but overall the trough widths are lower than before low tide, especially if the outliers are disregarded. This is explained by the fact that, with the duration of exposure, the water has more time to drain off the flats and troughs. Also, no relation of trough width and wind velocity or wind direction (source: DWD, hourly means) could be found by direct comparison, nor by plotting the trough widths with the wind components up-trough, down-trough and cross-trough (Fig. 5.2-5b, c).

To examine the variability of trough edges during the time of exposure, field investigations were carried out at the edges of 100% water-covered troughs. In all, 17 troughs measured during four tidal cycles in 2014/2015 persistently show a clearly less pronounced waterline regression on their west side: maximum values of waterline regression measured over a period of 5 h are 8 m, and 12 m at the eastern trough edges. The corresponding edges receded by only 1.60 m and 0.40 m respectively over the same time interval. In 14 measurements over periods of up to 3 h, average waterline shifts of up to 2.40 m at the eastern edges and up to 0.8 m at the western edges were observed. This illustrates the steeper inclinations at the western sides of the troughs, consistent with RTK measurements (Fig. 5.2-3; also see Adolph et al. 2016, this special issue).

5.2.4.2 Bedform dynamics

Bedform dynamics are reported in Figs. 5.2-6 to 5.2-9. From late winter to late summer, the trough positions extracted from TerraSAR-X data generally remain stable. This is exemplified in Fig. 5.2-7 for the year 2013 when the trough positions were stable from February to August, despite slightly differing levels of residual water cover. In contrast, the TerraSAR-X image from 17 December 2013 shows an eastward shift of most bedforms (Fig. 5.2-8), explained by the impact of the heavy gales "Christian" and "Xaver" with maximum wind speeds exceeding 130 and 120 km/h in late October and early December respectively (Deutscher Wetterdienst, DWD 2013a, 2013b). These bedform positions of December 2013 persisted throughout the year 2014.

Further analysis of TerraSAR-X images indicates that this stable pattern during much of the year and a shift to the east during winter recur regularly. The resulting general bedform shift is documented by TerraSAR-X images from 2009 to 2015 (cf. TerraSAR-X acquisition dates in ESM Table 5.2-A1 in the electronic supplementary material) and is demonstrated for the years 2012–2015 in Fig. 5.2-9. The data also show that the shift of the troughs is strongest in the upper part of the bedform area. Here, the trough positions of February 2015 have reached the position of the former eastward neighbouring trough of 2009. The western edge of the westernmost trough crossed by the D6–D5 transect thus shifted by 57.3 m along the profile perpendicular to the bedform. About 150 m to the south, the offset is 47.4 m.

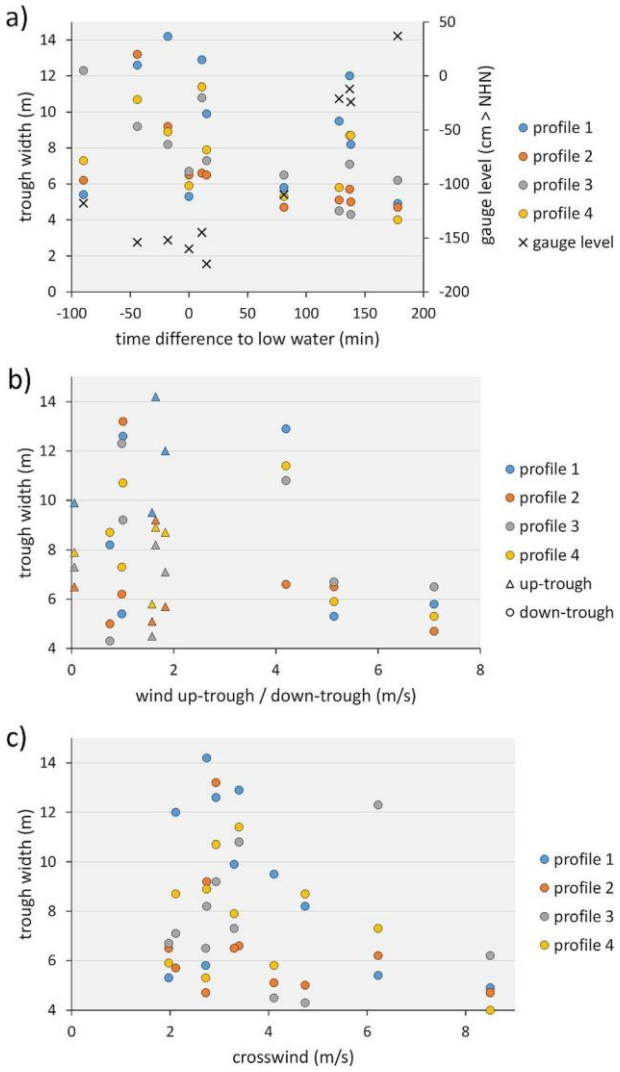

Fig. 5.2-5 Width of water-covered troughs measured along four profiles based on TerraSAR-X images of 2011 at different stages of the tidal cycle versus **a** Riffgat gauge level (© WSV), **b** up-trough and down-trough wind components and **c** cross wind components based on wind speed and direction (both © DWD)

The magnitude of the bedform shifts can vary from year to year. Regarding the time span 2012–2015 depicted in Fig. 5.2-9, the large shift from 2013 to 2014 (orange to green) is striking, presumably reflecting the effect of the heavy gales of October and December 2013 (see above). In contrast, only a small relocation is detected from 2014 to 2015. Height profiles gained from RTK-GPS measurements in 2013, 2014 and 2015 confirm the eastward shift of the troughs as well as the larger shift from 2013 to 2014 (Fig. 5.2-6).

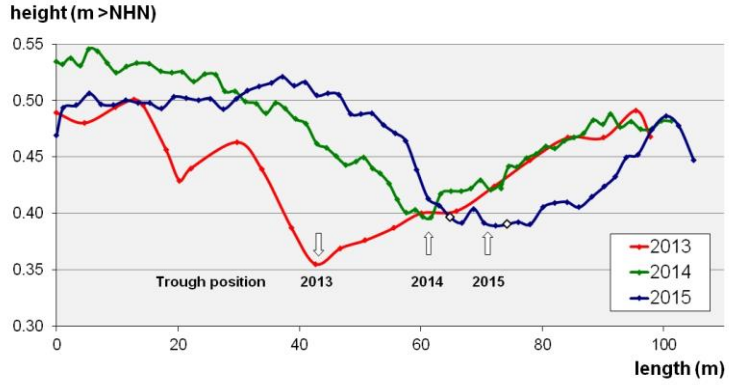

Fig. 5.2-6 RTK-DGPS height profiles (m above normal height null, NHN) crossing a trough along transect D13–D12 (cf. Fig. 5.2-3) in spring 2013 (17th May), winter 2014 (6th February) and winter 2015 (15th February). *White dots:* Trough edges measured by RTK-GPS in 2015. *White arrows:* Troughs

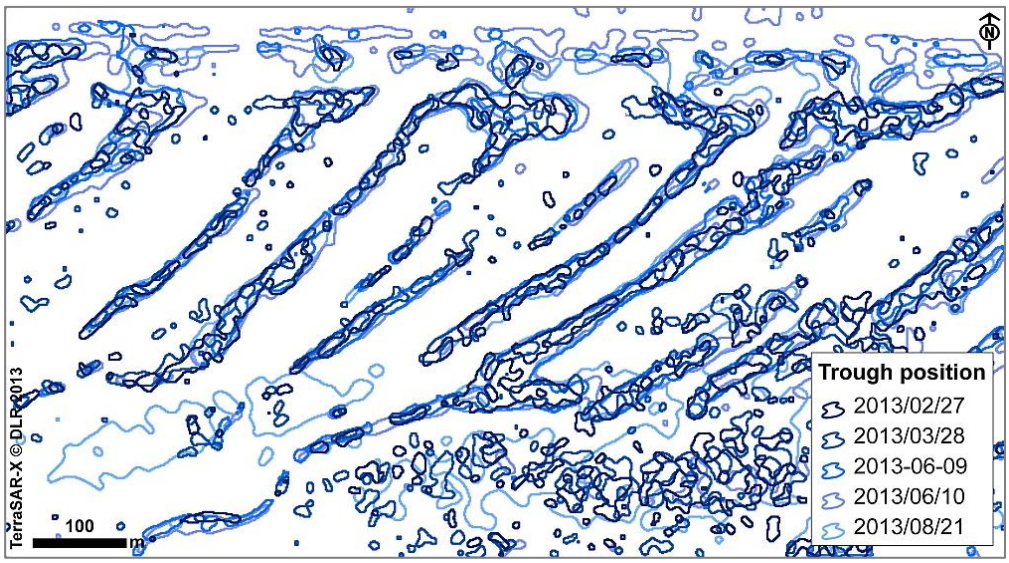

Fig. 5.2-7 Trough positions extracted from TerraSAR-X images of February to August 2013

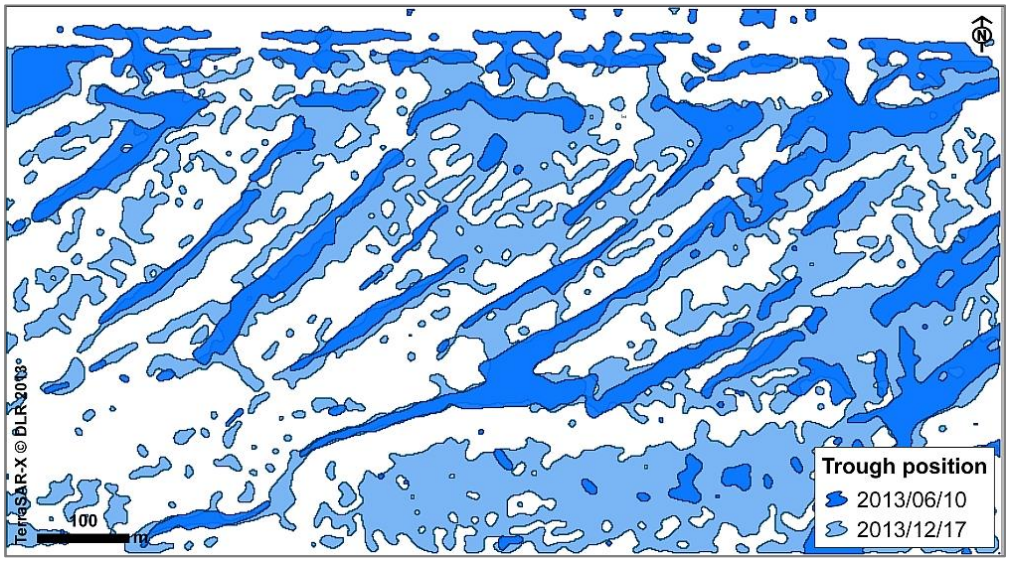

Fig. 5.2-8 Trough positions extracted from TerraSAR-X images of 2013 contrasting the "summer" (*light blue*) and "winter" situation (*dark blue*)

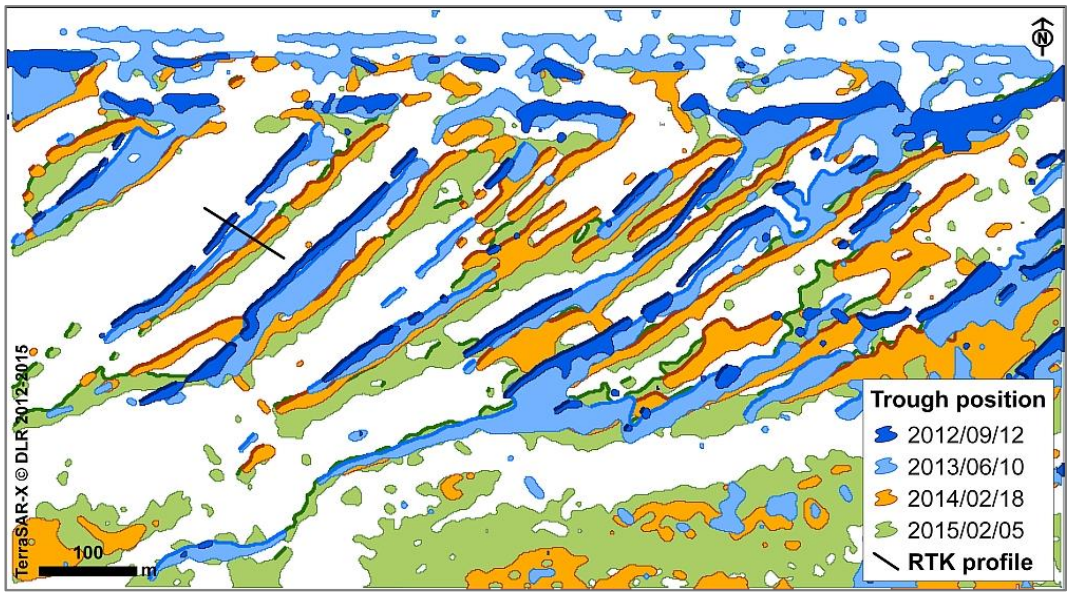

Fig. 5.2-9 Trough positions extracted from TerraSAR-X images of 2012–2015. *Black line:* Position of the height profile D13–D12 in Fig. 5.2-6

5.2.4.3 Sediments

The characteristic grain-size parameters of surface sediments (Table 5.2-1) reveal that the bedforms are composed mainly of fine sand (2–3 phi). The mean grain sizes of the crests are slightly but not significantly finer compared to those of the troughs. Moreover, all sediments in both crests and troughs are very well sorted (sorting value <0.35 phi) and the mud contents are less than 3%. Additional samples from the bedform area show that mud content ranges from 0.59 to 4.85% during summer and from 0.37 to 2.22% during winter. This means that the mud content in the bedform area is generally less than 5% regardless of sampling positions and seasonal variations. On the other hand, on the lower flats in the non-bedform area between the bedform field and the main channel (stations S-6 to S-9 in Fig. 5.2-2), the mud content ranges from ca. 4–30% during summer and drops below 2.5% during winter. The trend of decreasing mud content recorded at all locations (bedform and non-bedform areas) during winter can be attributed to relatively strong waves induced by winter storms.

The sedimentary structures of the bedforms revealed by the box-cores can overall be subdivided into two facies: (1) an intensively bioturbated lower part and (2) a cross-bedded upper part. The cross-bedded sand overlies the intensively bioturbated sand with a sharp boundary. The thickness of the laminated upper part ranges from 5 to 10 cm and occasionally reaches up to 20 cm. During winter, the cross-bedded tops tend to be slightly thicker.

Tab. 5.2-1 Textural parameters of bedform sediments (φ phi, C crest, T trough)

sampling station	Mean grain size (φ)		Sorting (φ)		Mud content (dry wt %)	
	C	**T**	**C**	**T**	**C**	**T**
S-1	2.448	2.319	0.282	0.266	2.33	2.13
S-2	2.461	2.375	0.293	0.278	2.92	2.43
S-3	2.385	2.375	0.24	0.298	2.77	2.53
S-4	2.385	2.355	0.259	0.252	0.69	1.09
S-5	2.366	2.293	0.276	0.261	1.73	0.88

5.2.4.4 Macrofauna

In total, 30 macrofauna taxa were identified. *Scoloplos armiger* (46%), *Aphelochaeta spp*. (15%), *Cerastoderma edule* (10%) *Tubificoides benedii* (9%) and *Capitella capitata* (5%) are the five most common species, constituting ca. 85% of the total macrofauna abundance. Densities of macrofauna species are greater in trough areas compared to crests.

Results from the statistical analysis (Fig. 5.2-10, ESM Table 5.2-A2 in the electronic supplementary material) reveal significant differences in macrofauna community structure among crest and trough areas (F=4.783, p=0.001***). However, evidence against the null hypothesis of no differences in community structure between the stations MZB1 and MZB2 (Fig. 5.2-2) is weak between trough_MZB1 and trough_MZB2 (p=0.05). Highest dissimilarity is found between crest_MZB1 and crest_MZB2 (F=8.683, p=0.001***).

Crest areas are dominated by deposit feeders such as *S. armiger*, *T. benedii* and *Aphelochaeta spp*., suspension feeding bivalves such as *C. edule* and sand-licking amphipods such as *Corophium arenarium*. Trough areas are inhabited predominantly by the deposit feeding polychaetes *S. armiger*, *Aphelochaeta* spp. and *C. capitata*, followed by *C. edule*. Densities of macrofaunal species are higher in the crests of the lower part of the bedform area (crest_MZB2) dominated by *S. armiger*, *T. benedii*, *C. arenarium*, *C. edule*, *C. capitata* and *Macoma balthica*. On the other hand, higher densities of *Aphelochaeta spp.* are found in the upper bedform area (crest_MZB1). Higher densities of the sand-licking amphipod *Urothoe poseidonis* and the omnivorous polychaete *Hediste diversicolor* occur only in the upper bedform area (trough_MZB1 compared to trough_MZB2; ESM Table5.2-A3 in the electronic supplementary material).

Densities of *Arenicola marina* are higher in the lower MZB2 area, with 18.4±8.2 ind. (individuals)/m^2 at the crest and 16.0±6.7 ind./m^2 in the trough (mean of 10 samples). For the higher MZB1 area, the values are 10.8±7.8 ind./m^2 for the crest and 8.8±6.1 ind./m^2 for the trough. Significant differences are found between sites MZB1 and MZB2 (crest: p=0.04625, trough: p=0.04142). No significant difference of lugworm numbers is found between troughs and crests (MZB1: p=0.5437, MZB2: p=0.5146).

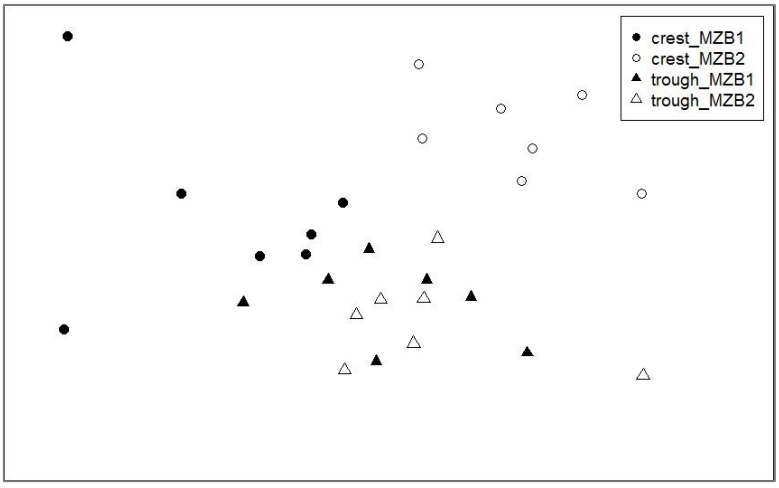

Fig. 5.2-10 nMDS plot based on macrobenthic species abundance data at crest and trough sites. Stress: 0.14

5.2.5 Discussion

This study shows that analysis of TerraSAR-X data allows to determine the trough positions of intertidal bedforms via discrimination of water cover and sediment surface. Due to the topography of the study area and the location of the bedforms on the highest flats close to the East Frisian island of Norderney, the residual water in the troughs is not directly connected to the tide level in the Riffgat channel. Both

the analysis of the TerraSAR-X images and the field observations confirm a slight decrease of the water cover in the troughs over the course of a tidal cycle once the bedforms are exposed. The detection of bedform position is not affected by these minor changes. Variations observed in water cover extent primarily affect the position of the eastern trough edges. The minor variability of especially the western trough edges leads to a consistent core area defining the trough position in the majority of the satellite images. In Fig. 5.2-7, this is demonstrated by the clear congruence of all troughs detected from TerraSAR-X images covering the stable bedform situation from February to August of 2013.

Initial tests on using the shifting of the troughs' centroids as a measure for the study of bedform migration performed in ArcGIS yielded no useful results, due to the higher variability of the smoother eastern trough edges. Therefore, a further determination of bedform migration rates from SAR data should focus on the steeper—in this case, western—trough edges and preferably use images acquired after low tide.

The asymmetry of the bedform edges implies the formation of a stoss side and a lee side as a sign of sediment transport. This supports the notion that the relocation of the bedforms observed in the TerraSAR-X data is due to bedform migration. As the lee sides correspond to the eastward edges of the bedforms in this area, and in view of the shifting direction of the bedforms as detected in TerraSAR-X images from 2009 to 2015, a net sediment transport from west to east is suspected during this time interval. This notion is supported by the sedimentary structure of the bedform area, i.e. the cross-bedded upper part suggests sediment reworking and most likely bedform migration.

In the present study, evidence of differences in species composition and community structure between crests and troughs hint at bio-geomorphological interrelations. Although the macrozoobenthic communities revealed a large overlap of dominant species, significant differences between crest and trough areas were found. Trough areas show higher densities of macrofaunal species dominated by suspension as well as surface and subsurface deposit feeding species. As mentioned above, trough areas were covered with water over the tidal cycle, which offers the opportunity to withstand desiccation during the exposure time and leads to longer feeding periods for macrofaunal species, especially for suspension and deposit feeders. In contrast, crest areas were dominated by the amphipod *C. arenarium*, which feeds on microalgae and detritus (Morrisey 1988). Primary factors that positively regulate microalgae production and biomass are exposure time and related factors like irradiance, wind speed and air temperature (de Jonge et al. 2012). The observed distribution of *C. arenarium* can therefore probably be considered as a close relationship between the feeding preference of this species and microalgae biomass. That distinct distribution patterns of intertidal macrofaunal species are related to exposure time, food availability as well as sediment characteristics has been shown in several Wadden Sea studies (e.g. Schückel et al. 2013).

A key finding of the present study of the upper flats of the East Frisian island of Norderney from 2009–2015 is that the bedforms overall migrated eastwards during the commonly stormy winter season. This contrasts with the bidirectional migration of intertidal bedforms reported by Dolch and Reise (2010) for the North Frisian island of Sylt (cf. Fig. 5.2-1a) over the period 1998–2006. Moreover, those authors documented a spatial expansion of bedform fields in the List tidal basin since 1936/1945, which they related to possible effects of climate change associated with negative impacts on benthic habitats such as seagrass beds and initial mussel beds. Expanding the presented TerraSAR-X-based monitoring approach to other East Frisian or North Frisian Wadden Sea islands should shed light on these regionally contrasting, long-term dynamics of intertidal bedforms, with both ecological and geomorphological implications. Indeed, the pivotal role of the Wadden Sea intertidal zone has attracted increasing attention these last few years (e.g. Wang et al. 2012, and other articles in this special issue).

5.2.6 Conclusions

- Trough extraction from TerraSAR-X imagery is applicable for the detection of intertidal bedforms characterised by residual water cover.
- The method proposed in this study is easy to implement and, with the high potential of data availability offered by satellite SAR, it enables remote sensing investigations of intertidal bedform dynamics which can conveniently be coupled with assessments of faunal diversity.
- The high temporal resolution of SAR satellite data enables precise identification of possible bedform migration.
- In particular the relocation of bedforms over longer periods or strong shifts due to episodic extreme events can be determined using satellite SAR data.
- Easily applicable remote sensing of exposed intertidal geomorphic structures with the use of SAR data helps improve our understanding of bedform dynamics and associated processes of sediment transport.

Acknowledgements

This study forms part of the “Wissenschaftliche Monitoringkonzepte für die Deutsche Bucht – WIMO” (“Scientific Monitoring Concepts for the German Bight”) project jointly funded by the Ministry for Environment, Energy and Climate Protection, and the Ministry for Science and Culture of the Federal State of Lower Saxony. Sedimentological work was facilitated by a fellowship of the Hanse Institute for Advanced Study, and a grant from the Korean Ministry of Oceans and Fisheries (PJT200538). The authors thank the German Aerospace Center for supplying the TerraSAR-X images. Udo Uebel (ICBM-Terramare, Wilhelmshaven) helped with the RTK-DGPS measurements. Also acknowledged are constructive assessments by two anonymous reviewers.

Conflict of interest: The authors declare that there is no conflict of interest with third parties.

5.2.7 References

Adolph W, Jung R, Schmidt A, Ehlers M, Heipke C, Bartholomä A, Farke H (2016) Integration of TerraSAR-X, RapidEye and airborne lidar for remote sensing of intertidal bedforms on the upper flats of Norderney (German Wadden Sea). Geo-Mar Lett 36 (accepted)

Airbus Defence & Space (2014) Radiometric calibration of TerraSAR-X Data. Beta Naught and Sigma Naught coefficient calculation. Airbus Defence & Space. TSXX-ITD-TN-0049-radiometric_calculations_I3.00.doc

Allen JRL (1980) Sand waves: a model of origin and internal structure. Sediment Geol 26:281–328. doi:10.1016/0037-0738(80)90022-6

Anderson MJ (2001) A new method for non-parametric multivariate analysis of variance. Austral Ecol 26:32–46. doi:10.1111/j.1442-9993.2001.01070.pp.x

Ashley GM (1990) Classification of large-scale subaqueous bedforms: a new look at an old problem. J Sediment Petrol 60:160–172. doi:10.1306/212F9138-2B24-11D7-8648000102C1865D

Baptist MJ, van Dalfsen J, Weber A, Passchier S, van Heteren S (2006) The distribution of macrozoobenthos in the southern North Sea in relation to meso-scale bedforms. Estuar Coast Shelf Sci 68(3-4): 538–546. doi:10.1016/j.ecss.2006.02.023

Bartholdy J, Bartholomae A, Flemming BW (2002) Grain-size control of large compound flow-transverse bedforms in a tidal inlet of the Danish Wadden Sea. Mar Geol 188(3-4):391–413. doi:10.1016/S0025-3227(02)00419-X

Borsje BW, de Vries MB, Bouma TJ, Besio G, Hulscher SJMH, Herman PMJ (2009) Modeling bio-geomorphological influences for offshore sandwaves. Cont Shelf Res 29(9):1289–1301. doi:10.1016/j. csr.2009.02.008

Brezina J (1986) Macrogranometer MC86, Laboratory manual. Macrogranometry, Heidelberg

Buijsman MC, Ridderinkhof H (2008) Long-term evolution of sand waves in the Marsdiep inlet. II: relation to hydrodynamics. Cont Shelf Res 28(9):1202–1215. doi:10.1016/j.csr.2008.02.014

Core Team R (2015) R: a language and environment for statistical computing. R Foundation for Statistical Computing, Vienna, https://www.R-project.org/

CWSS (2008) Nomination of the Dutch-German Wadden Sea as World Heritage Site. Volume 1. Wilhelmshaven. http://www.waddensea-secretariat.org/management/whs/whs.html. Accessed 20 Dec 2015

de Jonge VN, de Boer WF, de Jong DJ, Brauer VS (2012) Long-term mean annual microphytobenthos chlorophyll *a* correlates with air temperature. Mar Ecol Prog Ser 468:43–56. doi:10.3354/meps09954

Dalrymple RW, Knight RJ, Lambiase JJ (1978) Bedforms and their hydraulic stability relationships in a tidal environment, Bay of Fundy, Canada. Nature 275(5676):100–104. doi:10.1038/275100a0

Davies RA, Flemming BW (1991) Time-series study of mesoscale tidal bedforms, Martens Plate, Wadden Sea, Germany. Can Soc Petrol Geol Mem 16:275–282

Dellepiane S, De Laurentiis R, Giordano F (2004) Coastline extraction from SAR images and a method for the evaluation of the coastline precision. Pattern Recogn Lett 25(13):1461–1470. doi:10.1016/j. patrec.2004.05.022

Diesing M, Kubicki A, Winter C, Schwarzer K (2006) Decadal scale stability of sorted bedforms, German Bight, southeastern North Sea. Cont Shelf Res 26(8):902–916. doi:10.1016/j.csr.2006.02.009

Dolch T, Reise K (2010) Long-term displacement of intertidal seagrass and mussel beds by expanding large sandy bedforms in the northern Wadden Sea. J Sea Res 63(2):93–101. doi: 10.1016/j. seares.2009.10.004

DWD (2013a) Orkantief CHRISTIAN am 28. Oktober 2013. Deutscher Wetterdienst. https://www.dwd.de/DE/presse/hintergrundberichte/2013/Orkantief_Christian_PDF.pdf?__blob=publicationFile&v=3. Accessed 3 Dec 2015

DWD (2013b) Orkantief XAVER über Nordeuropa vom 5. bis 7. Dezember 2013. Stand: 30. Dezember 2013. Deutscher Wetterdienst. https://www. dwd.de/DE/presse/hintergrundberichte/2013/XAVER_PDF.pdf%3F. Accessed 3 Dec 2015

Eitner V, Kaiser R, Niemeyer HD (1996) Nearshore sediment transport processes due to moderate hydrodynamic conditions. In: Batist M de, Jacobs P (eds) Geology of siliciclastic shelf seas. Geol Soc Lond Spec Publ 117:267–288. doi:10.1144/GSL.SP.1996.117.01.16

Ernstsen VB, Noormets R, Winter C, Hebbeln D, Bartholomä A, Flemming BW, Bartholdy J (2005) Development of subaqueous barchanoid-shaped dunes due to lateral grain size variability in a tidal inlet channel of the Danish Wadden Sea. J Geophys Res 110, F04S08. doi:10.1029/2004JF000180

Flemming BW, Ziegler K (1995) High-resolution grain size distribution patterns and textural trends in the back-barrier environment of Spiekeroog Island (southern North Sea). Senckenberg Marit 26:1–24

Fritz T, Eineder M (2010) TerraSAR-X, ground segment, basic product specification document. CAF - Cluster Applied Remote Sensing. DLR TX-GS-DD-3302, Issue 1.7

Frost VS, Stiles JA, Shanmugan KS, Holtzman JC (1982) A model for radar images and its application to adaptive digital filtering of multiplicative noise. IEEE Trans Pattern Anal Mach Intell 4(2): 157–166. doi:10.1109/TPAMI.1982.4767223

Gómez EA, Cuadrado DG, Pierini JO (2010) Sand transport on an estuarine submarine dune field. Geomorphology 121(3-4):257–265. doi:10.1016/j.geomorph.2010.04.022

Haralick RM, Shanmugam K, Dinstein I (1973) Textural features for image classification. IEEE Trans Syst Man Cybern 3(6):610–621. doi:10.1109/TSMC.1973.4309314

Hayes MO (1979) Barrier islands morphology as a function of tidal and wave regime. In: Leatherman SP (ed) Barrier islands. Academic Press, New York, pp 1–27

Heygster G, Dannenberg J, Notholt J (2010) Topographic mapping of the German tidal flats analyzing SAR images with the waterline method. IEEE Trans Geosci Remote Sensing 48(3):1019–1030. doi:10.1109/TGRS.2009.2031843

Hoekstra P, Bell P, van Santen P, Roode N, Levoy F, Whitehouse R (2004) Bedform migration and bedload transport on an intertidal shoal. Cont Shelf Res 24(11):1249–1269. doi:10.1016/j. csr.2004.03.006

Kim D-J, Moon WM, Kim G, Park S-E, Lee H (2011) Submarine ground-water discharge in tidal flats revealed by space-borne synthetic aperture radar. Remote Sens Environ 115(2):793–800. doi:10.1016/j.rse.2010.11.009

Legendre P, Gallagher ED (2001) Ecologically meaningful transformations for ordination of species data. Oecologia 129:271–280. doi:10.1007/s004420100716

Lehner S, Tings B (2015) Maritime products using TerraSAR-X and Sentinel-1 imagery. International Archives Photogrammetry Remote Sensing Spatial Information Sciences XL-7/W3:967–973. doi:10.5194/isprsarchives-XL-7-W3-967-2015

Li Z, Heygster G, Notholt J (2014) Intertidal topographic maps and morphological changes in the German Wadden Sea between 1996–1999 and 2006–2009 from the waterline method and SAR images. IEEE J Sel Top Appl Earth Observations Remote Sensing 7(8):3210–3224. doi:10.1109/JSTARS.2014.2313062

Markert E, Kröncke I, Kubicki A (2015) Small scale morphodynamics of shoreface-connected ridges and their impact on benthic macrofauna. J Sea Res 99:47–55. doi:10.1016/j.seares.2015.02.001

Mason DC, Davenport LJ (1996) Accurate and efficient determination of the shoreline in ERS-1 SAR images. IEEE Trans Geosci Remote Sens 34(5):1243–1253. doi:10.1109/36.536540

McCave IN (1971) Sand waves in the North Sea off the coast of Holland. Mar Geol 10(3):199–225. doi:10.1016/0025-3227(71)90063-6

Moreira A, Prats-Iraola P, Younis M, Krieger G, Hajnsek I, Papathanassiou KP (2013) A tutorial on synthetic aperture radar. IEEE Geosci Remote Sens Mag 1(1):6–43. doi:10.1109/MGRS.2013.2248301

Morrisey DJ (1988) Differences in effects of grazing by deposit-feeders *Hydrobia ulvae* (Pennant) (Gastropoda: Prosobranchia) and *Corophium arenarium* Crawford (Amphipoda) on sediment microalgal populations. II Quantitative effects. J Exp Mar Biol Ecol 118:43–53. doi:10.1016/0022-0981(88)90121-9

Niedermeier A, Hoja D, Lehner S (2005) Topography and morphodynamics in the German Bight using SAR and optical remote sensing data. Ocean Dyn 55(2):100–109. doi:10.1007/s10236-005-0114-2

Niemeyer HD (1987) Measurements of tidal currents in groyne fields (in German). Jber 1986 Forsch-Stelle Küste, vol 38

Niemeyer HD (1994) Long-term morphological development of the East Frisian Islands and coast. In: Edge BL (ed) Coastal Engineering 1994. Proc 24th Int Conf Coastal Engineering, Kobe, vol 1, p 2417–2433. doi:10.1061/9780784400890.176

Oksanen J, Blanchet FG, Friendly M, Kindt R, Legendre P, McGlinn D, Minchin PR, O'Hara RB, Simpson GL, Solymos P, Stevens MHH, Szoecs E, Wagner H (2016) vegan: Community Ecology Package. R package version 2.4-0. https://CRAN.R-project.org/package=vegan

Pratt WK (2007) Digital image processing. PIKS Scientific inside, 4th edn. Wiley-Interscience, Hoboken

Schückel U, Beck M, Kröncke I (2013) Spatial variability in structural and functional aspects of macrofauna communities and their environmental parameters in the Jade Bay Wadden Sea Lower Saxony, southern North Sea. Helgol Mar Res 67:121–136

Shi Z, Fung KB (1994) A comparison of digital speckle filters. In: Proc IGARSS 94, p 2129–2133. doi:10.1109/IGARSS.1994.399671

Tou JT, Gonzalez RC (1974) Pattern recognition principles. Addison-Wesley, Reading. doi:10.1002/zamm.19770570626

Wang ZB, Hoekstra P, Burchard H, Ridderinkhof H, de Swart HE, Stive MJF (2012) Morphodynamics of the Wadden Sea and its barrier island system. Ocean Coast Manag 68:39–57. doi:10.1016/j. ocecoaman.2011.12.022

Whitmeyer SJ, FitzGerald DM (2008) Episodic dynamics of a sand wave field. Mar Geol 252(1-2):24–37. doi:10.1016/j.margeo.2008.03.009 Wiehle S, Lehner S (2015) Automated waterline detection in the Wadden Sea using high-resolution TerraSAR-X images. J Sensors 2015: 450857. doi:10.1155/2015/450857

Winter C, Herrling G, Bartholomä A, Capperucci R, Callies U, Heipke C, Schmidt A, Hillebrand H, Reimers C, Bremer P, Weiler R (2014) Scientific concepts for monitoring the ecological state of German coastal seas (in German). Wasser und Abfall 07-08/2014:21–26. doi:10.1365/s35152-014-0685-7

Zarillo GA (1982) Stability of bedforms in a tidal environment. Mar Geol 48:337–351. doi:10.1016/0025-3227(82)90103-7

5.2.8 Electronic supplementary material

APPENDIX

Tab. 5.2-A1 TerraSAR-X data: date of acquisition, relative orbit, path (*A* ascending, *D* descending), incidence angle (inc.), polarisation (pol., *VV* vertically co-polarised, *HH* horizontally co-polarised), acquisition time related to low tide (Δ LT, *positive values* acquisition at rising tides), Riffgat gauge level (source: Federal Waterways and Shipping Administration WSV, provided by the Federal Institute for Hydrology BFG), wind speed (ws) and wind direction (wd) hourly means (source: German Weather Service DWD). *Bold* TerraSAR-X data represented in Figures 5.2-3, 5.2-4, 5.2-7 to 5.2-9

Date	Orbit	Path	Inc. [°]	Pol.	Δ LT [minute]	Gauge level [cm>NHN]	ws [m/s]	wd [°]
22/06/2009	25	A	53.2	VV	80	-96	6.5	350
21/07/2009	131	A	20.8	VV	63	-111	3.9	60
21/04/2011	139	D	23.3	VV	-44	-154	3.1	110
01/05/2011	131	A	20.8	HH	81	-110	7.6	60
02/06/2011	116	A	45.1	VV	11	-145	5.4	360
04/06/2011	139	D	23.3	VV	0	-160	5.5	60
15/06/2011	139	D	23.4	VV	137	-12	2.8	170
16/07/2011	116	A	45.1	VV	-18	-152	3.2	160
29/07/2011	139	D	22.9	VV	178	37	8.5	310
14/10/2011	139	D	23.6	VV	15	-174	3.2	130
26/10/2011	154	D	46.2	VV	128	-21	4.4	150
08/11/2011	25	A	53.2	VV	138	-24	4.8	120
16/11/2011	139	D	23.1	VV	-90	-118	6.3	120
09/01/2012	131	A	20.9	VV	16	-108	7.6	270
21/02/2012	116	A	45.1	VV	44	-112	6.1	240
23/03/2012	78	D	54.3	VV	20	-176	3.5	60
21/06/2012	116	A	45.1	VV	-44	-162	6.9	70
17/08/2012	139	D	23.3	HH/VV	102	-30	3.2	150
01/09/2012	**40**	**A**	**34.4**	**VV**	**-11**	**-157**	**4.0**	**230**
15/09/2012	78	D	54.2	VV	104	27	10.0	310
17/10/2012	63	D	36.2	VV	26	-117	5.1	170
28/11/2012	40	A	34.4	VV	40	-117	8.6	20
30/11/2012	63	D	36.4	VV	21	-129	5.4	10
27/02/2013	**78**	**D**	**54.2**	**VV**	**-9**	**-181**	**4.1**	**70**
28/03/2013	**25**	**A**	**53.2**	**VV**	**-4**	**-173**	**6.6**	**70**
09/06/2013	**131**	**A**	**21.2**	**VV**	**-23**	**-144**	**6.9**	**360**

Date	Orbit	Path	Inc. [°]	Pol.	Δ LT [minute]	Gauge level [cm>NHN]	ws [m/s]	wd [°]
10/06/2013	**139**	**D**	**23.1**	**VV**	**27**	**-144**	**4.8**	**350**
21/08/2013	**63**	**D**	**36.3**	**HH/VV**	**86**	**-74**	**3.0**	**170**
17/12/2013	**25**	**A**	**53.1**	**VV**	**45**	**-109**	**2.2**	**200**
18/02/2014	**139**	**D**	**23.2**	**VV**	**-38**	**-155**	**5.7**	**170**
28/02/2014	131	A	21.1	VV	63	-67	3.4	60
18/03/2014	63	D	36.3	VV	8	-151	5.0	230
03/04/2014	139	D	23.2	VV	-58	-144	6.8	60
14/06/2014	**63**	**D**	**36.1**	**VV**	**46**	**-132**	**9.9**	**350**
28/06/2014	116	A	45.1	VV	-19	-137	2.0	360
11/08/2014	116	A	45.1	VV	6	-111	8.5	220
10/09/2014	63	D	36.2	VV	41	-125	9.6	350
07/12/2014	63	D	36.1	VV	56	-102	7.6	190
21/01/2015	78	D	54.3	VV	33	-149	2.6	150
03/02/2015	116	A	45.0	VV	30	-127	9.1	20
05/02/2015	**139**	**D**	**23.2**	**VV**	**20**	**-159**	**10.5**	**30**

Tab. 5.2-A2 Results of pair-wise comparisons among crest and trough areas. Significance level: < 0.001 = ***; < 0.01 = **, < 0.05 = *

Pair-wise comparisons	F	p
Crest vs. trough areas	4.783	**0.001*** **
Crest_MZB1 vs. trough_MZB1	3.923	**0.003** **
Crest_MZB1 vs. crest_MZB2	8.683	**0.001*** **
Crest_MZB1 vs. trough_MZB2	4.887	**0.001*** **
Trough_MZB1 vs. crest_MZB2	8.949	**0.002*** **
Trough_MZB1 vs. trough_MZB2	2.078	**0.05**
Crest_MZB2 vs. trough_MZB2	8.335	**0.001*** **

Tab. 5.2-A3 Average abundances (ind./m²) per groups and cumulative contribution (%) of the most discriminating species occurring in the different communities in crest and trough areas. Feeding types are abbreviated as follows: SD = surface deposit feeder, SSD = subsurface deposit feeder, IF = interface feeder, SL = sandlicker, SF = suspension feeder.

Species	Feeding type	ind./m²	ind./m²	cumContri%
crest_MZB1 vs trough_MZB1				
Scoloplos armiger	*SSD*	1071.43	1942.86	25.53
Aphelochaeta spp.	*SD*	685.71	871.43	37.24
Urothoe poseidonis	*SL*	42.86	442.86	47.82

Species	Feeding type	ind./m^2	ind./m^2	cumContri%
Capitella capitata	*SSD*	242.86	471.43	58.05
Cerastoderma edule	*SF*	242.86	471.43	67.08
Tubificoides benedii	*SSD*	371.43	214.29	73.97
crest_MZB1 vs crest_MZB2				
Scoloplos armiger	*SSD*	1071.43	2214.29	23.32
Tubificoides benedii	*SSD*	371.43	1342.86	41.38
Corophium arenarium	*SL,SD*	100.00	971.43	58.12
Aphelochaeta spp.	*SD*	685.71	171.43	68.13
Capitella capitata	*SSD*	242.86	585.71	78.05
Cerastoderma edule	*SF*	242.86	542.86	84.56
Macoma balthica	*IF*	114.29	228.57	87.22
crest_MZB1 vs trough_MZB2				
Scoloplos armiger	*SSD*	1071.4	2300.0	27.83
Aphelochaeta spp.	*SD*	685.7	1271.4	44.21
Cerastoderma edule	*SF*	242.8	928.5	59.95
Capitella capitata	*SSD*	242.8	714.2	71.24
Tubificoides benedii	*SSD*	371.4	385.7	77.37
trough_MZB1 vs crest_MZB2				
Tubificoides benedii	*SSD*	214.29	1342.86	19.59
Corophium arenarium	*SL,SD*	14.29	971.43	36.70
Scoloplos armiger	*SSD*	1942.86	2214.29	49.33
Aphelochaeta spp.	*SD*	871.43	171.43	61.71
Capitella capitata	*SSD*	471.43	585.71	72.35
Cerastoderma edule	*SF*	471.43	542.86	78.84
trough_MZB1 vs trough_MZB2				
Scoloplos armiger	*SSD*	1942.8	2300.0	16.31
Aphelochaeta spp.	*SD*	871.4	1271.4	31.55
Capitella capitata	*SSD*	471.4	714.2	46.00
Cerastoderma edule	*SF*	471.4	928.5	59.14
Urothoe poseidonis	*SL*	442.8	157.1	68.32
Tubificoides benedii	*SSD*	214.2	385.7	75.90
crest_MZB2 vs trough_MZB2				
Aphelochaeta spp.	*SD*	171.4	1271.4	18.76
Tubificoides benedii	*SSD*	1342.8	385.7	35.04
Corophium arenarium	*SL,SD*	971.4	28.57	51.21
Scoloplos armiger	*SSD*	2214.2	2300.0	63.69
Capitella capitata	*SSD*	585.7	714.2	76.04

5.3 Integration of TerraSAR-X, RapidEye and Airborne Lidar for Remote Sensing of Intertidal Bedforms on the Upper Flats of Norderney (German Wadden Sea)

Adolph, W.; Jung, R.; Schmidt, A.; Ehlers, M.; Heipke, C.; Bartholomä, A.; Farke, H. (2017). *Geo-Mar. Lett.* 37 (2), 193–205. DOI: 10.1007/s00367-016-0485-z.

Abstract

The Wadden Sea is a large coastal transition area adjoining the southern North Sea uniting ecological key functions with an important role in coastal protection. The region is strictly protected by EU directives and national law and is a UNESCO World Heritage Site, requiring frequent quality assessments and regular monitoring. In 2014 an intertidal bedform area characterised by alternating crests and water-covered troughs on the tidal flats of the island of Norderney (German Wadden Sea sector) was chosen to test different remote sensing methods for habitat mapping: airborne lidar, satellite-based radar (TerraSAR-X) and electro-optical sensors (RapidEye). The results revealed that, although sensitive to different surface qualities, all sensors were able to image the bedforms. A digital terrain model generated from the lidar data shows crests and slopes of the bedforms with high geometric accuracy in the centimetre range, but high costs limit the operation area. TerraSAR-X data enabled identifying the positions of the bedforms reflecting the residual water in the troughs also with a high resolution of up to 1.1 m, but with larger footprints and much higher temporal availability. RapidEye data are sensitive to differences in sediment moisture employed to identify crest areas, slopes and troughs, with high spatial coverage but the lowest resolution (6.5 m). Monitoring concepts may differ in their remote sensing requirements regarding areal coverage, spatial and temporal resolution, sensitivity and geometric accuracy. Also financial budgets limit the selection of sensors. Thus, combining differing assets into an integrated concept of remote sensing contributes to solving these issues.

5.3.1 Introduction

Preserving the integrity of the Wadden Sea ecosystem (southern North Sea) poses substantial challenges in terms of the natural distribution of habitats and their temporal variability. This includes sediments as well as morphological features such as sand and mud flats, tidal channels and creeks. Therefore, the status and development of these elements are a major focus for the monitoring and environmental assessment of the Wadden Sea, required at regular temporal intervals by international directives (European Commission 1992, 2000, 2008) integrated into national laws. Modern remote sensing techniques employing high-resolution sensors open up new possibilities to detect, describe and map habitats and surface structures in tidal areas which are difficult to access.

Airborne lidar (light detection and ranging) provides both backscatter intensity and height information, and has become a standard method to generate digital terrain models (DTMs) in coastal zones such as the Wadden Sea. It is used for operational monitoring of the German mainland coast and islands (Schmidt et al. 2013). Spectral reflectance data from electro-optical sensors have been used with a focus on the distinction of different grain sizes or sediment types (e.g. sand and mud), as well as the examination of the influence of water or biofilms on reflectance. Spectral contrast between sediments of different grain sizes is influenced by interstitial moisture (Rainey et al. 2000; Small et al. 2009) but also by target properties such as organic matter content, iron oxides, cyanobacteria and mineralogy. These effects have been studied extensively in the laboratory and under field conditions (e.g. Rainey et al. 2000; Decho et al. 2003; Sørensen et al. 2006; Ryu et al. 2010). For instance, Ibrahim et al. (2009)

have analysed the specific influences exerted on spectral reflectance by the grain size, chlorophyll a and organic matter of different sediment types. Synthetic aperture radar (SAR), on the other hand, can be regarded as a measure of surface roughness (e.g. Van der Wal et al. 2005; Aubert et al. 2011; Moreira et al. 2013). Satellite SAR imagery has been investigated in various environments including intertidal sediments (e.g. Van der Wal and Herman 2007; Gade et al. 2008), mussel beds (e.g. Choe et al. 2012; Kim et al. 2013; Nieuwhof et al. 2015) and salt marshes (e.g. Lee et al. 2012). Stelzer et al. (2010), Dehouck et al. (2012), Gade et al. (2014, 2015), Jung et al. (2015) and Müller et al. (2016) demonstrated the potential of SAR data as a synergistic input to multi-sensor approaches for the remote sensing of intertidal areas. SAR imagery has also allowed to distinguish water cover from sediment surfaces in the intertidal zone of the Wadden Sea, and has been applied for topographic mapping by Niedermeier et al. (2005), Heygster et al. (2010), Mason et al. (2010), Li et al. (2014) and Wiehle and Lehner (2015).

With the overall aim of evaluating the specific qualities of modern remote sensing technologies in identifying and mapping intertidal seabed habitats and geomorphic structures of the Wadden Sea, in this study an intertidal bedform area was investigated using airborne lidar and satellite remote sensing by electro-optical and high-resolution SAR sensors. A joint campaign was carried out in autumn 2014 employing airborne lidar, RapidEye, TerraSAR-X and in situ verification performed by RTK-DGPS measurements. Additionally, SAR and lidar data from 2010 and 2012 were analysed. As test site, a tidal flat area directly bordering the island of Norderney in the German Wadden Sea sector was chosen because it is characterised by regular geomorphic surface structures (bedforms) representing a sediment surface differing in height and moisture as well as in water cover (Fig. 5.3-1). The site has been described in detail by Adolph et al. (2016, this special issue), investigating spatiotemporal trends of the bedform area with an extensive set of TerraSAR-X data from 2009–2015.

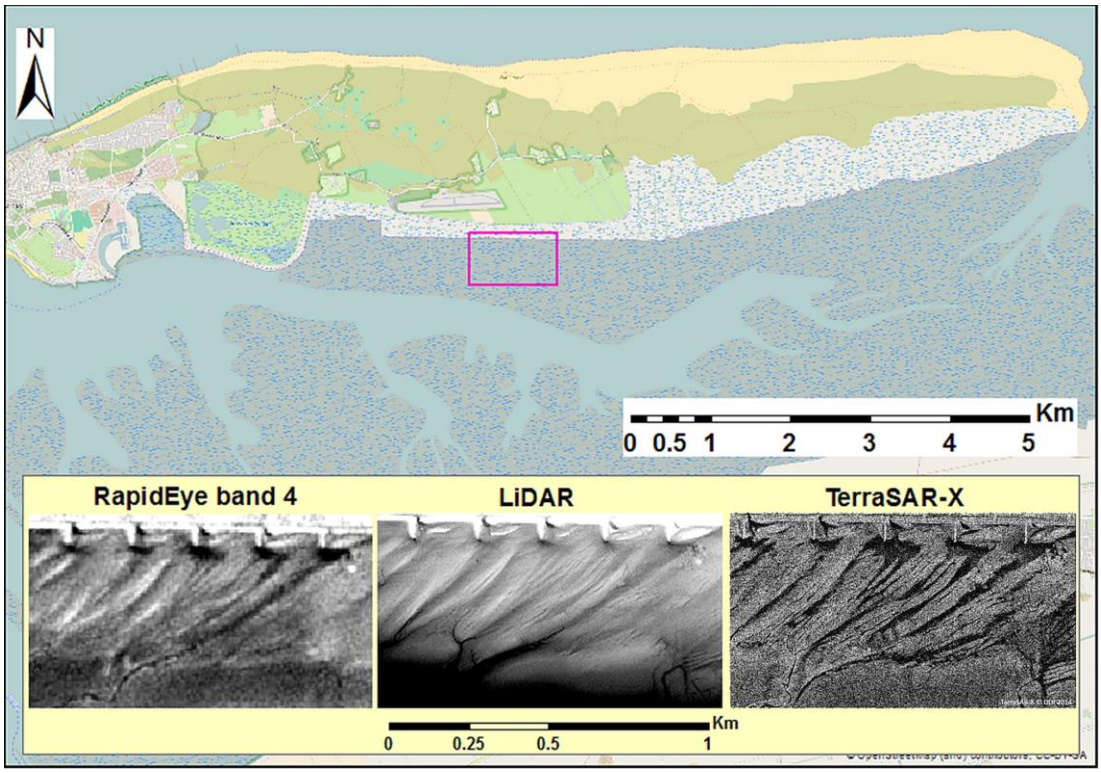

Fig. 5.3-1 Study site on the upper tidal flats of Norderney (German Wadden Sea sector, southern North Sea) with subset images of RapidEye (2014/09/19), lidar (2016/10/04) and TerraSAR-X (2016/09/10) data. Background map ©AOI_V3-OpenStreetMap (and) contributors CC-BY-SA

The aim of this study is to identify the specific strengths of the different sensors to recognise intertidal geomorphic features and their positioning, based on the example of these bedforms. Remote sensing studies of intertidal geomorphic structures and their dynamics could benefit the understanding of basic processes shaping the Wadden Sea, in turn supporting national and local authorities responsible for coastal management. The ultimate aim is to propose a combination of different sensor data types in an integrated application of advanced remote sensing techniques for future Wadden Sea monitoring or long-term ecological research in the intertidal zone. This requires a cost-effective combination of, for example, SAR, lidar and electro-optical data to satisfy spatial coverage and resolution as well as application frequency and availability. The present study forms part of the German scientific project "WiMo" carried out by an interdisciplinary research consortium addressing various European and German regulations to assess the state of the marine environment in the German Bight (for overviews, see Winter et al. 2014; Winter et al., Introduction article for this special issue).

5.3.2 Study area

The study area on the back-barrier tidal flats south of the barrier island of Norderney is part of the Lower Saxony Wadden Sea National Park in the southern North Sea. On the upper tidal flats directly bordering the island, bedform fields form a pattern of alternating crests and troughs diagonally to the southern shoreline of the island. Such intertidal bedforms can be seen along all East Frisian islands. Due to the permanent water cover of the troughs, the bedforms are clearly recognised in situ as well as in most remote sensing data. A study of trough positions derived from TerraSAR-X data from 2009–2015 suggests a long-term shifting of the bedforms to the east (Adolph et al. 2016, this special issue).

The study site of approx. 0.64 km^2 is situated in between the main channel of the tidal basin and the island, comprising part of the western bedform field of Norderney (Fig. 5.3-1). Fine sand (2–3 phi) is the predominant grain size fraction characterising the sediments of the bedform area, the mud content being less than 5%; in the southern, non-bedform part of the subset near the tidal channel, the sediments consist of fine sand with higher mud (silt and clay) content (Adolph et al. 2016, this special issue). During exposure, in the bedform area the pore water quite quickly seeps from the ridges, leaving the crests relatively dry compared to the moist or wet slopes and the troughs.

5.3.3 Materials and methods

One set of remote sensing data including lidar, RapidEye and TerraSAR-X as well as in situ measurements by RTK-DGPS was acquired within 1 month in autumn 2014 (Table 5.3-1). A comparative view of the observed terrain as reflected in the data from the different sensors is used to illustrate the respective characteristics of reproduction regarding the test site within an intertidal bedform area. From the lidar data, a DTM and height profiles are drawn. The electro-optical imagery is classified to discriminate between three classes based on water cover and sediment moisture. From the SAR data, total water cover is distinguished from the exposed sediment surface. The results are verified with in situ measurements. Based on additional data from 2010 and 2012, the detection of shifting bedform position from SAR data is tested against lidar data. Furthermore, Fourier analysis is applied on profiles of each sensor dataset to check for periodicity of the bedforms.

Analysis of lidar data

Lidar data are available from three different flight campaigns performed in the framework of coastal protection by the Lower Saxony State Department for Waterway, Coastal and Nature Conservation (NLWKN). The flights took place in spring 2010 and 2012 and in autumn 2014 using the lidar sensor Riegl LMS-Q 820G (version of 2014) from an airplane at 400–650 m altitude. Data acquisition was carried out around low water in order to ensure minimal water coverage of the tidal flat areas. The

accuracy of a given lidar point is >20 cm in the horizontal direction and 5–15 cm (absolute) or up to 2 cm (relative) in the vertical direction.

For the data of 2010, the irregular point cloud was interpolated to generate a regular DTM of 1 m grid size using the SCOP++ software (SCOP-WWW 2001). For the data of 2012 and 2014, the DTM was generated by the data provider using commercial software. As the test site (Fig. 5.3-1) has a size of 1,075×600 m, this leads to about 0.64 million points in the DTM. Bedform shape and height characteristics are analysed using a profile selected from the DTM of 2014. This profile also forms the basis for the Fourier analysis to derive further characteristics of the bedforms. Height profiles recorded in 2010, 2012 and 2014 were compared to measure relocation distances of the bedforms. For this purpose, the curve maxima were defined as the crests of the bedform ridges marking the bedform positions of 2010, 2012 and 2014.

Tab. 5.3-1 Acquisition dates of remote sensing and RTK datasets used in this study

Lidar	RapidEye	TerraSAR-X	RTK-DGPS
05/2010			
06/04/2012		21/04/2012	
04/10/2014	19/09/2014	10/09/2014	04/09/2014

Analysis of electro-optical data

Electro-optical data were acquired by the RapidEye satellite constellation composed of five identical satellites phased in a sun-synchronous orbit plane with an inclination angle of 97.8°. The sensors have a swath width of nearly 77 km and acquire the data from a nominal altitude of 630 km, recording five discrete spectral bands at a spatial resolution of 6.5 m (re-sampled to 5 m) at nadir (BlackBridge 2015). The image used in this study was taken on 19/9/2014 approx. 1 h before low water, and is fully cloud-free. It was delivered as RapidEye 3A Ortho Product, which offers the highest processing level with respect to radiometric, sensor and geometric corrections. The digital numbers of the RapidEye image pixels represent absolute calibrated radiance values (BlackBridge 2013).

As the crest area, slopes and troughs are characterised by the same sediment but ranging from water-covered trough to relatively dry crest, the differences in the spectral properties of the test area are mainly caused by the water content of the sediment. Thus, areas with variably water-saturated sediments can be distinguished from the electro-optical data with the aid of training areas. As a first step, a principal component analysis (PCA) is carried out to improve the radiometric quality of the satellite image by reducing the spectral variability. Spectral variability in this study addresses the fact that an area of homogenous land cover (e.g. water) may have a wide range of values, implying heterogeneity. To reduce most of the spectral variability, the first two PCA bands are selected for the inverse PCA. Subsequent to this radiometric improvement, an atmospheric correction is carried out based on the ENVI atmospheric correction module FLAASH of Manakos et al. (2011) and Matthew et al. (2002). Next, several indices such as NDWI (normalized difference water index), MSAVI (modified soil adjusted vegetation index) and NDVI (normalized difference vegetation index) are calculated. Especially the NDWI enables the demarcation between different moisture contents of the sediments. From the resulting index images and from the RapidEye bands 3, 4 and 5, the Haralick texture measures contrast, mean and variance are calculated in the direction perpendicular to the bedforms in a 3×3 window with one pixel distance (Haralick et al. 1973). In Table 5.3-2 the bands, indices and texture results are listed; these are layer-stacked and subsequently applied to the supervised classification

approach “maximum likelihood classifier” (MLC). For the training step, training data for the classes “crest area” (dry sediment), “slope” (wet sediment) and “trough” (water-covered sediment) are derived from the input images by visual interpretation based on ground-truth data.

Tab. 5.3-2 Information derived from RapidEye bands for supervised classification with the maximum likelihood classifier

Band 3	NDWI	Contrast of NDWI	Mean of NDWI	Variance of NDWI
Band 4	MSAVI	Contrast of NDVI	Mean of NDVI	Variance of NDVI
Band 5	NDVI		Mean of Band 5	

Analysis of SAR data

SAR data were acquired by the high-frequency (9.6 GHz) X-band sensor of TerraSAR-X with a wavelength of 3.1 cm, operating at 514 km altitude. The acquisitions used in this study were taken in high-resolution mode, vertically co-polarised and delivered as Geocoded Ellipsoid Corrected (GEC) intensity images in Universal Transverse Mercator (UTM) coordinates. The images were taken on 21/04/2012 and 10/09/2014 shortly after low water (25 and 41 minutes respectively) and the pixel sizes are 0.75×0.75 and 0.5×0.5 m respectively, in both cases re-sampled to 1.25 m for comparison with the complete set of TerraSAR-X data. The TerraSAR-X acquisition of 10/09/2014 has been reported by Adolph et al. (2016, this special issue).

The differences in surface roughness caused by the pattern of sandy crests and slopes alternating with water-covered troughs in the bedform area are reflected in the radar backscatter measured by the SAR sensor. The bedform positions were determined by detection of the water-covered troughs according to the method proposed by Adolph et al. (2016, this special issue): the TerraSAR-X data were calibrated to “Sigma Naught” (σ^0), the radar reflectivity per unit area in ground range, to correct for geometry of acquisition (cf. Airbus Defence & Space 2014). Speckle reduction was performed by Frost and Median filtering and followed by a textural analysis calculating Gray Level Co-occurrence Matrix (GLCM) statistical parameters (variance, homogeneity and mean) according to Haralick et al. (1973). By means of unsupervised ISODATA classification, the water-covered troughs were derived from the resulting feature images using ERDAS Imagine (version 2013) and ENVI 4.7. Assignment of classes was verified by visual interpretation of the SAR images and in situ data. The shifting distance of the troughs from 2012–2014 was determined along the profile shown in Fig. 5.3-2 to be compared to the lidar data of the same years. To account for the asymmetry of the bedforms observed by Adolph et al. (2016, this special issue), the western edges of the water-covered troughs are used for these measurements.
Fourier analysis

Fourier analysis was applied to investigate the remote sensing datasets for periodicities of the bedform area. The signal was analysed for periodicities in the frequency domain after decomposition of the data into a sum of sine and cosine functions with different amplitude, phase and frequency. The fast Fourier transformation, optimized with regard to efficient computation, was employed as implemented in the Signal Processing Toolbox of MATLAB to 1D profiles used as input data. In a pre-processing step, the lidar height profiles were adjusted for mean and trend to suppress a systematic signal component due to the sloping area and make the height values fluctuate around a zero mean. Mean and trend adjustment was also performed for the RapidEye and the TerraSAR-X data.

Ground-truth

Ground-truth is provided by high-precision height measurements of the bedform surface recorded by Real Time Kinematic Differential GPS (RTK-DGPS) on 04/09/2014 with a Leica Differential-GPS SR530 and AT 502 antenna type. Reference data were supplied by the Satellite Positioning Service SAPOS® of the German land surveying authorities using the High Precision Real-Time Positioning Service SAPOS®-HEPS, with a horizontal accuracy of 1–2 cm and a vertical accuracy of 2–3 cm.

The measurements were carried out at intervals of approx. 2 m (three steps) along transects perpendicularly crossing the bedforms. Five profiles with a total length of 540 m (220, 100, 100, 80 and 40 m) were recorded at higher and lower ranges of the bedform area. Additionally, the troughs defined by the edges of total water cover were documented following the transects 2 h before and after low water.

5.3.4 Results

Bedform detection from lidar, electro-optical and SAR sensor data

The lidar DTM clearly displays the morphology of the bedforms (Fig. 5.3-2) with pixel brightness representing the ground level elevation. The crests are mapped as bright pixel values whereas the troughs can be seen in the darker areas. Main characteristics of the bedforms are demonstrated by height profiles (Fig. 5.3-2 and 5.3-3). Within the profile marked by the red arrow in Fig. 5.3-2, the height differences between crests (local maxima) and troughs (local minima) are about 10– 15 cm (Fig. 5.3-3). The large bedforms with lengths of almost 110 m and heights of nearly 20 cm vary and they are superimposed by small ripples. In general, the area slopes slightly towards the main tidal channel in a southern direction. Classification results for water cover, wet sediment and dry sediment of the RapidEye data from 19 September 2014 are shown in Fig. 5.3-4 (upper image) and can be compared with the NDWI result in Fig. 5.3-4 (lower image). Sediments covered by a water layer (e.g. water-covered trough) are represented by very bright pixels in the NDWI data; darker to black pixel values indicate the gradual transition from wet and moist to relatively dry sediment. In the bedform area, the classification results represent the troughs, slopes and crest areas of the bedforms. The crest area is assumed to be the highest and thus the driest part of the sediment surface. The results show that the NDWI is well suited to visualize the water-filled troughs and the wet and dry sediment of the slopes and the crest areas. The result of the supervised classification method is in good agreement with the NDWI; both patterns are very similar and show the diagonally oriented troughs. In many cases the crest area is located close to the western border of the troughs. Thus, a certain asymmetry of the bedform profiles, which is also visible in the lidar data, is reflected in the electro-optical data due to the differing moisture of the sediments.

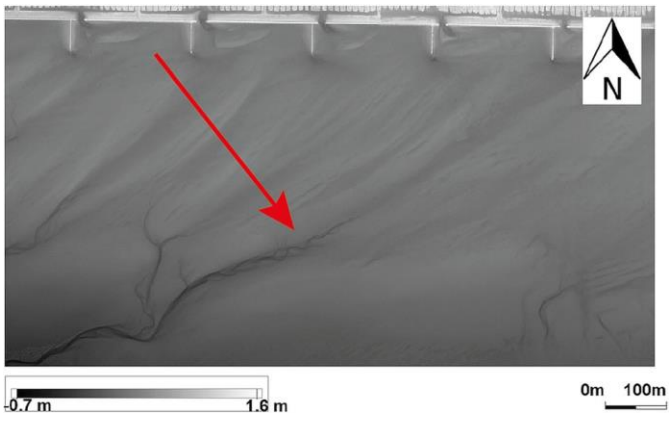

Fig. 5.3-2 DTM of the test site derived from lidar data of 2014, and location of NW–SE directed transect for detailed height and geometry analysis of the bedforms

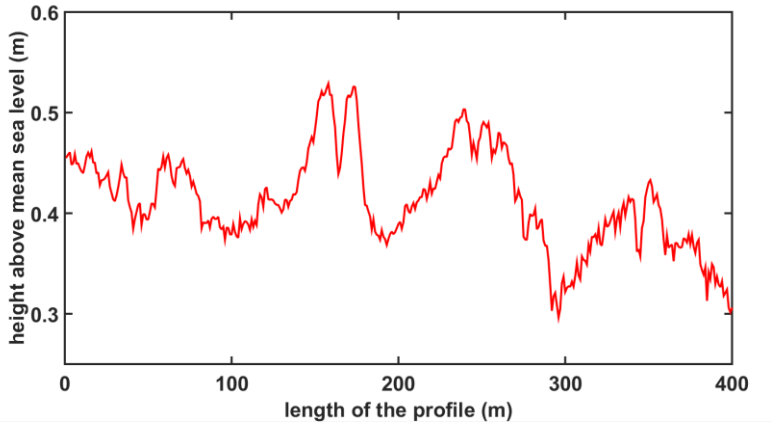

Fig. 5.3-3 Height profile of the lidar data of 2014 along the NW–SE directed transect showing a cross-section of bedform geometry

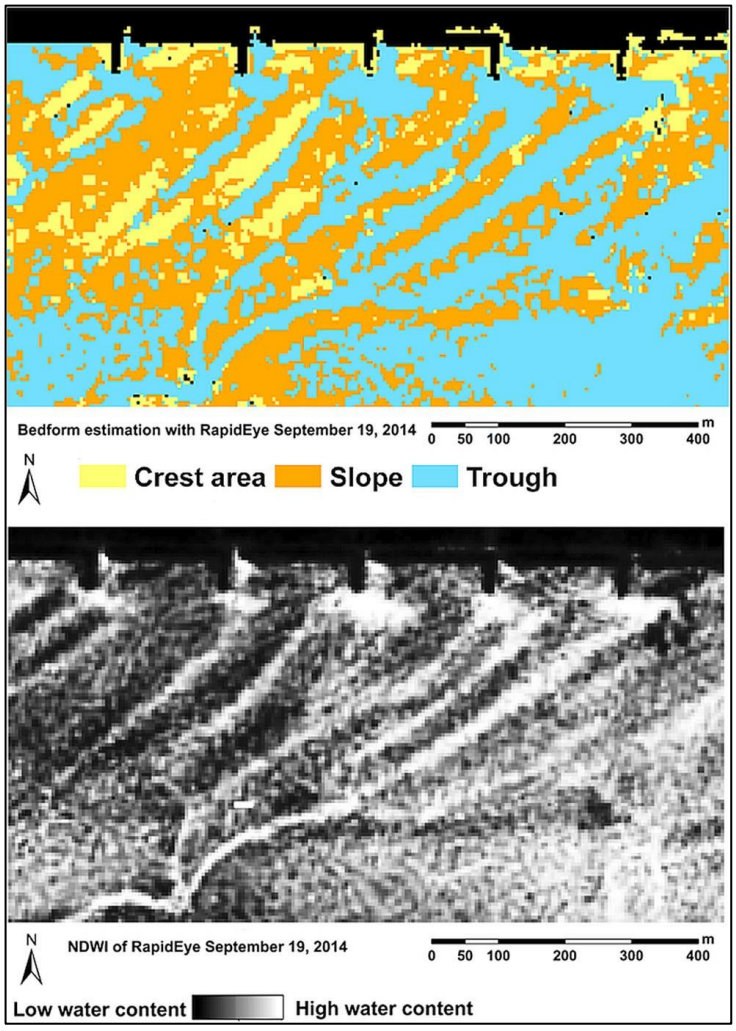

Fig. 5.3-4 Supervised classification of the bedforms (*upper*) compared to NDWI (*lower*), both based on RapidEye data

A detailed analysis of a smaller subset of the test area demonstrates the accuracy of the classification with RapidEye data. Figure 5.3-5 shows the lidar DTM superimposed with the RapidEye classification results and the RTK measurements of water-covered troughs carried out 15 days before image acquisition. While the smallest troughs could not be detected from the RapidEye data by the applied method, the locations of the larger troughs are determined correctly. Regarding the non-water-covered areas, the lidar DTM as well as the RTK-DGPS measurements confirm the classification and interpretation of the driest sediments as representing the highest parts of the bedforms, the crest areas (Fig. 5.3-6).

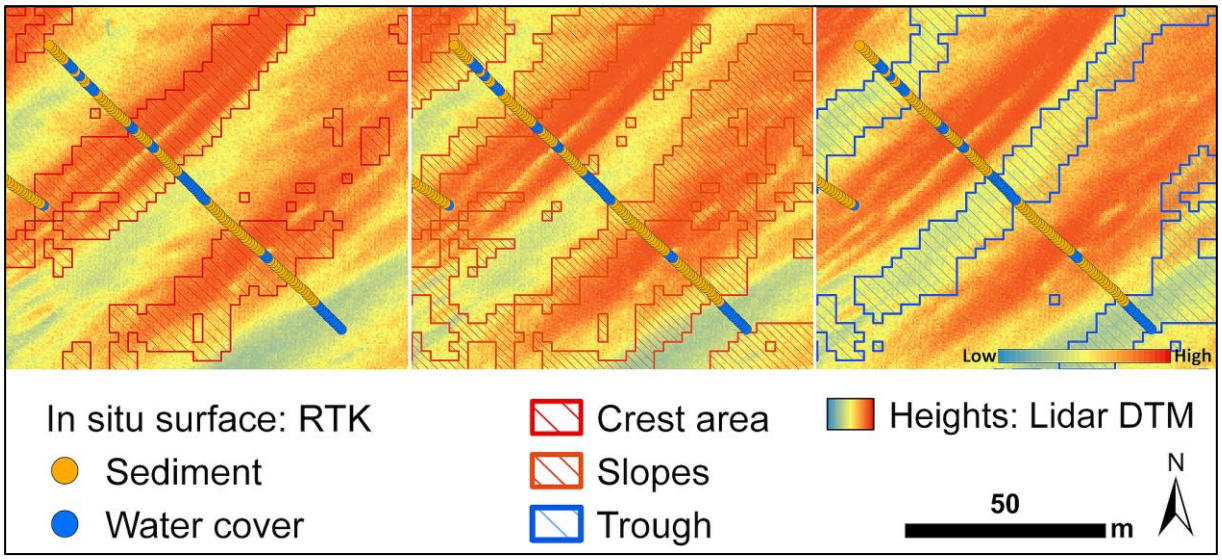

Fig. 5.3-5 Crest area (*left*), slope (*middle*) and trough (*right*) classified from RapidEye data compared to water cover recorded by RTK-DGPS (*profile*) and lidar DTM (*background*)

The classification results for trough detection from TerraSAR-X data are also in good agreement with the visual interpretation of the SAR image and with the positions of the trough edges measured by RTK-DGPS (Fig. 5.3-7). The subset in Fig. 5.3-8 shows the troughs derived from the TerraSAR-X image compared to the ground level elevation of the lidar DTM and the RTK-DGPS measurements. The class "trough" as derived from RapidEye and TerraSAR-X data in most cases is associated with low height values in the lidar DTM, which demonstrates the capability of both sensors and the applied methods to detect the troughs (Fig. 5.3-5 and 5.3-8). Accordingly, the classification results from RapidEye and TerraSAR-X data identify the same trough positions. However, the water-covered troughs based on TerraSAR-X data are more precise in planimetric location and width: the extent of the troughs extracted from the SAR data is more restricted to the central areas of the troughs with total water cover (Fig. 5.3-9). The southern area is free of any bedforms and characterised by wet sediments and water pools.

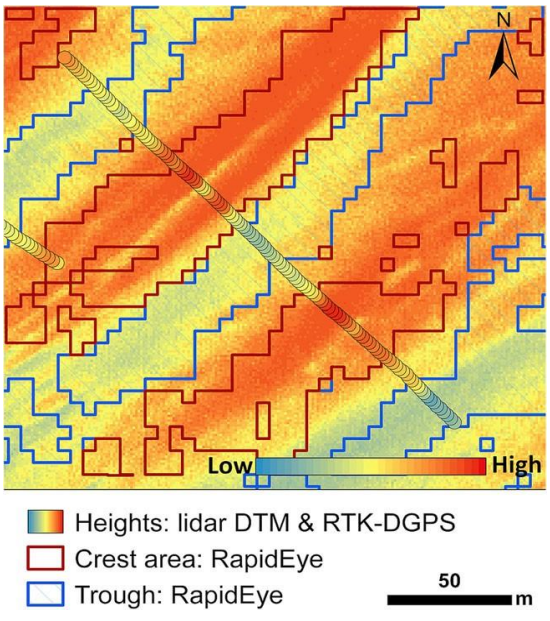

Fig. 5.3-6 Crest area (*red*) and trough (*blue*) classified from RapidEye data compared to ground level elevation from lidar (*background*) and RTK-DGPS (*profile*)

In addition to trough detection, the RapidEye data enable to distinguish different water contents of the sediment by using the NDWI. Thus, the exposed sediment surfaces can be attributed to the classes “crest area” and “slope” which, on the whole, correspond to the lidar and the RTK height data, as the slopes and crest areas are assigned to increasing heights according to the DTM (Fig. 5.3-5 and 5.3-6). A detailed analysis of height profiles, however, reveals that the crest areas cannot always be associated with the highest ground level elevations, which means that in some cases also slope sediments can be dry. For an overview, bedform parameters derived from the different sensor data are listed in Table 5.3-3. Distances are measured between the steep edges of the troughs (western edge) and the crests (eastern edge).

Fig. 5.3-7 Trough extraction (*white lines*) derived from TerraSAR-X data and water edges recorded with RTK-DGPS 6 days before image acquisition (*red dots*)

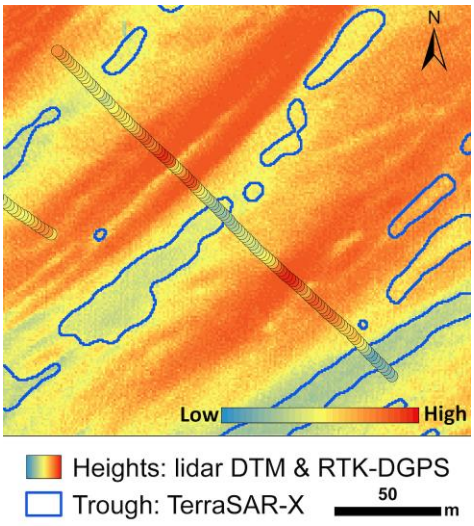

Fig. 5.3-8 Trough detection (*blue lines*) derived from TerraSAR-X data compared to ground level elevation based on lidar (*background*) and RTK-DGPS (*profile*)

Tab. 5.3-3 Bedform parameters based on lidar, RapidEye and TerraSAR-X data

Bedform parameter	Lidar	RapidEye	TerraSAR-X
Height crest C1 (cm)	16	–	–
Height crest C2 (cm)	14	–	–
Height crest C3 (cm)	15	–	–
Distance C1/C2 (m)	93	82	–
Distance C2/C3 (m)	99	94	–
Distance T1/T2 (m)	–	101	99
Distance T2/T3 (m)	–	70	73
Trough width T1 (m)	–	25	11
Trough width T2 (m)	–	18	14
Trough width T3 (m)	–	25	13
Wavelength FFT (m)	110	90	100

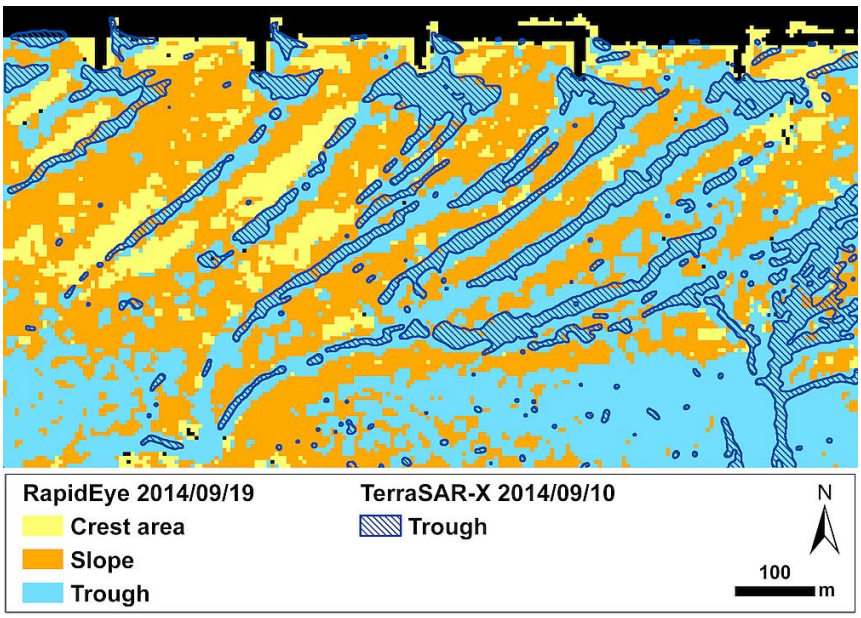

Fig. 5.3-9 Classification of crest area, slope and trough from RapidEye data compared to trough extraction from TerraSAR-X data

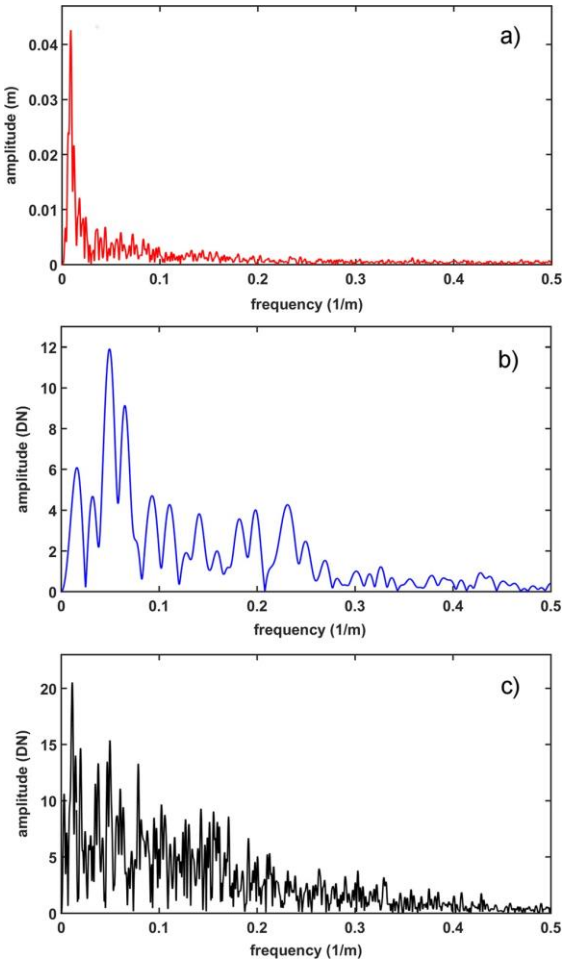

Fig. 5.3-10 Profiles of a) lidar data, b) electro-optical data and c) SAR data in the frequency domain

Fourier analysis

Figure 5.3-10 shows the amplitude of each signal component of the three sets of remote sensing data corresponding to the profile in Fig. 5.3-2. In the high-frequency range, no significant signal components can be detected for any of the sensors. In contrast, the low-frequency components show a significant peak for the lidar data at 0.0090 m^{-1}. In the spatial domain this value corresponds to a period of approx. 110 m. Delineating this period in the DTM demonstrates the good correlation with the input data (Fig. 5.3-11). The peak is less significant in the electro-optical data. However, the data show a maximum at the frequency of 0.0099 m^{-1}, approx. equal to 100 m. The difference between the wavelengths for the profiles of the RapidEye and the lidar data is thus about 10 m. This is probably a result of the lower geometric resolution of the electro-optical data and the fact that the bedforms are less obvious in the spectral data. For the SAR data, the maximal amplitude relates to the frequency of 0.011 m^{-1} or about 90 m. The deviation from the other sensor data is due to the noisy input data (Fig. 5.3-7), which is why the decomposition of the signal into few significant components fails. However, especially for the lidar data the Fourier analysis proves to be a suitable tool for the description of the bedforms.

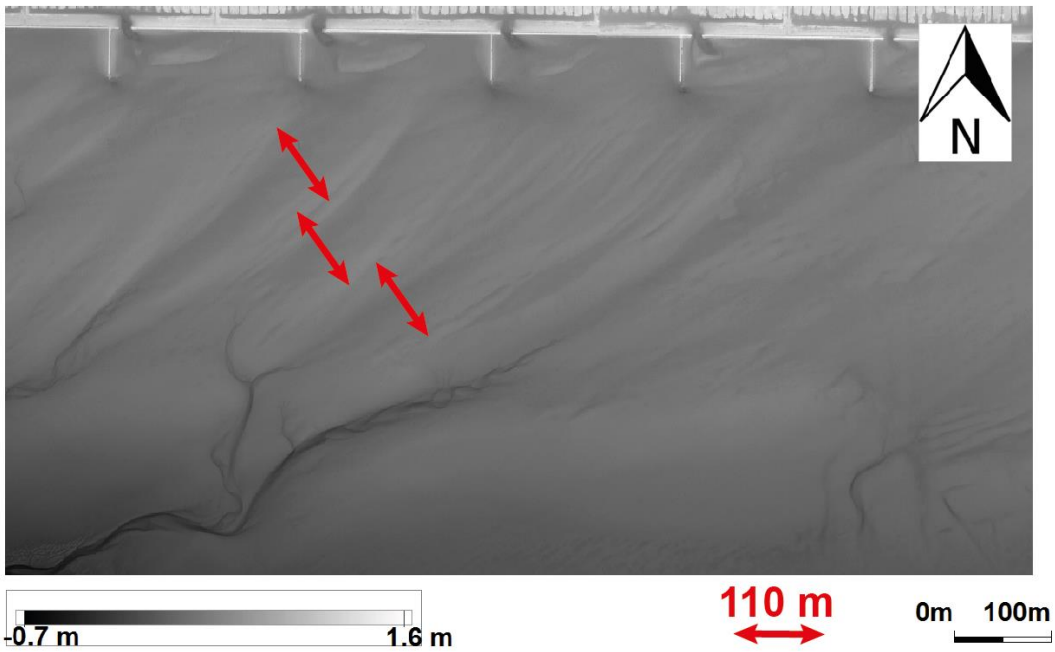

Fig. 5.3-11 Fourier analysis of lidar data showing a significant wavelength of about 110 m

Comparison of bedform migration based on lidar and TerraSAR-X data

As different features are used for bedform detection from lidar (crests) and from TerraSAR-X data (troughs), a comparison serves to assess whether this affects the results on bedform migration. Lidar data from the test site are available for the years 2010, 2012 and 2014. In Fig. 5.3-12 the height profiles corresponding to the transect presented in Fig. 5.3-2 are compared for the three snapshots. Both between 2010–2012 and 2012–2014, a shift of the bedforms can be observed (cf. arrows in Fig. 5.3-12; Table 5.3-4). Three individual bedforms lie along the profile—bedform 1 (crest in 2010 at 110 m of the profile), bedform 2 (crest at 196 m), bedform 3 (crest at 276 m). The troughs east of these crests are defined correspondingly.

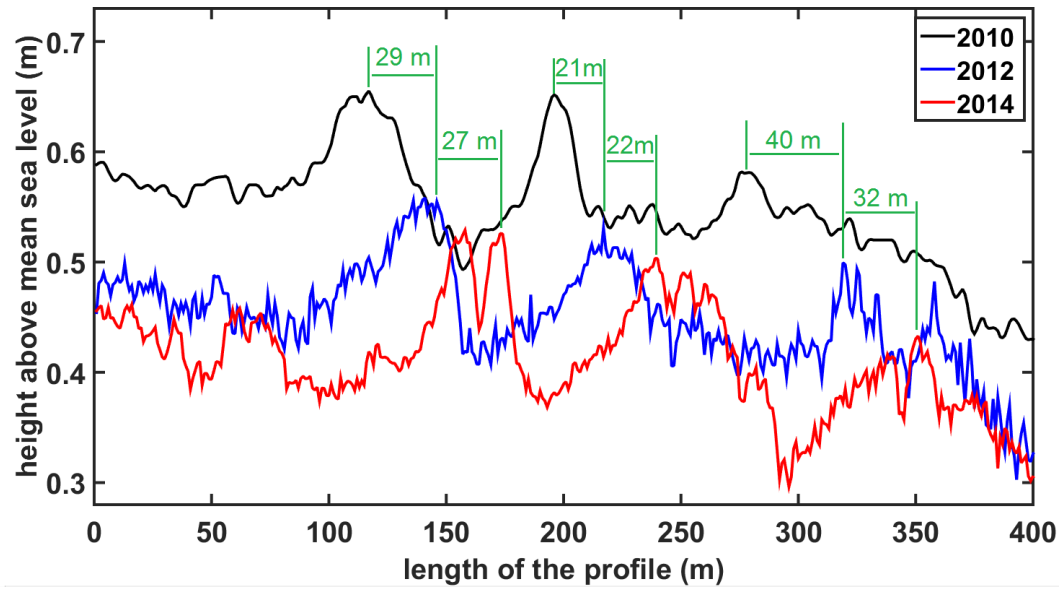

Fig. 5.3-12 Height profiles of lidar data from 2010, 2012 and 2014. The crests shifted from west to east by 21 to 40 m

TerraSAR-X data comparable to the dates of the lidar flights are available for 2012 and 2014. The shift of the bedform positions over this period is reflected by the water-covered troughs extracted from the TerraSAR-X images (Fig. 5.3-13). The positions of the steeper western trough edges in 2012 are at 156 m of the profile for bedform 1, 270 m for bedform 2 and 362 m for bedform 3. The distances of the resulting shifts are given in Table 4. Troughs T1, T2 and T3 show a shifting distance of 31, 20 and 27 m respectively, resembling those of the related crests (27, 22 and 32 m). Comparing the shift of trough edges to that of the crests as a measure for bedform migration, the resulting migration distances of 20–30 m can be regarded as rather similar although determined by completely different methods. For the pair of crest C2 and trough T2, some irregularities are due to the formation of small and shorter depressions, which might be initial or temporary trough-like structures in the space between C2 and T2 (Fig. 5.3-13). As for the profile, this is not counted as a trough.

Tab. 5.3-4 Shifting distances of crests (2010–2012 and 2012–2014) and troughs (2012–2014) along the profile marked in Fig. 5.3-13. Shifting distance of troughs is measured at the western trough edges

	Shift 2010–2012 (m)	Shift 2012–2014 (m)
Crest 1	29	27
Crest 2	21	22
Crest 3	40	32
Trough 1		31
Trough 2		20
Trough 3		27

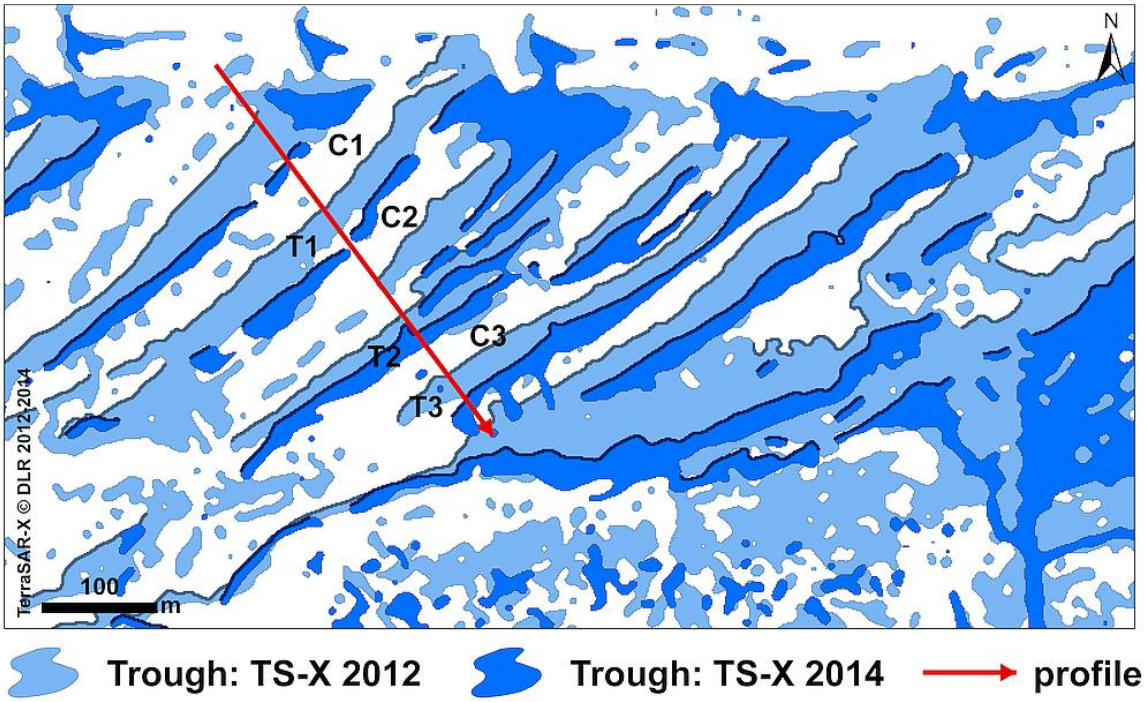

Fig. 5.3-13 Trough positions of 2012 and 2014 derived from TerraSAR-X data and position of lidar height profiles of Fig. 5.3-12 (*red arrow*)

5.3.5 Discussion

This study shows that the employed sensors and methods map the pattern and position of the bedforms consistently. Describing different properties of the intertidal bedforms, the individual results confirm and complement each other. The basic positioning of the bedforms is reflected by the three sensors with good consistency when comparing the trough-to-trough distance derived from TerraSAR-X and RapidEye and the crest-to-crest distance from RapidEye and lidar. The trough-to-trough distance differs by only 2–3 m and the crest-to-crest distance by 5–11 m (Table 5.3-3)—a good result in view only of the difference in the sensors' resolution. Accordingly (Table 5.3-4), bedform migration derived from the shifting distance of the western trough edges as detected by TerraSAR-X corresponds to the relocation of the crests in the lidar profiles. Further studies employing an extended data base may be requested, but these results strengthen the feasibility of bedform tracking with SAR imagery and the integration of data from different sensor systems into combined monitoring schemes.

Compared to the troughs extracted from SAR images, the extent of the area assigned to the class "trough" is clearly larger when RapidEye data are used (Fig. 5.3-9, Table 5.3-3). This results from the difference in spatial resolution (5 vs. 1 m), the classification method (all pixels are assigned to one class) and the transition areas which occur due to the variable moisture content of the sediments. In addition, the high sensitivity of the electro-optical data to moisture results in a blurry discrimination of very wet sediments and sediments covered by water. Very high sediment moisture, for example, results in high NDWI values independently of an existing water layer. The trough extraction from the TerraSAR-X data, in contrast, is solely based on the detection of water-covered surfaces. Figure 5.3-9 clearly shows the different representation of the slight depression in the southern part of the subset in the different sensor data (given the applied methods of classification). As both acquisitions took place in a period of stable weather conditions (but with an offset of 9 days), the exact magnitude of this deviation cannot be determined in this study. Regarding the non-water-covered sediments, on the other hand, electro-optical data like RapidEye imagery contributes to a comprehensive picture by adding spectral information which enables the discrimination of wet/moist and dry sediments. For the sandy bedform area, the dry expanses are most likely to result from the drying of the highest and steepest parts of the ridges, mainly the most distinct crests. For the westernmost bedform ridges, the positions of these dry areas confirm an asymmetry which also shows in the height profile drawn from the lidar data. Thus, by combining the different sensor data, we obtain a coherent overall assessment of the outer appearance of the geomorphic structures in the test area, containing information on the morphology and heights of the sediment surface, and the distribution of sediment moisture and water cover.

The most accurate and direct image of the bedform surface is given by the lidar data, which (with a resolution in the range of decimetres to centimetres) enables to precisely determine the crest positions within the exposed ridges of the bedforms. This facilitates the study of the shape and orientation of the bedforms, which could provide the basis for systematic investigations of, for example, the predominance or spatiotemporal occurrence of symmetric or asymmetric bedform shapes. Analysing a multitude of profiles or 3D data would allow to determine the local directions of bedform migration. Moreover, the lidar data provide absolute elevation: given a correct normalisation of water levels during data acquisition, possible trends of accumulation or erosion can be observed. However, the near-infrared laser pulses used in the systems investigated here cannot penetrate water. Thus, for the water-covered troughs, the lidar height represents the level of the water surface. Unless a water–land classification is carried out, the troughs cannot be detected as precisely as the slope and crest areas of the bedforms. With regard to large regions like the Wadden Sea, airborne acquisition of lidar data is limited by the maximum area the flight route can cover during low tide. Lidar acquisitions take much time and effort and are thus also expensive.

Due to the water cover, the bedform troughs are detected most clearly by TerraSAR-X data. Accuracy of trough detection verified by ground-truth is in the range of 1–2 m depending on pixel size and image qualities (e.g. influence of incidence angle, storm at acquisition time). Being an active sensor like the lidar, SAR is independent of daylight and of cloud cover. The repetition rate of TerraSAR-X is 11 days but images taken from differing orbits can be acquired more frequently so that yearly, seasonal or even shorter time intervals are feasible—e.g. to investigate the effects of high-energy events such as storms or storm surges. Therefore, Adolph et al. (2016, this special issue) were able to study the bedform dynamics over a period of 6 years (2009–2015) using trough detection from TerraSAR-X data showing a general shift of the bedforms from west to east. Indeed, SAR imagery would facilitate future investigations of the distribution and dynamics of intertidal bedform fields—e.g. are bedform dynamics the same at all East Frisian islands, and how stable are the characteristics of the bedform fields?

For Wadden Sea monitoring purposes, SAR imagery from TerraSAR-X can provide frequent acquisitions with a spatial resolution of up to 1.1 m (or 1.7 m) in high-resolution (or spotlight) mode and down to 3.5 m in stripmap mode. One high-resolution image covers an area of 10×5 km (10×10 km for spotlight image), which for Lower Saxony corresponds to the area of about one tidal basin. An image taken in stripmap mode covers 30×15 km for a larger overview and still maps the bedform troughs. Compared to lidar, this overview based on synchronous data presents a significant advantage of TerraSAR-X, or satellite imagery in general. For wider surveys, also larger footprints are available in ScanSAR and ScanSARWide mode, providing swath widths of 100 and 270 km although leading to much coarser resolutions down to 18.5 and 40 m.

While the spatial resolution of RapidEye data (6.5 m) lags behind that of the SAR and lidar sensors, the large spatial coverage (swath width 77 km) is a clear advantage in achieving a simultaneous overview over large areas which may only partly be accessible for ground-truth. Relating to basic monitoring needs rather than to bedform detection, application of spectral data is of importance to investigate the distribution of sediment types or plant cover such as seagrass and algal mats. A significant limitation associated with optical remote sensing is the dependency on daylight and a cloudless sky. The potential repetition rate of RapidEye is only 1 day (off-nadir) due to the constellation of five satellites, but in 2013 the data policy was changed by the data provider. Since that year, Germany is covered by RapidEye only every 45 days, considerably reducing the possibility of obtaining cloud-free images during low tide.

Similar to in situ investigations which may be hindered by limiting factors such as large distances, inaccessible or protected terrains, restricted daylight or the tides, it may be also difficult to achieve synchronous acquisitions by different sensors at the appropriate moment to map the intertidal zone. Adolph et al. (2016, this special issue) have shown that, during exposure, the bedforms slowly drain to a maximum stage defined by a minimum trough width shortly before the next inundation. Maximum waterline regression on the steeper west side of 17 troughs ranged from 0.4 to 1.6 m over nearly the whole exposure time (5 h) and up to 0.8 m over 3 h around low water. This corresponds to only a few centimetres of water level decrease in the troughs. A dependency of trough width variation on tidal gauge or wind speed and wind direction data could not be found (Adolph et al. 2016, this special issue).

In this study, all datasets were acquired within a period of calm and stable weather—the lidar data around low water, the RapidEye and TerraSAR-X data 1 h before and 40 minutes after low water respectively at a 9 day interval. On the one hand, this is quite close for satellite remote sensing. Thus, regarding the weather conditions, the acquisition dates are not expected to measurably influence the comparison. The lidar data are not much affected by sediment moisture, and trough extraction from TerraSAR-X data only concerns approx. 100% water cover. The electro-optical data, on the other hand,

are highly sensitive to sediment moisture. Even with a fast-drying sediment of fine sands (2–3 phi), the exact conditions of sediment moisture and water cover might not be directly comparable between the acquisition dates of TerraSAR-X and those of RapidEye. Trough areas detected from RapidEye data might also generally be wider than SAR-detected troughs because of a more gradual perception of moisture and the coarser resolution of the RapidEye data. These differences have no effect on the general position of the bedforms but should be considered when interpreting the data. For a quantitative comparison and assessment, extensive in situ measurements adapted to the resolutions of the different sensors would be necessary. For monitoring purposes, however, acquisition time as late as possible after low water and closest to inundation is recommended.

For the monitoring of geomorphic structures and habitats of the intertidal zone of the Wadden Sea as well as for long-term ecological research, however, the sensors should be used in a way that ensures the regular surveying of the entire area while obtaining all information needed at minimum expense. This leads to a spatially and temporally structured concept combining the advantages of the respective sensor classes according to the footprint area and the resolution, frequency and costs of acquisition. Regarding the example of intertidal bedforms, a basic overview could be achieved by lidar data—e.g. every 5 to 10 years, the lidar flights performed regularly by the local authorities could be employed. The yearly or seasonal migration of the troughs can be surveyed using a series of SAR images. The combination of lidar data and more frequently acquired SAR images also allows to identify the crests corresponding to the troughs in the lidar data even if these are taken at intervals of years. Although the electro-optical RapidEye data cannot be scheduled as reliably as the data of active sensors like lidar or SAR, one or two images in between the lidar flights would provide a large overview of the distribution of troughs and crest areas, covering more than twice the size of a TerraSAR-X stripmap image.

Besides monitoring purposes, the remote sensing data presented in this study can support systematic investigations of the driving forces governing the origin and dynamics of intertidal bedforms. To this end, remote sensing data should be combined with ground-truth such as sedimentological in situ studies. For smaller study areas, the lidar data or, alternatively, high-quality ortho-images can also be provided by drones with higher temporal availability. The fusion of different sensor data has lead to promising approaches for a synergistic classification of intertidal habitats (e.g. Stelzer et al. 2010; Gade et al. 2014; Jung et al. 2015). The conceptual combination of remote sensing data with differing spatial or temporal advantages presented in this study likewise enables the investigation of the intertidal zone due also to a more flexible supply of data.

Continuing advances in satellite and sensor technology are to be expected. For further investigations on the use of satellite remote sensing as an input for Wadden Sea monitoring, the ESAs Sentinel fleet and their open data policy (amongst others) could ensure that SAR data as well as electro-optical data would continue to be available. To what extent the individual satellites and sensor systems are suitable for general and special tasks in monitoring the Wadden Sea has to be investigated. For example, the bedforms are reproduced by vertically co-polarised acquisitions of Sentinel-1 but, with a resolution of 10 m, the trough extraction would have to be adapted and it is arguable whether this resolution would be sufficient to detect smaller or even larger bedform shifts. Sentinel-2, however, can replace the RapidEye data and could even improve their use, as demonstrated recently by Jung and Ehlers (2016) for the most usable wavelengths retrieved from hyperspectral data. Most of the wavelength ranges are covered by Sentinel-2, which is not the case for RapidEye. In general, the adaptation of these new techniques for monitoring concepts is challenging but also an advantage for monitoring and research.

5.3.6 Conclusions

The pros and cons of three remote sensing methods applied to intertidal bedforms as an example for the monitoring or long-term research of Wadden Sea surface structures show that all these methods are able to reproduce the bedforms in general. Differences exist in the resolution, coverage and temporal availability as well as the cost of data acquisition.

Lidar is most precise with clear indications of crests and slopes but is limited in space and time and is expensive. TerraSAR-X reproduces the positions of troughs in a high quality, especially the western waterlines adjoining the steep slopes in the present study area. Together with the high temporal availability, the area charted and moderate expenses, SAR imagery should be preferred for monitoring as well as studies on bedform migration and effects of single events. Detailed information about crests and slopes cannot be obtained by this method. From the RapidEye sensor, additional information on the sediment can be obtained, especially the water content (dry, moist, water-covered), and the area recorded encompasses nearly the whole Lower Saxony Wadden Sea in the present case. The main advantage of the electro-optical approach, i.e. the spectral information obtained by the high number of separate wave length measurements, is of minor importance for bedform records but of substantial importance for other structures and habitats such as vegetation, diatoms and algal mats.

Acknowledgements

This study forms part of the interdisciplinary research project "Wissenschaftliche Monitoringkonzepte für die Deutsche Bucht – WIMO" ("Scientific Monitoring Concepts for the German Bight"), jointly funded by the Ministry for Environment, Energy and Climate Protection and the Ministry for Science and Culture of the Federal State of Lower Saxony. The authors thank the German Aerospace Centre (DLR) for delivering an extensive set of TerraSAR-X images relating to Proposal ID COA1075 and the Lower Saxony State Department for Waterway, Coastal and Nature Conservation (NLWKN) for providing lidar data. Also acknowledged are constructive assessments by V.B. Ernstsen and an anonymous reviewer.

5.3.7 References

Adolph W, Schückel U, Son CS, Jung R, Bartholomä A, Ehlers M, Kröncke I, Lehner S, Farke H (2016) Monitoring spatiotemporal trends in intertidal bedforms of the German Wadden Sea in 2009–2015 with TerraSAR-X, including links with sediments and benthic macrofauna. Geo-Mar Lett 37 (in press). doi:10.1007/s00367-016-0478-y

Airbus Defence & Space (2014) Radiometric calibration of TerraSAR-X Data. Beta Naught and Sigma Naught coefficient calculation. Airbus Defence & Space, TSXX-ITD-TN-0049-radiometric_calculations_I3.00.doc

Aubert M, Baghdadi N, Zribi M, Douaoui A, Loumagne C, Baup F, El Haji M, Garrigues S (2011) Analysis of TerraSAR-X data sensitivity to bare soil moisture, roughness, composition and soil crust. Remote Sens Environ 115(8):1801–1810. doi:10.1016/j.rse.2011.02.021

BlackBridge (2013) Satellite imagery product specifications. BlackBridge. Accessed 25 November 2013. http://blackbridge.com/rapideye/upload/RE_Product_Specifications_ENG.pdf

BlackBridge (2015) http://www.blackbridge.com/rapideye/upload/RE_Product_Specifications_ENG.pdf

Choe B-H, Kim D-J, Hwang J-H, Oh Y, Moon WM (2012) Detection of oyster habitat in tidal flats using multi-frequency polarimetric SAR data. Estuar Coast Shelf Sci 97:28–37. doi: 10.1016/j. ecss.2011.11.007

Decho AW, Kawaguchi T, Allison MA, Louchard EM, Reid RP, Stephens FC, Voss KJ, Wheatcroft RA, Tyloe BB (2003) Sediment properties influencing upwelling spectral reflectance signatures: the "biofilm gel effect". Limnol Oceanogr 48(1):431–443. doi:10.4319/lo.2003.48.1_part_2.0431

Dehouck A, Lafon V, Baghdadi N, Marieu V (2012) Use of optical and radar data in synergy for mapping intertidal flats and coastal salt-marshes (Arcachon lagoon, France). In: IGARSS 2012 I.E. Int Geoscience and Remote Sensing Symp, Munich, Germany, pp 2853–2856. doi:10.1109/IGARSS.2012.6350837

European Commission (1992) Council Directive 92/43/EEC of 21 May 1992 on the conservation of natural habitats and of wild fauna and flora. Off J Eur Communities, L 206, 22.07.1992, pp 1–66

European Commission (2000) Directive 2000/60/EC of the European Parliament and of the Council of 23 October 2000 establishing a framework for Community action in the field of water policy. Off J Eur Communities, L 327, 22.12.2000, pp 1–72

European Commission (2008) Directive 2008/56/EC of the European Parliament and of the Council of 17 June 2008 establishing a frame-work for community action in the field of marine environmental policy (Marine Strategy Framework Directive). Off J Eur Communities, L 164, 25.6.2008, pp 19–40

Gade M, Alpers W, Melsheimer C, Tanck G (2008) Classification of sediments on exposed tidal flats in the German Bight using multi-frequency radar data. Remote Sens Environ 112(4):1603–1613. doi:10.1109/IGARSS.2012.6350837

Gade M, Melchionna S, Stelzer K, Kohlus J (2014) Multi-frequency SAR data help improving the monitoring of intertidal flats on the German North Sea coast. Estuar Coast Shelf Sci 140:32–42. doi:10.1109/IGARSS.2012.6350837

Gade M, Melchionna S, Kemme L (2015) Analyses of multi-year synthetic aperture radar imagery of dry-fallen intertidal flats. Int Arch Photogramm Remote Sens Spat Inf Sci XL-7(W3):941–947. doi:10.5194/isprsarchives-XL-7-W3-941-2015

Haralick RM, Shanmugam K, Dinstein I (1973) Textural features for image classification. IEEE Trans Syst Man Cybern 3(6):610–621. doi:10.1109/TSMC.1973.4309314

Heygster G, Dannenberg J, Notholt J (2010) Topographic mapping of the German tidal flats analyzing SAR images with the waterline method. IEEE Trans Geosci Remote Sens 48(3):1019–1030. doi:10.1109/TGRS.2009.2031843

Ibrahim E, Adam S, van der Wal D, De Wever A, Sabbe K, Forster R, Monbaliu J (2009) Assessment of unsupervised classification techniques for intertidal sediments. eProc EARSeL 8:158–179, doi:10.1.1.535.1691

Jung R, Ehlers M (2016) Comparison of two feature selection methods for the separability analysis of intertidal sediments with spectrometric datasets in the German Wadden Sea. Int J Appl Earth Obs Geoinf 52:175–191. doi:10.1016/j.jag.2016.06.009

Jung R, Adolph W, Ehlers M, Farke H (2015) A multi-sensor approach for detecting the different land covers of tidal flats in the German Wadden Sea – a case study at Norderney. Remote Sens Environ 170: 188–202. doi:10.1016/j.rse.2015.09.018

Kim D-J, Choe B-H, Moon WM (2013) Remote sensing of oyster reefs and groundwater discharge in coastal area using synthetic aperture radar. In: IEEE/GRSS (ed) Proc IEEE Int Geoscience and Remote Sensing Symp (IGARSS), 21–26 July 2013, Melbourne, Australia. Institute of Electrical and Electronics Engineers, Piscataway, NJ, pp 2435–2438. doi:10.1109/IGARSS.2013.6723312

Lee Y-K, Park J-W, Choi J-K, Oh Y, Won J-S (2012) Potential uses of TerraSAR-X for mapping herbaceous halophytes over salt marsh and tidal flats. Estuar Coast Shelf Sci 115:366–376. doi:10.1016/j.ecss.2012.10.003

Li Z, Heygster G, Notholt J (2014) Intertidal topographic maps and morphological changes in the German Wadden Sea between 1996–1999 and 2006–2009 from the waterline method and SAR images. IEEE J Sel Top Appl Earth Obs Remote Sens 7(8):3210–3224. doi:10.1109/JSTARS.2014.2313062

Manakos IK, Manevski C, Kalaitzidis S, Edler D (2011) Comparison between FLAASH and ATCOR atmospheric correction modules on the basis of WorldView-2 Imagery and in situ spectroradiometric measurements. In: EARSeL 7th SIG-Imaging Spectroscopy Workshop, Edinburgh

Mason DC, Scott TR, Dance SL (2010) Remote sensing of intertidal morphological change in Morecambe Bay, U.K., between 1991 and 2007. Estuar Coast Shelf Sci 87(3):487–496. doi:10.1016/j. ecss.2010.01.015

Matthew MW, Adler-Golden SM, Berk A, Felde G, Anderson GP, Gorodetsky D, Paswaters S, Shippert M (2002) Atmospheric correction of spectral imagery: evaluation of the FLAASH algorithm with AVIRIS data. In: Proc 31st Applied Imagery Pattern Recognition Workshop From Color to Hyperspectral: Advancements in Spectral Imagery Exploitation, Washington, pp 157–163. doi:10.1109/AIPR.2002.1182270

Moreira A, Prats-Iraola P, Younis M, Krieger G, Hajnsek I, Papathanassiou KP (2013) A tutorial on synthetic aperture radar. IEEE Geosci Remote Sens Mag 1(1):6–43. doi:10.1109/MGRS.2013.2248301

Müller G, Stelzer K, Smollich S, Gade M, Adolph W, Melchionna S, Kemme L, Geißler J, Millat G, Reimers H-C, Kohlus K, Eskildsen K (2016) Remotely sensing the German Wadden Sea—a new approach to address national and international environmental legislation. Environ Monit Assess 188(10):595. doi:10.1007/s10661-016-5591-x

Niedermeier A, Hoja D, Lehner S (2005) Topography and morphodynamics in the German Bight using SAR and optical remote sensing data. Ocean Dyn 55(2):100–109. doi:10.1007/s10236-005-0114-2

Nieuwhof S, Herman P, Dankers N, Troost K, van der Wal D (2015) Remote sensing of epibenthic shellfish using synthetic aperture radar satellite imagery. Remote Sens 7(4):3710–3734. doi:10.3390/rs70403710

Rainey MP, Tyler AN, Bryant RG, Gilvear DJ, McDonald P (2000) The influence of surface and interstitial moisture on the spectral characteristics of intertidal sediments: implications for air-borne image acquisition and processing. Int J Remote Sens 21(16):3025–3038. doi:10.1080/01431160050144938

Ryu J-H, Eom JA, Choi J-K (2010) Application of airborne remote sensing to the surface sediment classification in a tidal flat. In: 2010 I.E. Int Geoscience and Remote Sensing Symp (IGARSS), pp 942–945. doi:10.1109/IGARSS.2010.5653413

Schmidt A, Rottensteiner F, Soergel U (2013) Water-land-classification in coastal areas with full waveform lidar data. PFG 2:71–81

SCOP-WWW (2001) Institute of Photogrammetry and Remote Sensing, Vienna University of Technology. http://www.ipf.tuwien.ac. at/produktinfo/scop/scopdtmsheet.htm

Small C, Steckler M, Seeber L, Akhter SH, Goodbred S, Mia B, Imam B (2009) Spectroscopy of sediments in the Ganges-Brahmaputra delta: spectral effects of moisture, grain size and lithology. Remote Sens Environ 113:342–361.doi:10.1016/j. rse.2008.10.009

Sørensen TH, Bartholdy K, Christiansen C, Pedersen JBT (2006) Intertidal surface type mapping in the Danish Wadden Sea. Mar Geol 235:87–99. doi:10.1016/j.margeo.2006.10.007

Stelzer K, Geißler J, Gade M, Eskildsen K, Kohlus J, Farke H, Reimers HC (2010) DeMarine Umwelt: Operationalisierung mariner GMES-Dienste in Deutschland. Integration optischer und SAR Erdbeobachtungsdaten für das Wattenmeermonitoring. Jahresbericht 2009–2010, pp 37–55

Van der Wal D, Herman PMJ (2007) Regression-based synergy of optical, shortwave infrared and microwave remote sensing for monitoring the grain-size of intertidal sediments. Remote Sens Environ 111(1): 89–106. doi:10.1016/j.rse.2007.03.019

Van der Wal D, Herman PMJ, Wielemaker-van den Dool A (2005) Characterisation of surface roughness and sediment texture of intertidal flats using ERS SAR imagery. Remote Sens Environ 98(1):96– 109. doi:10.1016/j.rse.2005.06.004

Wiehle S, Lehner S (2015) Automated waterline detection in the Wadden Sea using high-resolution TerraSAR-X images. J Sens 2015: 450857. doi:10.1155/2015/450857

Winter C, Herrling G, Bartholomä A, Capperucci R, Callies U, Heipke C, Schmidt A, Hillebrand H, Reimers C, Bremer P, Weiler R (2014) Scientific concepts for monitoring the ecological state of German coastal seas (in German). Wasser und Abfall 07-08/2014:21–26. doi:10.1365/s35152-014-0685-7

6 Summary and Assessment of Findings

By investigation of more than 100 acquisitions from a period of seven years (2009–2016), the attempt for a comprehensive assessment of the potential of TerraSAR-X data to monitor tidal habitats and macrostructures was made.

6.1 Image Analysis

With regard to image analysis, initial tests have shown that mere statistical analysis of backscatter values such as brightness, mean value, amplitude or variance were not sufficient to significantly identify and distinguish the different tidal habitats and surface structures. Moreover, grouping the images according to geometry of acquisition for reasons of comparability also reduced the data basis. It soon became very clear that more of the properties contained in the image information had to be used for interpretation. In general, the challenges are extremely high to a valid classification of the various and permanently variable intertidal surface types which are continuously influenced by tidal dynamics, wind effects or biological processes. Very likely, a whole series of specific classification procedures will have to be developed for future automated interpretation of the SAR data from the tidal Wadden Sea. In the studies presented here, visual image analysis proved to be effective as a non-specific and generic approach to recognize a multitude of different tidal surfaces, taking into account not only backscatter intensity and contrast but also shapes, spatial configuration, patterns of internal structures and textures of the reflected surfaces. In an iterative process as already described by Albertz (2009), also context information such as environmental data (i.a. weather and gauge level data) and in particular the extensive in situ data specifically collected for this purpose contributed significantly to the interpretation process. Particularly noteworthy in this context are in situ data recorded synchronously with the acquisition of the satellite images, which contributed enormously to the understanding of imaging properties of the sensor. Based on these findings, such an iterative approach with regular reviews based on current terrain data is highly recommended for future development of automated classification procedures.

Referring to the available products of the TerraSAR-X itself, data collected in SpotLight (SL) and in High Resolution SpotLight (HS) mode proved most suitable to investigate typical intertidal habitats and large-scale surface structures. Both products have the same slant range resolution of 1.2 m while the azimuth resolution is 1.7–3.4 m for SL and 1.1–2.2 m for HS respectively. The scene sizes are technically defined to 10 km x 10 km (width x length) for the SpotLight and to 10 km x 5 km for High Resolution SpotLight. For the research carried out here, the compromise that needs to be made in gathering (satellite) data between the required spatial resolution and the footprint coverage is best met with these products. The StripMap mode (SM) with a standard scene size of 30 km x 50 km (acquisition length extendable up to 1 650 km) offers a somewhat lower azimuth resolution of 1.7–3.4 m. In these studies, the higher resolution offered by HS and a little less pronounced by SL mode facilitated the visual interpretation process, if it did not make it possible at all. Only with sufficient spatial resolution, perceptible details given by internal patterns or textures of the tidal surface types are transmitted. On the other hand, the footprint even of images taken in High Resolution SpotLight mode covers about the area of a tidal basin, a sub-unit of the Wadden Sea which was used in this study to fundamentally map the essential tidal habitats and large-scale structures. The even higher resolution of up to 0.25 m provided by Staring SpotLight mode (ST) since 2013 would result in a footprint area of only 4 km x 3.7 km depending on incidence level. With regard to an area-wide monitoring of the Wadden Sea however, this compromise indicates the potential for further development in SAR sensor technology.

An extensive set of TerraSAR-X data, including detailed time series and recordings before and after extreme events such as storms, storm tides or ice drift could be obtained during the investigations.

Data acquisition was tied to a narrow time slot related to low water time, therefore varying orbits and incidence angles had to be accepted. In general, the visual interpretation of the SAR data turned out to be quite robust with respect to changing geometries of acquisition but a basic trend from stronger contrasts to more and more differentiated backscatter differences is to be mentioned for increasing angles of incidence. For most intertidal surface types, collection at incidence angles between 30–47° is to be considered most suitable: Differentiated backscatter intensities allow for a good distinction even of rough or otherwise strongly backscattering surfaces such as mussel beds, humpy mud fields or steep sandy slopes. Internal structures can well be recognized as well as fine structures of the sediment surface. Water surfaces appear predominantly uniform and darker than the emerged intertidal area and both can be quite well distinguished. Yet, for specific questions smaller or higher incidences can be useful. In near range, at incidence angles < 24° e.g. contrasts are extremely sharp and any roughness of the water surface is highlighted, so that eddies and currents can clearly be seen, especially when surface-active agents are present. At incidences higher that 50° on the other hand, the differentiation of backscatter intensity becomes increasingly finer, transitions become more and more fluent, and contours become less distinct. Taking these differences into account would be of advantage also in the development of automatable classification methods, e.g. in the separation of water-covered areas from exposed areas.

6.2 Determination of Habitats and Geomorphic Surface Structures from the TerraSAR-X Data

In the course of the investigations different habitats and large-scale surface structures characterizing the tidal flats have been visually identified and analyzed from the TerraSAR-X data so that characteristic elements essentially structuring the area of the tidal basin of Norderney can be described. Two principles of perception can be distinguished: Due to outstanding surface roughness, specific patterns and textures mussel beds and fields of shell detritus are successfully recognized. The same holds for edges and steep slopes of channels, gullies and of high sandflats, especially those inclined towards the sensor. Other tidal structures, mostly of geomorphological origin and predominantly rather inconspicuous, are specifically reproduced due to the contrast of water and sediment surface reflected in the SAR data. This refers to residual water caught in depressed areas, any kind of drainage systems or the troughs which in turn mark the intertidal bedforms. On the other hand and most obvious, recognition of water level lines enables to distinguish between exposed flats and sub-littoral areas at low water time or, more generally, areas flooded and submerged in the course of the tides.

6.2.1 Mussel Beds

Mussel beds are a focus of attention in the Wadden Sea due to the environmental key role of mussels as an ecosystem engineer on the one hand, and their importance for fisheries on the other. As an example, annual surveys on mussel beds are required under a mussel management plan. Intertidal settlements of Blue Mussels (*M. edulis*) associated with Pacific Oysters (*M. gigas*) form solid structures surmounting the sediment surface which makes them seem almost predestined for monitoring with SAR data. The mussels and the even larger oysters, which often grow upright effectuate a pronounced roughness of the surface resulting in a high backscatter reflected in the SAR images. In fact, the mussel beds and their various forms of appearance are characteristically depicted by the sensor and can be easily recognized. An essential feature of identification is provided by the internal structures that develop in mature mussel beds: More or less elevated areas actually populated by the bivalves form an organic pattern with free interspaces and flood ponds. This pattern is reflected in the SAR data accordingly. Young mussel beds, on the other hand, cause an evenly textured backscatter as they are formed relatively homogeneously by Blue Mussels or mussel patches – oysters usually settle most of

such beds during the following years. Visual recognition of mussel beds in the SAR images was highly correlated with the results of in situ surveys and with current monitoring results obtained from aerial photography.

Yet, in some cases visual interpretation is hampered by a risk of misinterpretation. In the example of the mussel beds, fields of shell detritus can give rise to confusion. They may show a similarly high backscatter in the SAR data but not the internal structures indicating the mussel beds. Slight differences in backscatter and texture are gradual and vary, therefore shell detritus could be taken for dense mussel bed areas or for young beds of Blue Mussels. This also applies to strongly backscattering features such as steeply sloping high sands inclined to the sensor or even very humpy mud flats. If such cases cannot be clarified by contextual information, e.g. by a typical location of the surface type or a comparison with data acquired with other geometry, in situ data is required for identification. The further development of clearly identified surfaces that differ well from their direct surroundings can then be observed with relatively little effort using the SAR data.

6.2.2 Sediment Composition

Another topic of great importance for monitoring is sediment composition of tidal flats. Especially in view of rising sea levels, and in particular of increasing flow velocities and number of extreme events, the effects on the sedimentary conditions in the Wadden Sea have to be observed carefully. Sediment grain size of course could not be obtained from visual interpretation of the SAR data but at least some reference points can be drawn from the images.

One example is given by the detection of mud fields characterized by a sediment surface varying from wavy to humpy interspersed with extremely dense and highly branched gully structures and puddles of residual water. The mixture of these properties leads to a specific reproduction of the mud field in the SAR images which is characterized by a high backscatter and the recognizable texture created by the gullies and the puddles. The mud field studied in detail in this study, is located close to the watershed of the tidal basin of Norderney, it was several hundred meters wide and had a length of 1.8 km. Due to its position between the Riffgat channel and a large depression mostly holding residual water, the detection of the mud field´s contours was facilitated, resulting in very high agreement of the interpretation results with in situ GPS measurements. Therefore, the extent of the field could be observed through the seasons and over the years. Similar mud fields of different sizes were also found in the tidal basins of the other East Frisian Islands. Regarding the mud field in the Norderney basin, it was shown that the humpy surface was more pronounced during the calmer season of the year than after the stormy time of winter. At the same time, a regular decrease of the width of the mud field surface in the winter season was found during the observation period 2011–2015. Based on these dynamics, conclusions can also be drawn i.a. on the range of hydrodynamic forces which have an effect on the sedimentation conditions.

Hints at sediment composition of tidal flats can also be drawn from assessment of channel network features: The meandering and branching patterns, the density and complexity of tidal creeks and gullies in muddy areas differ considerably from those observed in areas with coarser sediments. Analyses of this kind allow at least qualitative statements, however, they seem quite suitable for automated procedures.

6.2.3 Tidal Channels, Gullies and Water Level Lines

It has been demonstrated, that channels and gullies are well captured by visual interpretation of TerraSAR-X imagery. Detection depends on their width, on the slope and inclination of the edges and on the water-level within the tidal course. Contours of water-filled channels are marked by the

waterline, whereas smaller and dry-fallen gullies are imaged by the backscatter of their edges, especially the steep edges and erosion banks. Stability and relocation of tidal creeks have been shown as an example for a section in which the channel shifted locally by a maximum of 100 m from 2009–2012. The branching arms located higher up on the flats by contrast, largely remained stable. Apart from shedding light on morphodynamic processes constantly forming the characteristic Wadden Sea landscape, such observations of tidal channel dynamics are also valuable again with regard to climate change-induced alteration of hydrodynamics in the Wadden Sea area.

The same applies to the potential of SAR data to detect water level lines. Various in situ GPS measurements performed during the investigations have confirmed that they are imaged accurately and reliably. As described in chap. 3.2.3, automated detection methods have already been developed though they may need to be adapted for use in the Wadden Sea. With their application and further development, not only mudflats and their relocations can be mapped, but also the ratio of intertidal area to sublittoral area at given low water level can be determined which represents an important measure to assess the ability of tidal flats to adapt to rising water levels.

6.2.4 Intertidal Bedforms

In the course of the investigations, special attention was paid to the detection of geomorphic structures, which are indirectly mapped in the TerraSAR-X data via their correlation with residual water trapped in cavities. The collected SAR data showed, that large areas of the sandy upper back-barrier tidal flats of the East Frisian Islands are characterized by periodic bedforms, that is, patterns of long-stretched crests alternating with water-covered troughs. The differences in surface roughness between the sediment surface and the water surface enabled a clear identification of the water-covered troughs. Basically, the distinction of water cover from exposed sediment is predominantly clear, irrespective of the variable appearance the water surface may display in different acquisitions due to environmental influences. When looking at residual water however, the separation is made even easier because these water surfaces are not affected by currents or swell and often they are relatively sheltered from the wind. As a result, the relatively smooth and undisturbed water surface of the bedform troughs is displayed in the SAR images with very low backscatter intensity. By this means, the orientation and length of the bedforms, their distance from each other and the size of the entire bedform area could be determined on the basis of the SAR data, verified by in situ GPS measurements. In general, the bedforms were oriented in a north-easterly direction, the exact dimensions varied from island to island. These bedforms, determination of bedform position and their dynamics have been investigated in detail within the main study area at Norderney.

Around low tide, the residual water caught in the troughs is not directly connected to tide level and from in situ measurements as well as from analysis of the TerraSAR-X data only a slight loss of water cover was observed during exposition time of the bedforms, which will not affect detection of the bedform positions in general. To be sure, SAR data was taken at maximum drained situation during the two hours after low tide. Additionally, variations primarily affected the position of the eastern trough edges that turned out to be more gently sloped than the western edges which was confirmed by high-precision RTK-DGPS measurements. Consequently, the steeper western trough edges, whose positions in the SAR images are hardly affected, were used as a measure of the bedform position in the spatiotemporal analyses of bedform positions.

The documented bedform asymmetry implies the formation of stoss sides and lee sides as a sign of sediment transport. It supports the notion that the bedforms visually observed in the SAR data were migrating which explicitly motivated further investigation (see Publication II, chap. 5.2). Studies of the

sedimentary structure of the bedforms carried out by Dr. Son 2013–2014 (during a fellowship at Hanse-Wissenschaftskolleg, Delmenhorst) revealed a general subdivision into two facies within a depth of 30 cm. An intensively bioturbated lower part was overlain – with a sharp boundary – by a cross-bedded upper part which also suggests sediment reworking and most likely bedform migration. Overall, the bedforms are composed mainly of fine sand.

Evidence for direct ecological implications of the bedforms were found by Dr. Schückel (WIMO cooperation partner "Senckenberg am Meer") who assessed possible differences in macrofaunal species composition and community structure among and between crest and trough areas by means of multivariate analyses. Despite a large overlap of dominant species, significant differences between crest and trough areas have been discovered which can be related to differing exposure time and differing feeding preferences of the species. However, more detailed information on this topic would require more extensive samples to be taken and evaluated.

6.3 Observing Dynamics of Intertidal Features and Areas

6.3.1 Bedform dynamics

For spatiotemporal analyses of bedform dynamics, 41 TerraSAR-X scenes taken from 2009–2015 were collected to capture seasonality of bedform dynamics and effects of storm events as well as inter-annual developments. To evaluate this amount of data effectively, a simple and straightforward method was developed to extract the outlines of the water-covered troughs for comparison in a GIS. This procedure includes steps of speckle reduction and an unsupervised ISODATA classification of the textural parameters variance, homogeneity and mean backscatter intensity. In contrast to the general comprehensive and image-covering evaluation of the TerraSAR-X data for which visual interpretation was chosen, this approach proved suitable for this particular demand. Trough detection results were synchronously validated by high-precision RTK-DGPS and corresponded also to regularly collected in situ data and to visual interpretation of the SAR scenes. Overall, the method proved to be sufficiently insensitive to the imaged variability of water and sediment surfaces shown in the set of images.

The subsequent analysis of the vectorized trough contours indicating the bedform positions, to be specific the western trough edges, resulted in an overall eastward shift over the observed period. This confirms the first results of the visual examination of the data. The extent of the relocations varied between the years, which for the Winter 2013/2014 could be related to the impact of two heavy gales. In addition, it could be shown that the bedform shift regularly occurred during the stormy season from late summer to late winter, whereas during summer, the positions generally remained stable. These findings are supported by results of the sediment analysis, which documented slightly thicker cross-bedded top facies in the bedform crests and decreasing mud content during winter which can be attributed to stronger waves induced by winter storms.

The sandy bedforms described in this study are a prime example of how relatively inconspicuous, shallow surface structures of geomorphological origin in the intertidal area are specifically reproduced due to the contrast of residual water and sediment backscatter reflected in the SAR data. The detection of the residual water in the troughs proved to be an applicable indicator of the overall structure and the location of the bedforms. Similarly, the spatial resolution of the TerraSAR-X products used – HS and SL mode – proved to be suitable for tracking inter-annual developments as well as effect-related and seasonal dynamics. A particular advantage in this context was the high availability of data over time, especially when compared to electro-optical sensors, which are often obstructed by weather conditions. In this way, SAR imagery can be used to map geomorphic surface structures holding residual water, e.g. depressions, puddles or temporary linear surface structures, providing insights into intertidal water drainage systems and morphodynamic processes.

6.3.2 Tidal Flat Dynamics (Neßmer Watt)

The development of an intertidal sub-area in its complete coverage over time and its reproduction by TerraSAR-X has been demonstrated using a time-series of acquisitions from 2009–2015 in the "Neßmer Watt" region. Some of the observed structures do not change, or hardly do so, over the entire period; this applies, for example, to the Riffgat channel and its branching, as well as to the large mud field and the gully structures within. Minor changes affect the course of smaller gully branches and the exact course of the southern mud field boundary. The mud field area has become slightly larger. All of this is clearly visible in the SAR scenes.

In other areas, however, there is fundamental change in surface types. The intermediate stages and sometimes vague structures occurring in these processes are equally reflected in the SAR images. On the whole, the large water-covered depression south of the mud field is increasingly populated by mussels in the east and filled with muddy sediments in the central part. Mussel settlement in this case is initiated by the polychaete Sand Mason (*L. conchilega*) whose tubes in dense occurrence cause significantly increased backscatter, albeit without specifically recognizable pattern. The same applies to the first mussel settlement whereas the subsequent formation of the mussel bed and its internal structures is clearly evident in the SAR scenes. In the same way, the development and the ensuing decline of another mussel bed in the west are clearly depicted by the SAR data. The accumulation of muddy sediment within the initially depressed area, however, is indicated again by generally higher backscatter values. Intermittently, this newly formed sediment surface is characterized by temporary linear bedforms, also reflected by the SAR imagery, probably as a result of storm and wave action. In addition, there were indications in this sub-area that the effects of seagrass settlement on the sediment surface could also lead to increased backscatter in the SAR data. However, such indirect mapping of seagrass induced structures has not necessarily been associated to the occurrence of seagrass at other sites within the course of the investigations.

The overall picture shows that some habitats, structures and developments can be clearly identified from the SAR data due to typical characteristics, while others are recorded as general events whose specific qualities or exact dimensions must be determined via ground truth. The latter applies, in this example, to the extensive field of Sand Mason, to young mussel settlements or to oyster scree scattered by storm events. Correct identification by field observation provided, further development and spatial dynamics of such surfaces can then be remotely monitored via TerraSAR-X data again for a time.

6.4 The Contribution of TerraSAR-X Data to Wadden Sea Monitoring

In summary, the studies have shown that high-resolution SAR data as recorded by TerraSAR-X enables the detection of essential geomorphic surface structures and habitats of the tidal flats and their dynamics. Especially surfaces characterized by distinctive roughness, edges, or specific patterns and textures are clearly identified. But even smooth, intrinsically inconspicuous surface structures, which are marked by residual water, are clearly recognized, as shown by the bedforms example, which was also used for a comparative study integrating different remotely operating sensors (Publication III, chap. 5.3).

6.4.1 A Multi-sensor View on the Bedform Area

Comparing bedform detection from TerraSAR-X data with airborne lidar data and electro-optical data acquired by RapidEye, the individual findings confirmed and complemented each other, each reflecting different properties of the intertidal bedforms. Overall, the positioning of the bedforms was consistently determined by the three sensors. Bedform migration derived from TerraSAR-X data also corresponded to relocations measured in the lidar profiles. RapidEye only had one acquisition from the relevant period, so no relocation could be investigated.

In view of the special sensor characteristics, TerraSAR-X data is the most accurate in terms of trough detection due to the residual water cover. Depending on pixel size and image qualities, the accuracy of trough detection verified by ground truth is in the range of 1–2 m. The most precise determination of the entire bedform surface, however, is given by the three-dimensional lidar data with a resolution in the scale of decimeters to centimeters. This data enables to precisely determine the positions of the crests within the exposed bedform ridges and to study the shape and orientation of the bedforms, which is valuable information for a systematic research on intertidal bedforms and their dynamics. As the near-infrared laser pulses used in the study cannot penetrate water, the troughs, on the other hand, are not detected as precisely as the crest and slope areas of the bedforms. The electro-optical data provided by RapidEye adds highly sensitive detection of sediment moisture to the general view of the bedforms. The spectral properties of the bedform area mainly vary due to varying water content of the sediment surface. Therefore, from the RapidEye data crest, slope and trough areas could be classified by calculating an NDWI (normalized difference water index). Overall, the crests and slopes detected from the electro-optical data are in good agreement with the lidar and RTK height measurements. The asymmetry of the bedform profiles visible in the lidar data is reflected in the RapidEye data as well, as in many cases the crest areas are located close to the western border of the adjoining troughs. The trough positions obtained from RapidEye are consistent with those from TerraSAR-X data (as well as with low height values in the lidar DTM), only the smallest troughs were not recognized at this spatial resolution. The area classified as trough, however, is clearly larger when calculated from RapidEye data which is due to the coarser spatial resolution (6.5 m), but also to the classification method and the high moisture sensitivity of the spectral data, which on the other hand does not well distinguish between high moisture levels and water coverage. The trough area derived from the SAR data, on the contrary, is confined to the central trough areas which are about 100% water-covered.

On the one hand, the results of this multi-sensor view confirm the findings from the visual interpretation of the SAR data and support the assumption that these data are well suited to observe the dynamics of geomorphic structures, in this case the intertidal bedforms. This ability should be emphasized, as remote sensing studies of intertidal geomorphic structures and their dynamics could benefit the understanding of basic processes shaping the Wadden Sea, supporting national and local authorities responsible for coastal management. On the other hand, the study also provides an example of how various sensor data can be integrated to generate a coherent overall view of the bedform surface in the test site which contains the relevant information.

For systematic use in monitoring, not only the system-related imaging properties and sensitivity of the different sensor classes must be considered. Especially with a view to future Wadden Sea Monitoring and long-term ecological research, the most effective use of available sensor technology is of vital interest. A regular survey of the entire area providing the mandatory information characterizing geomorphic structures and habitats of the intertidal area is needed reliably and at minimum expense. These requirements are best ensured by a spatially and temporally structured concept combining the advantages of the respective sensor classes according to characteristics such as footprint area and

spatial resolution, frequency and costs of acquisition. In this regard, the sensors presented in the bedforms example differ significantly:

Airborne lidar provides backscatter intensity and height information with highest spatial resolution and accuracy. It has become a standard method to generate digital terrain models in coastal zones but is limited by the maximum area the flight route can cover during time of exposure. Lidar acquisitions are expensive as they take much time and effort.

Electro-optical sensors, represented by RapidEye, contribute spectral information which in this example enable the discrimination of wet/moist and dry sediments. The spatial resolution of RapidEye (6.5 m) lags behind that of the SAR and the lidar sensors but the swath width of 77 km is a clear advantage in achieving a simultaneous overview over large and hardly accessible areas. A significant limitation associated with optical remote sensing is the dependency on daylight and cloudless skies thus reducing the prospects of capturing data at low water time (reinforced by the provider`s data policy to survey German area only every 45 days). The main strength of the electro-optical data, i.e. the spectral information obtained by the high number of separate wave length measurements, is not fully reflected in the example of bedform detection but related to Wadden Sea monitoring it is of substantial importance to investigate the distribution of sediment types or vegetation such as seagrass, algal mats or diatoms.

As an active sensor, like the lidar, TerraSAR-X operates independent of daylight and cloud cover. The repetition rate is 11 days but scenes taken from differing orbits can be acquired more frequently. The high temporal availability is a great advantage of the SAR data, not only in terms of reliability of data delivery, it also allows to acquire data at yearly, seasonal and even shorter time intervals. Based on this data not only long-term developments and annual courses can be monitored, but also effects of individual high-energy events such as storms or storm surges can be analyzed.

As an outcome of the present study, an exemplary monitoring scheme has been set up to effectively assess bedform dynamics in the long term. It is based on the use of the three-dimensional but expensive lidar at large intervals of 5-10 years, while annual and seasonal developments are surveyed with series of SAR data. The electro-optical RapidEye data cannot be scheduled as reliably as the active sensor`s data, but one or two acquisitions in between the lidar flights should provide larger overviews, covering more than twice the size of even TerraSAR-X StripMap data. For research into the driving forces governing the origin and dynamics of intertidal bedforms, this data can also be complemented by field studies or additional acquisition of lidar data or high-quality ortho-images provided by drones with higher temporal frequency for smaller test sites.

7 Outlook

Radar backscatter measured by high-resolution satellite SAR sensors such as TerraSAR-X contributes information on surface roughness with a high reliability and frequency of data availability. It has been demonstrated, that especially those habitats and geomorphic structures characterized by their surface roughness in combination with specific patterns and textures are clearly recognizable in TerraSAR-X scenes. Additionally, geomorphic surface structures can be virtually marked by residual water which makes an outstanding advantage of this sensor technology.

The pursued approach of visual interpretation of the SAR scenes combined with ground truth, monitoring results and environmental data, integrated in a GIS has met the expectations and proved

to be a technically unsophisticated and quick access to the information contained in the backscatter intensity images. Both, the approach and the information have their own value in support of monitoring and research in tidal areas and can be used by nature protection managers, coastal management in general or by researchers of various disciplines. The results and insights gained from visual interpretation of the TerraSAR-X data also provide suitable knowledge and pointers for further development of automatable classification methods. Dealing with large amounts of data, and with regard to the large area of the Wadden Sea, a visual evaluation of the remote sensing data will be too labor-intensive and time-consuming so that automatable evaluation methods become necessary.

Resulting from the present studies it has become clear that the development of automatic classification methods will encounter some difficulties that are less crucial in the visual interpretation: Above all, the enormous temporal variability of all surface properties in the tidal area must be taken into account, but the same applies to the very different manifestations that certain habitats may have. For example, in contrast to the characteristic internal pattern, both roughness and spectral properties of mussel beds may change with the density of settlement, the content of shell detritus, proportions of Blue Mussel and Pacific Oyster coverage or with brown algae cover (Bladder Wrack, *Fucus vesiculosus*). Also, i.e. the orientation of certain structures in relation to the sensor can affect their reproduction in the data. On the side of the sensor, different recording geometries also influence the image properties.

On the other hand, it has been shown in which cases visual interpretation of backscatter values reaches its limits. Misinterpretation can i.e. relate to fields of shell detritus that can be taken for dense and homogenously covered parts of a mussel bed. In particular, directly adjoining or merging surfaces of i.e. shell detritus or humpy mud can obstruct the exact delineation of mussel beds. Therefore, it is important to identify automatable and additional distinguishing characteristics and to design specific classification tools to fully exploit the information provided by SAR technology for monitoring purposes. By now, various authors have investigated the polarimetric information also provided by the current SAR sensors (TerraSAR-X, Radarsat-2, ALOS/PalSAR) and have demonstrated the potential of multi-polarization SAR imagery for the detection of mussel beds. To this aim, fully polarimetric (Choe et al. 2012, Cheng et al. 2013) or dual-copolarized SAR data (Gade et al. 2015, Gade & Melchionna 2016) have been used. Wang et al. (2017b) who introduce new polarimetric SAR indicators also based on dual-copolarized SAR data, conclude that mussel beds can be detected at all radar wavelengths (X-, C- and L-band), but best results were obtained using X-Band (TerraSAR-X) data. The suggested indicators worked well with acquisition geometries ranging from 31° to 37° incidence. The operational applicability of such methods should be tested in cooperation with potential users.

The recognition of mussel beds has been studied most extensively, but also the use of polarimetric information from the SAR data to identify further surface types in the tidal area has already been pointed out e.g. by Geng et al. (2016) and Gade et al. (2018). It remains to be examined to what extent these methods can also be developed to recognize even vaguely pronounced phenomena such as e.g. Sand Mason (*L. conchilega*) fields or transitional zones and stages which also complicate the visual interpretation. After all, even characteristics of seagrass beds reproduced by SAR data have been found by Gade et al. (2018) for the Schleswig-Holstein Wadden Sea where seagrass stocks are known to grow denser and more pronounced than in Lower Saxony where the sites of this study are located.

For future development of the Wadden Sea monitoring, a multi-sensor approach, containing both SAR and multi-spectral data, seems to be the most promising, and SAR data and algorithm-based evaluation methods of SAR data will make an important contribution. The advances in satellite and sensor technology have accelerated the development of classification tools including methods of data fusion

to refine resolutions and differentiation of targets or to determine intertidal sediment types (listed in Adolph et al. 2018). Also, integrative procedures in general are tested to design comprehensive classification methods for tidal habitats. The latter was particularly in focus of the two projects DeMarine and WIMO, the results of which suggest the beneficial combination of multi sensor data. Neural network deep learning methods may lead to further advances in exploiting satellite remote sensing data for tidal flat monitoring.

The open data policy for an increasing number of sensors such as the sentinel missions from the ESA Copernicus program contributes to drive further development of information extraction and provide reliable data availability. The radar mission, Sentinel-1, uses C-band SAR with a wavelength of 6 cm and supporting operation in single polarization (HH or VV) and dual cross-polarization (HH+HV or VV+VH). Spatial resolution is approximately 5 m by 5 m maximum in stripmap mode with a swath width of 80 km. It has to be worked out to what extent the lower resolution of Sentinel-1 data compared to TerraSAR-X allows the identification of habitats and structures and how the available polarization can be utilized.

The development of operational methods or of contributions to operative classification tools for Wadden Sea monitoring and long-term ecological research based on satellite SAR data is promising but will still be a challenge. For this purpose, interdisciplinary research and collaboration of experts for SAR remote sensing and conservation managers is required and will be of absolute benefit.

References

The references listed here refer to the chapters 1–4 and to chapter 6 framing the cumulating section (chap. 5).

Abt, K.F. (2002): Phänologie und Populationsdynamik des Seehundes (*Phoca vitulina*) im Wattenmeer. Grundlagen zur Messung von Statusparametern. Forschungs-u. Technologiezentrum Westküste der Univ. Kiel.

Adolph, W., Schückel, U., Son, C.-S., Jung, R., Bartholomä, A., Ehlers, M. et al. (2017a): Monitoring spatiotemporal trends in intertidal bedforms of the German Wadden Sea in 2009–2015 with TerraSAR-X, including links with sediments and benthic macrofauna. Geo-Mar. Lett. 37 (2), 79–91. DOI: 10.1007/s00367-016-0478-y.

Adolph, W., Jung, R., Schmidt, A., Ehlers, M., Heipke, C., Bartholomä, A. & Farke, H. (2017b): Integration of TerraSAR-X, RapidEye and airborne lidar for remote sensing of intertidal bedforms on the upper flats of Norderney (German Wadden Sea). Geo-Mar. Lett. 37 (2), 193–205. DOI: 10.1007/s00367-016-0485-z.

Adolph, W., Farke, H., Lehner, S. & Ehlers, M. (2018): Remote sensing intertidal flats with TerraSAR-X. A SAR perspective of the structural elements of a tidal basin for monitoring the Wadden Sea. Remote Sens. 10 (7), 1085–1108. DOI: 10.3390/rs10071085.

Albertz, J. (2009): Einführung in die Fernerkundung. Grundlagen der Interpretation von Luft- und Satellitenbildern. 4th ed., Wissenschaftliche Buchgesellschaft: Darmstadt, Germany, ISBN 978-3-534-23150-8.

Asmus, H. (1987): Secondary production of an intertidal mussel bed community related to its storage and turnover compartments. Mar. Ecol. Prog. Ser. 39 (3), 251–266.

Aubert, M., Baghdadi, N., Zribi, M., Douaoui, A., Loumagne, C., Baup, F. et al. (2011): Analysis of TerraSAR-X data sensitivity to bare soil moisture, roughness, composition and soil crust. Remote Sens. Environ. 115 (8), 1801–1810. DOI: 10.1016/j.rse.2011.02.021.

Bartholdy, J. & Folving, S. (1986): Sediment classification and surface type mapping in the Danish Wadden Sea by remote sensing. Neth. J. Sea Res. 20 (4), 337–345. DOI: 10.1016/0077-7579(86)90001-3.

Beukema, J.J. (1978): Biomass and species richness of the macrobenthic animals living on the tidal flats of the Dutch Wadden Sea: long-term changes during a period with mild winters. Neth. J. Sea Res. 1, 236–261.

Beukema, J.J., Cadée, C.G. & Dekker, R. (2002): Zoobenthic biomass limited by phytoplankton abundance: evidence from parallel changes in two long-term data series in the Wadden Sea. J. Sea Res. 48 (2), 111–125.

Blew, J., Günther, K., Hälterlein, B., Kleefstra, R., Laursen, K., Ludwig, J. & Scheiffarth, G. (2017): Migratory birds. In: Kloepper, S. et al. (eds.): Wadden Sea Quality Status Report 2017. Common Wadden Sea Secretariat, Wilhelmshaven, Germany. Available online: https://qsr.waddensea-worldheritage.org/reports/migratory-birds (accessed on 24 Oct. 2019).

Blew, J., Günther, K., Laursen, K., Van Roomen, M., Südbeck, P., Eskildsen, K. et al. (2005): Overview of numbers and trends on migratory waterbirds in the Wadden Sea 1980–2000. In: Blew, J. & Südbeck,

P. (eds.): Migratory waterbirds in the Wadden Sea 1980–2000. Wadden Sea Ecosystem 20, 1-148. Common Wadden Sea Secretariat, Trilateral Monitoring and Assessment Group, Joint Monitoring Group of Migratory Birds in the Wadden Sea, Wilhelmshaven, Germany. Available online: https://www.waddensea-secretariat.org/resources/ecosystem-20-migratory-waterbirds-wadden-sea-1980-2000 (accessed on 24 Oct. 2019).

Brockmann Consult (2007): OFEW: Operationalisierung von Fernerkundungsmethoden. Summary. Available online: https://docplayer.org/7506004-Operationalisierung-von-fernerkundungsmethoden-fuer-das-wattenmeermonitoring-zusammenfassung.html (accessed on 10 Nov. 2019).

Brzank, A., Heipke, C., Göpfert, J. & Sörgel, U. (2009): Ableitung Digitaler Geländemodelle im Wattenmeer aus luftgestützten Laserscannerdaten. Die Küste 76, 91–120.

Cheng, T.-Y., Yamaguchi, Y., Chen, K.-S., Lee, J.-S. & Cui, Y. (2013): Sandbank and oyster farm monitoring with multi-temporal polarimetric SAR data using four-component scattering power decomposition. IEICE Trans. Commun. 96 (10), 2573–2579. DOI: 10.1587/transcom.E96.B.2573.

Choe, B.-H., Kim, D.-J., Hwang, J.-H., Oh, Y. & Moon, W.M. (2012): Detection of oyster habitat in tidal flats using multi-frequency polarimetric SAR data. Estuar. Coast. Shelf Sci. 97, 28–37. DOI: 10.1016/j.ecss.2011.11.007.

CWSS (1997): Stade Declaration. Trilateral Wadden Sea Plan. Ministerial declaration of the eighth trilateral governmental conference on the protection of the Wadden Sea. Stade, October 22. Available online: https://www.waddensea-worldheritage.org/resources/1997-stade-declaration (accessed on 24 Oct. 2019).

CWSS (2008): Nomination of the Dutch-German Wadden Sea as World Heritage Site. Volume one. Wilhelmshaven, Germany. Available online: https://www.waddensea-worldheritage.org/resources/2008-dossier-nomination-dutch-german-wadden-sea-world-heritage-site (accessed on 24 Oct. 2019).

CWSS (2017): Introduction. In: Kloepper, S. et al. (eds.): Wadden Sea Quality Status Report 2017. Common Wadden Sea Secretariat, Wilhelmshaven, Germany. Available online: https://qsr.waddensea-worldheritage.org/reports/introduction (accessed on 24 Oct. 2019).

Dehouck, A., Lafon, V., Baghdadi, N., Roubache, A. & Rabaute, T. (2011): Potential of TerraSAR-X imagery for mapping intertidal coastal wetlands. Proceedings of the 4th TerraSAR-X Science Team Meeting, Oberpfaffenhofen, Germany, 14–16.

Dehouck, A., Lafon, V., Baghdadi, N. & Marieu, V. (2012): Use of optical and radar data in synergy for mapping intertidal flats and coastal salt-marshes (Arcachon lagoon, France). IGARSS 2012. IEEE International Geoscience and Remote Sensing Symposium, Munich, Germany, 2853–2856.

Delafontaine, M.T., Flemming, B.W. & Mai, S. (2000): The Wadden Sea squeeze as a cause of decreasing sedimentary organic loading. In: Flemming, B.W. et al. (eds.): Muddy coast dynamics and resource management. Elsevier, Amsterdam, The Netherlands, 273–286.

Dellepiane, S., De Laurentiis, R. & Giordano, F. (2004): Coastline extraction from SAR images and a method for the evaluation of the coastline precision. Pattern Recognition Letters 25 (13), 1461–1470. DOI: 10.1016/j.patrec.2004.05.022.

Dennert-Möller, E. (1982): Erstellung einer Sedimentkarte der nordfriesischen Wattgebiete aus LANDSAT-Bilddaten. Bildmessung und Luftbildwesen, 50, 204-206.

Deroin, J.-P. (2012): Combining ALOS and ERS-2 SAR data for the characterization of tidal flats. Case study from the Baie des Veys, Normandy, France. Int. J. Applied Earth Observation Geoinformation 18, 183–194. DOI: 10.1016/j.jag.2012.01.019.

Dijkema, K.S. (1991): Towards a habitat map of the Netherlands, German and Danish Wadden Sea. Ocean and shoreline management 16 (1), 1–21. DOI: 10.1016/0951-8312(91)90036-2.

Dijkema, K.S., Van Tienen, G. & Van Beek, J.G. (1989): Habitats of the Netherlands, German and Danish Wadden Sea 1: 100 000. Research Institute for Nature Management, Texel. Leiden: Veth Foundation, 24 habitat maps 1: 100 000.

Dolch, T., Folmer, E.O., Frederiksen, M.S., Herlyn, M., Van Kartwijk, M.M., Kolbe, K. et al. (2017): Seagrass. In: Kloepper, S. et al. (eds.): Wadden Sea Quality Status Report 2017. Common Wadden Sea Secretariat, Wilhelmshaven, Germany. Available online: https://qsr.waddensea-worldheritage.org/reports/seagrass (accessed on 24 Oct. 2019).

EC (2000): Directive 2000/60/EC of the European Parliament and of the Council of 23 October 2003 establishing a framework for Community action in the field of water policy. OJ L327, 22.12.2000, 1–73. Available online: http://data.europa.eu/eli/dir/2000/60/oj (accessed on 17 Oct. 2019).

EC (2008): Directive 2008/56/EC of the European Parliament and of the Council of 17 June 2008 establishing a framework for community action in the field of marine environmental policy. OJ L 164, 25.6.2008, 19–40. Available online: http://data.europa.eu/eli/dir/2008/56/oj (accessed on 17 Oct. 2019).

EC (2009): Council Directive 2009/147/EC of the European Parliament and of the Council of 30 November 2009 on the conservation of wild birds. OJ L 20, 26.01.2010, 7–25. Available online: http://data.europa.eu/eli/dir/2009/147/oj (accessed on 17 Oct. 2019).

EEC (1992): Council Directive 92/43/EEC of 21 May 1992 on the conservation of natural habitats and of wild fauna and flora. OJ L 206, 22.7.1992, 7–50. Available online: http://data.europa.eu/eli/dir/1992/43/oj (accessed on 17 Oct. 2019).

Ehlers, J. (1994): Geomorphologie und Hydrologie des Wattenmeeres. In: Lozán J.L. et al. (eds.): Warnsignale aus dem Wattenmeer. Blackwell Wissenschaftsverlag, Berlin, Germany, 1-11.

ESA Earth Online 2000−2019: SAR. Available online: https://earth.esa.int/web/guest/missions/esa-operational-eo-missions/ers/instruments. (accessed on 06 Nov. 2019).

Esselink, P., Petersen, J., Arens, S., Bakker, J.P., Bunje, J., Dijkema, K.S. et al. (2009): Salt marshes. In: Marencic, H. & De Vlas, J. (eds.): Wadden Sea Quality Status Report 2009. Common Wadden Sea Secretariat, Wilhelmshaven, Germany. Available online: https://qsr.waddensea-worldheritage.org/reports/salt-marshes (accessed on 24 Oct. 2019).

Folmer, E.O., Drent, J., Troost, K., Büttger, H., Dankers, N., Jansen, J. et al. (2014): Large-scale spatial dynamics of intertidal mussel (Mytilus edulis L.) bed coverage in the German and Dutch Wadden Sea. Ecosystems 17 (3), 550–566. DOI: 10.1007/s10021-013-9742-4.

Gade, M., Alpers, W., Melsheimer, C. & Tanck, G. (2008): Classification of sediments on exposed tidal flats in the German Bight using multi-frequency radar data. Remote Sens. Environ. 112 (4), 1603–1613. DOI: 10.1016/j.rse.2007.08.015.

Gade, M. & Melchionna, S. (2016): Joint use of multiple Synthetic Aperture Radar imagery for the detection of bivalve beds and morphological changes on intertidal flats. Estuar. Coast. Shelf Sci. 171, 1–10. DOI: 10.1016/j.ecss.2016.01.025.

Gade, M., Melchionna, S. & Kemme, L. (2015): Analyses of multi-year synthetic aperture radar imagery of dry-fallen intertidal flats. Int. Arch. of Photogramm. Remote Sens. Spatial Inf. Sci. 40 (7), 941–947. DOI: 10.5194/isprsarchives-XL-7-W3-941-2015.

Gade, M., Melchionna, S., Stelzer & K., Kohlus, J. (2014): Multi-frequency SAR data help improving the monitoring of intertidal flats on the German North Sea coast. Estuar. Coast. Shelf Sci. 140, 32–42. DOI: 10.1016/j.ecss.2014.01.007.

Gade, M., Wang, W. & Kemme, L. (2018): On the imaging of exposed intertidal flats by single- and dual-co-polarization Synthetic Aperture Radar. Remote Sens. Environ. 205, 315–328. DOI: 10.1016/j.rse.2017.12.004.

Geng, X.M., Li, X.-M., Velotto, D. & Chen, K.-S. (2016): Study of the polarimetric characteristics of mud flats in an intertidal zone using C- and X-band spaceborne SAR data. Remote Sens. Environ. 176, 56–68. DOI: 10.1016/j.rse.2016.01.009.

GEOSCAN (1996): Demonstration der Anwendungs- und Nutzungsmöglichkeiten von ERS-1 Daten im Rahmen eines Überwachungsprogramms für das Ökosystem Wattenmeer. Pilotprojekt gefördert durch die Deutsche Agentur für Raumfahrtangelegenheiten (DARA) GmbH FKZ: 50 EE 9314. Hildesheim, Germany.

Goethe, F. (1961): A survey of moulting Shelduck on Knechtsand. British Birds 54 (3), 106–119.

Hellwig, U. & Stock, M. (2014): Dynamic islands in the Wadden Sea. Wadden Sea Ecosystem 33, 1-134. Common Wadden Sea Secretariat. Wilhelmshaven, Germany. Available online: https://www.waddensea-worldheritage.org/resources/ecosystem-33-dynamic-islands-wadden-sea (accessed on 24 Oct. 2019).

Herlyn, M. (2005): Quantitative assessment of intertidal Blue Mussel (Mytilus edulis L.) stocks: combined methods of remote sensing, field investigation and sampling. J. Sea Res. 53 (4), 243–253. DOI: 10.1016/j.seares.2004.07.002.

Herlyn, M. & Millat, G. (2004): Wissenschaftliche Begleituntersuchungen zur Aufbauphase des Miesmuschelmanagements im Nationalpark “Niedersächsisches Wattenmeer”. Abschlussbericht der Niedersächsischen Wattenmeerstiftung, Wilhelmshaven, Germany. (unpublished data).

Heygster, G., Dannenberg, J. & Notholt, J. (2010): Topographic mapping of the German tidal flats analyzing SAR images with the waterline method. IEEE Trans. Geosci. Remote Sens. 48 (3), 1019–1030. DOI: 10.1109/TGRS.2009.2031843.

Holler, P., Markert, E., Bartholomä, A., Capperucci, R., Hass, H.C., Kröncke, I. et al. (2017): Tools to evaluate seafloor integrity: comparison of multi-device acoustic seafloor classifications for benthic macrofauna-driven patterns in the German Bight, southern North Sea. Geo-Mar. Lett. 37 (2), 93–109. DOI: 10.1007/s00367-016-0488-9.

Jensen, L.F., Teilmann, J., Galatius, A., Pund, R., Czeck, R., Jess, A. et al. (2017): Marine mammals. In: Kloepper, S. et al. (eds.): Wadden Sea Quality Status Report 2017. Common Wadden Sea Secretariat, Wilhelmshaven, Germany. Available online: https://qsr.waddensea-worldheritage.org/reports/marine-mammals (accessed on 24 Oct. 2019).

Jung, R. (2016): A multi-sensor approach for land cover classification and monitoring of tidal flats in the German Wadden Sea. Dissertation. University of Osnabrueck, Germany.

Jung, R., Adolph, W., Ehlers, M. & Farke, H. (2015): A multi-sensor approach for detecting the different land covers of tidal flats in the German Wadden Sea — A case study at Norderney. Remote Sens. Environ. 170, 188–202. DOI: 10.1016/j.rse.2015.09.018.

Kim, D.-J., Choe, B.-H. & Moon, W.M. (2013): Remote sensing of oyster reefs and groundwater discharge in coastal area using synthetic aperture radar. IGARSS 13. IEEE International Geoscience and Remote Sensing Symposium, Melbourne, Australia, 2435–2438. DOI: 10.1109/IGARSS.2013.6723312.

Kim, D.-J., Moon, W.M., Kim, G., Park, S.-E. & Lee, H. (2011): Submarine groundwater discharge in tidal flats revealed by space-borne synthetic aperture radar. Remote Sens. Environ. 115 (2), 793–800. DOI: 10.1016/j.rse.2010.11.009.

Kolbe, K. (2011): Erfassung der Seegrasbestände im niedersächsischen Wattenmeer über visuelle Luftbildinterpretation - 2008. NLWKN. Küstengewässer und Ästuare (4/2011).

Kuipers, B.R. (1977): On the ecology of juvenile plaice on a tidal flat in the Wadden Sea. Neth. J. Sea Res. 11 (1), 56–91. DOI: 10.1016/0077-7579(77)90021-7.

Lee, Y.-K., Park, J.-W., Choi, J.-K., Oh, Y. & Won, J.-S. (2012): Potential uses of TerraSAR-X for mapping herbaceous halophytes over salt marsh and tidal flats. Estuar. Coast. Shelf Sci. 115, 366–376. DOI: 10.1016/j.ecss.2012.10.003.

Lehner, S. & Tings, B. (2015): Maritime products using TerraSAR-X and Sentinel-1 imagery. Int. Arch. Photogramm. Remote Sens. Spatial Inf. Sci. XL-7/W3, 967–973. DOI: 10.5194/isprsarchives-XL-7-W3-967-2015.

Lehner, S., Winkel, N., Hija, D., Horstmann, J., Niedermeier, A., Ricklefs, K. et al. (2001): Synergien von Fernerkundung und mathematischen Tidemodellen zur Optimierung divergierender Nutzungsansprüche in Ästuaren. Forschungsbericht DLR 2001-18, ISSN 1434-8454. Deutsches Zentrum für Luft- und Raumfahrt (DLR).

Li, Z., Heygster, G. & Notholt, J. (2014): Intertidal topographic maps and morphological changes in the German Wadden Sea between 1996–1999 and 2006–2009 from the waterline method and SAR images. IEEE J. Sel. Top. Appl. Earth Observations Remote Sensing 7 (8), 3210–3224. DOI: 10.1109/JSTARS.2014.2313062.

Lienau, P. (2010): Über die Entstehung von „Heulern“ im Nationalpark Niedersächsisches Wattenmeer. Dissertation. Georg-August-Universität Göttingen, Germany. Available online: http://ediss.uni-goettingen.de/handle/11858/00-1735-0000-0006-B141-E (accessed on 25 Oct. 2019).

Marencic, H. (2009): The Wadden Sea - Introduction. In: Marencic, H. & De Vlas, J. (eds.): Wadden Sea Quality Status Report 2009. Common Wadden Sea Secretariat, Wilhelmshaven, Germany. Available online: https://www.waddensea-worldheritage.org/resources/ecosystem-25-wadden-sea-quality-status-report-2009 (accessed on 24 Oct. 2019).

Markert, E., Kröncke, I. & Kubicki, A. (2015): Small scale morphodynamics of shoreface-connected ridges and their impact on benthic macrofauna. J. Sea Res. 99, 47–55. DOI: 10.1016/j.seares.2015.02.001.

Mason, D.C. & Davenport, I.J. (1996): Accurate and efficient determination of the shoreline in ERS-1 SAR images. IEEE Trans. Geosci. Remote Sens. 34 (5), 1243–1253. DOI: 10.1109/36.536540.

Millat, G. (1996): Entwicklung eines methodisch-inhaltlichen Konzeptes zum Einsatz von Fernerkundungsdaten für ein Umweltmonitoring im niedersächsischen Wattenmeer. Dissertation, Hochschule Vechta, Germany. Schriftenreihe der Nationalparkverwaltung Niedersächsisches Wattenmeer 1, Wilhelmshaven, Germany.

Moreira, A., Prats-Iraola, P., Younis, M., Krieger, G., Hajnsek, I. & Papathanassiou, K.P. (2013): A tutorial on synthetic aperture radar. IEEE Geosci. Remote Sens. Mag. 1 (1), 6–43. DOI: 10.1109/MGRS.2013.2248301.

Müller, G., Stelzer, K., Smollich, S., Gade, M., Adolph, W., Melchionna, S. et al. (2016): Remotely sensing the German Wadden Sea—a new approach to address national and international environmental legislation. Environ. Monit. Assess. 188 (10), 26. DOI: 10.1007/s10661-016-5591-x.

NASA (2019a): The Multispectral Scanner System. Available online: https://landsat.gsfc.nasa.gov/the-multispectral-scanner-system/ (accessed on 06 Nov. 2019).

NASA (2019b): The Thematic Mapper. Available online: https://landsat.gsfc.nasa.gov/the-thematic-mapper/ (accessed on 06 Nov. 2019).

Nehls, G., Bräger, S., Meissner, J. & Thiel, M. (1988): Zum Bestand der Eiderente (Somateria mollissima) an der deutschen Nordseeküste. Corax 13 (1), 41–58.

Niedermeier, A., Hoja, D. & Lehner, S. (2005): Topography and morphodynamics in the German Bight using SAR and optical remote sensing data. Ocean Dyn. 55 (2), 100–109. DOI: 10.1007/s10236-005-0114-2.

Nieuwhof, S., Herman, P., Dankers, N., Troost, K. & Van der Wal, D. (2015): Remote sensing of epibenthic shellfish using Synthetic Aperture Radar satellite imagery. Remote Sens. 7 (4), 3710–3734. DOI: 10.3390/rs70403710.

Oost, A., Winter, C., Vos, P., Bungenstock, F., Schrijvershof, R., Röbke, B. et al. (2017): Geomorphology. In: Kloepper, S. et al. (eds.): Wadden Sea Quality Status Report 2017. Common Wadden Sea Secretariat, Wilhelmshaven, Germany. Available online: https://qsr.waddensea-worldheritage.org/reports/geomorphology (accessed on 24 Oct. 2019).

Park, S.-E., Moon, W.M. & Kim, D.-J. (2009): Estimation of surface roughness parameter in intertidal mudflat using airborne polarimetric SAR data. IEEE Trans. Geosci. Remote Sens. 47 (4), 1022–1031. DOI: 10.1109/TGRS.2008.2008908.

Petersen, J., Dassau, O., Dauck, H.-P. & Janinhoff, N. (2010): Applied vegetation mapping of large-scale areas based on high resolution aerial photographs - a combined method of remote sensing, GIS and near comprehensive field verification. In: Marencic, H. et al. (eds.) Science for Nature Conservation and Management: The Wadden Sea Ecosystem and EU Directives. Proceedings of the 12th International Scientific Wadden Sea Symposium in Wilhelmshaven, Germany, 30 March - 3 April 2009. Wadden Sea Ecosystem 26. Common Wadden Sea Secretariat, Wilhelmshaven, Germany, 75–

79. Available online: https://www.waddensea-secretariat.org/resources/ecosystem-26-science-nature-conservation-and-management (accessed on 24 Oct. 2019).

Piersma, T. (1987): Production by intertidal benthic animals and limits to their predation by shorebirds: a heuristic model. Mar. Ecol. Prog. Ser. 38, 187–196.

Pröber, C. (1981): Die Möglichkeiten der Fernerkundung in der Küstengeologie: eine Untersuchung am Beispiel der nordfriesischen Wattsedimente und der Schwebfracht in der Nordsee. Thesis. Christian-Albrechts-Universität zu Kiel, Germany.

Reise, K. (2005): Coast of change: habitat loss and transformations in the Wadden Sea. Helgol. Mar. Res. 59 (1), 9–21. DOI: 10.1007/s10152-004-0202-6.

Reise, K., Baptist, M., Burbridge, P., Dankers, N., Fischer, L., Flemming, B. et al. (2010): The Wadden Sea – A universally outstanding tidal wetland. Wadden Sea Ecosystem 29. Common Wadden Sea Secretariat, Wilhelmshaven, Germany, 7–24. Available online: https://www.waddensea-secretariat.org/resources/ecosystem-29-wadden-sea-2010 (accessed on 24 Oct. 2019).

Ringot, J.L. (1992/1993): Erstellen eines Interpretationsschlüssels und Kartierung der Biotoptypen terrestrischer Bereiche des Nationalparks Niedersächsisches Wattenmeer auf der Basis des CIR-Bildfluges vom 21.08.1991. unpublished.

Scheiffarth, G. (2004): Das Ökosystem Wattenmeer. In: Behrends, B. et al. (eds.): Gesamtsynthese Ökosystemforschung Wattenmeer. Zusammenfassender Bericht zu Forschungsergebnissen und Systemschutz im deutschen Wattenmeer. UBAFBNr 000190, Förderkennzeichen 296 85 905. UBA Texte 03/04, Berlin, Germany, 1–8.

Scheiffarth, G., Frank, D. (2005): Shellfish eating birds in the Wadden Sea - What can we learn from current monitoring programmes? Wadden Sea Ecosystem 20. Common Wadden Sea Secretariat, Trilateral Monitoring and Assessment Group, Joint Monitoring Group of Migratory Birds in the Wadden Sea, Wilhelmshaven, Germany, 187–200. Available online: https://www.waddensea-secretariat.org/resources/ecosystem-20-migratory-waterbirds-wadden-sea-1980-2000 (accessed on 25 Oct. 2019).

Scheiffarth, G. & Nehls, G. (1997): Consumption of benthic fauna by carnivorous birds in the Wadden Sea. Helgoländer Meeresunters. 51 (3), 373–387. DOI: 10.1007/BF02908721.

Schmidt, A., Rottensteiner, F. & Soergel, U. (2013): Monitoring concepts for coastal areas using lidar data. Int. Arch. Photogramm. Remote Sens. Spatial Inf. Sci. XL-1/W1, 311–316. DOI: 10.5194/isprsarchives-XL-1-W1-311-2013.

Smidt, E.L.B. (1951): Animal production in the Danish Waddensea. Fiskeri- og Havunders. Ser. Fiskeri 11 (6), 1–151.

Stelzer, K., Brockmann, C., Geißler, J., Kleeberg, U. & Doerffer, R. (2007): Abschlussbericht OFEW. Operationalisierung von Fernerkundungsmethoden für das Wattenmeermonitoring. Internal Report.

Stelzer, K., Geißler, J., Gade, M., Eskildsen, K., Kohlus, J., Farke, H. & Reimers, H.-C. (2010): DeMarine Umwelt: Operationalisierung mariner GMES-Dienste in Deutschland. Integration optischer und SAR Erdbeobachtungsdaten für das Wattenmeermonitoring. Jahresbericht 2009 - 2010.

Strasser, M. (2002): Reduced epibenthic predation on intertidal bivalves after a severe winter in the European Wadden Sea. Mar. Ecol. Prog. Ser. 241, 113–123. DOI: 10.3354/meps241113.

Swennen, C.G., Nehls, G. & Laursen, K. (1989): Numbers and distribution of Eiders Somateria mollissima in the Wadden Sea. Neth. J. Sea Res. 24, 83–92.

Van der Wal, D. & Herman, P.M.J. (2006): Quantifying the particle size of intertidal sediments with satellite remote sensing in the visible light, thermal infrared and microwave spectral domain. Proceedings of the ISPRS Commission VII Symposium "Remote Sensing: From Pixels to Processes, Enschede, The Netherlands, 618-622.

Van der Wal &D., Herman, P.M.J. (2007): Regression-based synergy of optical, shortwave infrared and microwave remote sensing for monitoring the grain-size of intertidal sediments. Remote Sens. Environ. 111 (1), 89–106. DOI: 10.1016/j.rse.2007.03.019.

Van der Wal, D., Herman, P.M.J. & Wielemaker-van den Dool, A. (2005): Characterisation of surface roughness and sediment texture of intertidal flats using ERS SAR imagery. Remote Sens. Environ. 98 (1), 96–109. DOI: 10.1016/j.rse.2005.06.004.

Wang, W., Yang, X., Li, X., Chen, K.-S., Liu, G., Li, Z. & Gade, M. (2017a): A fully polarimetric SAR imagery classification scheme for mud and sand flats in intertidal zones. IEEE Trans. Geosci. Remote Sens. 55 (3), 1734–1742. DOI: 10.1109/TGRS.2016.2631632.

Wang, W., Gade, M. & Yang, X. (2017b): Detection of bivalve beds on exposed intertidal flats using polarimetric SAR indicators. Remote Sens. 9 (10), 1047. DOI: 10.3390/rs9101047.

Wang, W., Yang, X., Liu, G., Zhou, H., Ma, W., Yu, Y. & Li, Z. (2016): Random Forest classification of sediments on exposed intertidal flats using ALOS-2 quad-polarimetric SAR data. Int. Arch. Photogramm. Remote Sens. Spatial Inf. Sci. 8, 1191–1194. DOI: 10.5194/isprsarchives-XLI-B8-1191-2016.

Wang, Y. & Koopmanns, B.N. (1995): Monitoring tidal flat changes using ERS-1 SAR images and GIS in the western Wadden Sea area, The Netherlands. EARSeL Advances in Remote Sensing 4 (1), 45–52.

Wang, Z.B., Hoekstra, P., Burchard, H., Ridderinkhof, H., De Swart, H.E. & Stive, M.J.F. (2012): Morphodynamics of the Wadden Sea and its barrier island system. Ocean & Coastal Management 68, 39–57. DOI: 10.1016/j.ocecoaman.2011.12.022.

Wiehle, S. & Lehner, S. (2015): Automated waterline detection in the Wadden Sea using high-resolution TerraSAR-X images. J. Sensors, Article ID 450857.

Winter, C. (2017): Monitoring concepts for an evaluation of marine environmental states in the German Bight. Geo-Mar. Lett. 37 (2), 75–78. DOI: 10.1007/s00367-017-0496-4.

Winter, C., Backer, V., Adolph, W., Bartholomä, A., Becker, M., Behr, D. et al. (2016): Wissenschaftliche Monitoringkonzepte für die Deutsche Bucht (WIMO). Abschlussbericht, 1–159. Available online: https://epic.awi.de/id/eprint/42706/ (accessed on 24 Oct. 2019).

Wolff, W.J. (1991): Ecology of the Wadden Sea. In: Prokosch, P. et al. (eds.): The common future of the Wadden Sea. Technical Report. World Wide Fund for Nature, Husum, Germany, 13–22.

Wolff, W.J. (2013): Ecology of the Wadden Sea: Research in the past and challenges for the future. J. Sea Res. 82, 3–9. DOI: 10.1016/j.seares.2013.03.006.

Acknowledgements

I wish to thank Prof. Dr.-Ing. Manfred Ehlers for taking on the supervision and for support but also for giving me the freedom I had in this study. He mentored and motivated me, even beyond the time of his professorship at the former Institute for Geoinformatics and Remote Sensing of the University of Osnabrück.

Thanks to Dr. Hubert Farke (NLPV) and Dr. Gerald Millat (NLPV) and to Dr. Susanne Lehner (DLR), who made this PhD position possible – they managed the funding acquisition (WIMO) and provided resources at their respective institutions, the Lower Saxon Wadden Sea National Park Authority (NLPV) and the German Aerospace Center (DLR). I have always been very grateful for that and all three of them have been of inspiration to me.

I am in particular deeply grateful to Dr. Hubert Farke for sharing his enthusiasm, for scientific advice, encouragement and for urging me to attend to international conferences and workshops to present and discuss my findings there. Thank you, I have learned a lot. Thanks for always taking your time helping me and for tirelessly accompanying me on countless days of fieldwork in often muddy terrain.

This research would not have been possible without the cooperative research project “Scientific Monitoring Concepts for the German Bight” (WIMO), jointly funded by the Ministry of Environment, Energy and Climate Protection (NMU) and the Ministry of Science and Culture (NMWK) of the Federal State of Lower Saxony. Funding was also received from the German Ministry of Economy (BMWi) for the projects DeMarine-1 Environment and DeMarine-2 SAMOWatt, from which data and knowledge have been included. Sedimentological work was facilitated by the fellowship of Dr. Chang Soo Son at the Hanse Institute for Advanced Study, and a grant from the Korean Ministry of Oceans and Fisheries (PJT200538). The Ministries are highly acknowledged for the funding. Thanks to the Institute for Advanced Study (HWK) in Delmenhorst, especially to Dr. Doris Meyerdierks and Verena Backer for the WIMO overall project management and the function of HWK as platform for discussions and workshops. Thanks also to the National Park Administration Lower Saxon Wadden Sea supporting my work, providing me with a working place and with many colleagues who were always willing to discuss or help – I would like to name Dr. Gerald Millat und Dr. Gregor Scheiffarth.

I have received a lot of support from the institutions and working groups, colleagues and friends that were involved or in cooperation with the WIMo and the DeMarine projects:

I am grateful to the colleagues with whom I worked together on the WIMO subproject “Remote Sensing”, especially Dr. Richard Jung from the Institute for Geoinformatics and Remote Sensing at the University of Osnabrück (IGF), Dr. Alena Schmidt from the Institute of Photogrammetry and GeoInformation at the University of Hannover (IPI) and Ruggero Capperucci and Dr. Alexander Bartholomä from Senckenberg Institute in Wilhelmhaven. Dr. Ulrike Schückel (Senckenberg, Wilhelmshaven) took the time to examine the benthos samples from the bedform area and Dr. Chang Soo Son (Chonnam National University, Gwangju, South Korea) travelled from South Korea to help with the sedimentological issues.

I am also thankful to the colleagues from the DeMarine-1 and DeMarine-2 subprojects (“Integration of optical and SAR Earth Observation Data and in situ data into Wadden Sea Monitoring” and SAMOWatt “Satellite data for Monitoring in the Wadden Sea”), particularly to Kerstin Stelzer from Brockmann Consult, Dr. Martin Gade from the University of Hamburg (Institut für Meereskunde), and Jörn Kohlus, Kai Eskildsen and Dr. Gabriele Müller, from the National Park Administration of the Schleswig Holstein Wadden Sea.

Thanks all of you for the good teamwork or cooperation, constructive discussions and joint field campaigns.

I owe a great thanks to Dr. Susanne Lehner (DLR) for scientific advice related to SAR remote sensing, for a multitude of ideas and for energetic encouragement. Thanks also for introducing me to her working groups at the Remote Sensing Technology Institute (IMF) located at Oberpfaffenhofen and Bremen Flughafen. There, I had fruitful discussions with colleagues who took their time and gave me valuable insights into SAR remote sensing and training in the acquisition and use of TerraSAR-X data. Many thanks especially to Dr. Stephan Brusch, Dr. Andrey Pleskachevsky, Dr. Wolfgang Rosenthal, Dr. Sven Jacobsen, Dr. Stephan Wiehle and Dr. Anja Frost who supported me in many ways. Thanks also to Ruth Kaps who helped me with all the formalities of the DLR workplace. The DLR also provided extensive TerraSAR-X data relating to project ID COA1075. I am very grateful to Ursula Marschalk und Achim Roth (DLR) for their support in acquiring scenes, which sometimes had to be in sync with field campaigns.

Thanks to the active support of Julius Schmidt and Helmo Nicolai from the Institute of Chemistry and Biology of the Marine Environment (ICBM) of the University of Oldenburg who boated the fieldworkers even to the most remote mudflats and back and to Udo Uebel (ICBM) who helped with processing the RTK-DGPS data.

Thanks to my former colleague and friend Dr. Gabi Petri for carefully reading this manuscript.

My family and friends are thanked for constant support and patience during the years of my studies.

Erklärung

Hiermit erkläre ich, daß ich die vorliegende Arbeit selbständig verfasst und nur die angegebenen Hilfsmittel benutzt habe.

Wilhelmshaven, den 03.06.2020

Winny Adolph